Optical and Electro-optical Impairment Mitigations for Large Capacity Optical Fiber Transmission

June 2018

Akira Hirano

Doctoral Thesis

Ph.D. (Engineering)

Optical and Electro-optical Impairment Mitigations for Large Capacity Optical Fiber Transmission

June 2018

Faculty of Science and Technology

Keio University

Akira Hirano

Forewords

Optical fiber transmission systems have been serving as social infrastructure for various Information Technologies-based (IT) services. Formerly, optical fiber transmission systems carried wire-line telephone services. After the saturation of wire-line telephone service traffic, mobile and data communication traffic has been expanding dramatically. As a result, over-all traffic demand is continuously increasing.

Thus, the need for optical transmission systems that support more capacity and sufficient optical reach with less cost still be indispensable.

In this Thesis, I will propose and present novel optical and electro-optical means to mitigate impairments induced by physical characteristics of optical transmission fibers. The means covers optical modulation formats which reveals high tolerance against such impairments, compensation techniques to reduce such impairment, and impairment evaluation methods to make possible efficient optical transmission systems design.

I have confirmed and presented higher tolerance, effective compensation performance, and successful evaluation of impairments in field environment, in both numerical estimation and experiments. In addition to that, two types of optical regeneration techniques are discussed. I have discussed effective suppression of waveform distortion and noise from optical amplifiers. Also I have provided precise analysis to treat nonlinear transmittance of optical gates with optical amplification for the first time as of 1999. These are candidates for more simple and power-efficient transmission systems.

To further extend transmission capacity, introduction of parallelism, namely wavelength division multiplexing in optical transport is indispensable. For such purposes, we need to tweak deviation of impairments beyond single channel case, invent a mechanism to handle parallel lambdas as a whole, and reduce failure rate resulted from expanding number of equipment which is inevitable consequence of wavelength division multiplexing where we use many channels.

I have proposed and verified novel deviation compensation techniques, a framework for consolidation of multiple channels as a whole, and transmission architecture to realize programmable robustness.

These techniques have significant advantages in scalability for capacity extension and for operational convenience. Moreover, at a time when the labor force is shrinking because of the

falling birth rate and the aging population, optical network itself should be maintained with less labor force. Programmable resiliency will be one of the key techniques to relax or reduce truck-roll to maintain optical network.

Nov. 19 2017

Akira Hirano

Index

1. Introduction

Optical communication systems overview 8

Major impairments (ISI and SNR degradation) 13

Contributions and structure of the Thesis 19

2. Optical phase and GVD tolerance

Optical time-division multiplexing with optical phase control 30

Numerical estimation of optical phase and duty ratio dependency 30

80-Gbit/s OTDM transmitter 34

Experimental setup for evaluation 35

Results 36

DSF transmission experiment 38

Section summary 40

3. Spectral mode splitting

Background 41

Spectral redundancy in carrier-suppressed RZ formats 41

Expansion of dispersion tolerance by spectral mode splitting 44

Automatic dispersion compensation by spectral mode splitting 49

Discussion 53

Section summary 54

4. PMD evaluation

The need for PMD mitigation 56

Field trial configuration 56

Tolerance against all-order and 2nd-order PMD 58

FEC performance against all-order PMD 59

Section summary 60

5. SNR recovery toward higher bitrate TDM

5.1 All-optical 2R (Reshaping and Regeneration) repeater

Signal-ASE beat noise suppression 62

FWM limiter circuit 62

Experimental setup 65

Results and discussion 65
Section summary 67

5.2 All-optical 3R (Retiming, Reshaping, and Regeneration) regenerator
All-optical approach for ASE noise suppression 68
Optical discrimination 70
Estimation of discrimination performance 70
Ultra-fast nonlinear gate: LOTOS 82
Experimental results 86
Discussion 88
Section summary 94

Summary of section 5 95

6. Approaches toward wider bandwidth WDM
6.1 Dispersion slope compensation
Background 96
3.2 THz bandwidth slope compensator 97
16-ch x 42.7-Gbit/s WDM transmission experiment 97
Section summary 101

6.2 Optical virtual concatenation
Background 102
The Terabit LAN Concept 103
The Scalable Adaptive Graphics Environment (SAGE) 107
The Technology and iGrid Real-time Demonstration 108
Section summary 113

6.3 Programmable resiliency
Background 115
i-ANP^2 architecture 115
Main advantages 116
Toward OPEX reduction 118
Change of maintenance operation 119
Enhanced agility with mesh-like topology 120
Section summary 120

Summary of section 6 122

7. Conclusion 123

Acknowledgments 127

Appendix 128

References 129

Journal papers used in the Thesis 140

Other journal papers 142

Full-length Papers in International Conferences 154

International Conference Papers 156

Domestic Conference Papers (in Japanese) 166

Holding Japanese Patents (in Japanese) 173

1. Introduction

Optical communication systems overview

Optical network overview

Basic configuration of optical network is summarized in Fig.1-1.

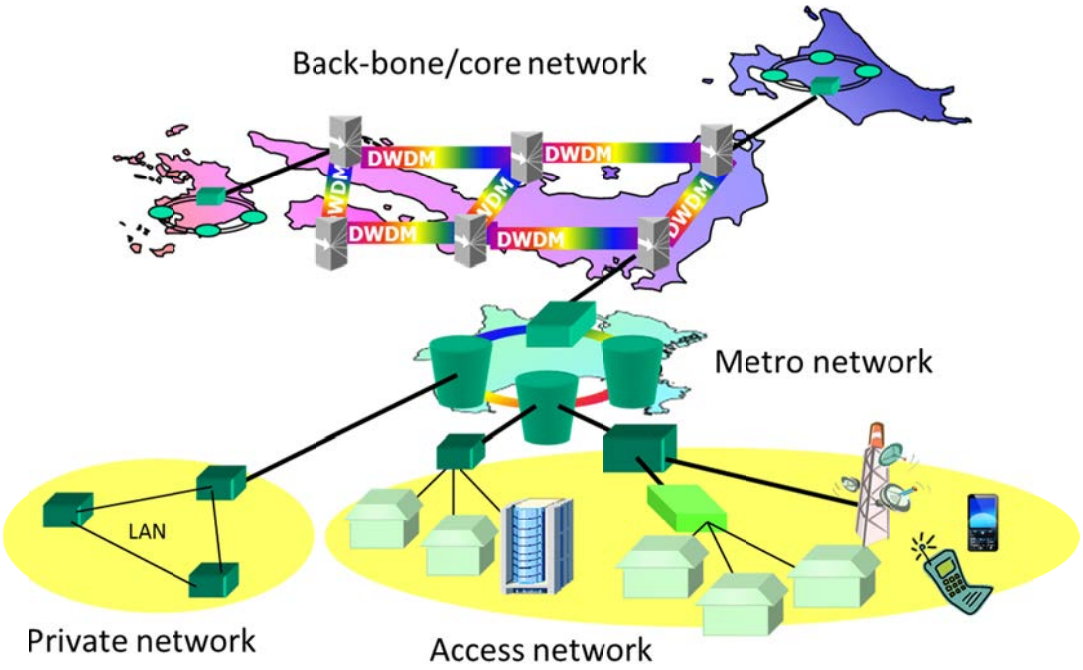

Fig. 1-1 Overview of optical network

It consists of back-bone/core, metro, and access network as shown in the figure. The access network aggregates traffic from subscribers including fixed/mobile phones, LANs, and some other devices. The metro network inter-connects and/or further aggregate the traffic from the access network. The back-bone/core network connects the metro traffic over long distance extending through several hundred's or thousands' of kilo meters.

To reduce expenditures for optical transport network, especially for the back-bone/core network, realizing optical transmission systems which can support larger transmission capacity and optical reach is essential and should be an research and development (R&D) target. Extending optical reach can reduce the number of regenerators (transmitters/receivers) to be needed to connect remote sites. Also, larger capacity transmission systems can support expanding traffic demand with smaller number of transmitters/receivers. Thus the more capacity and longer reach transmission should be one

of the rational goals of optical network R&D.

In addition to that, the number of working population in ageing society is expected to decrease in the following decades. Therefore, some countermeasures to reduce labor work to maintain optical network should be needed in the near future. That means some techniques which can reduce operational expenditure will be also needed.

In this thesis, I propose some novel optical and electro/optical techniques to enhance both transmission capacity and optical reach. Moreover, I propose a candidate technique that can be expected to reduce labor work needed to operate optical network.

Transmitter and receivers

Optical communication systems basically consist of optical transmitter and receivers.

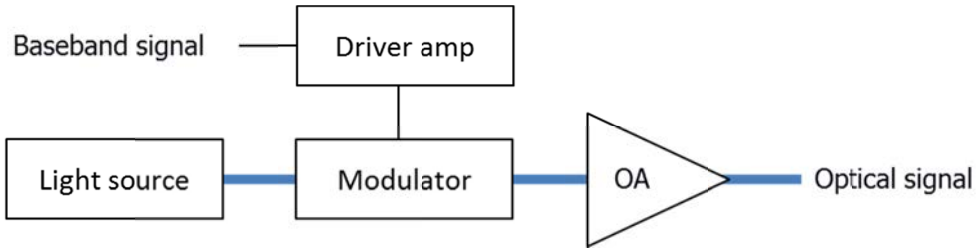

Fig. 1-2 Typical optical transmitter configuration

Optical transmitter, which is shown in Fig. 1-2, converts incoming electrical baseband signal into optical signal that can transmit through optical fibers. The transmitter usually consists of a light source, a modulator with a driver amplifier to adjust the amplitude of the electrical signal to fit the appropriate level for the modulator and an Optical Amplifier (OA) to enhance the optical signal to the level that will have sufficient Optical Signal-to-Noise Ratio (OSNR) at the receiver. We can use various characteristics of light-wave including optical amplitude, optical phase, states of polarizations, and so on.

Optical receiver, which is shown in Fig. 1-3, converts incoming optical signal transmitted over optical fibers into electrical baseband signal.

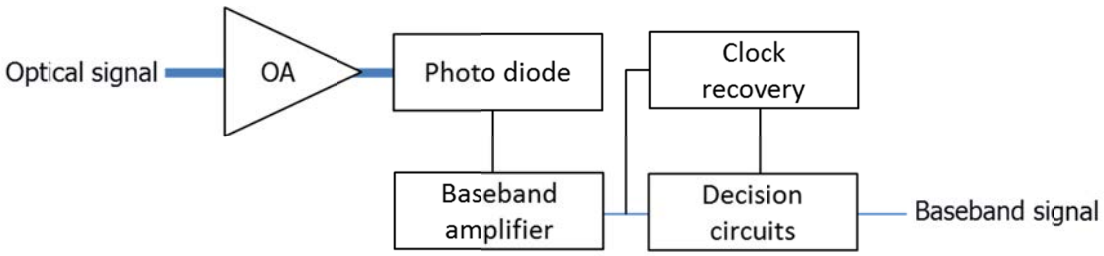

Fig. 1-3 Typical optical receiver configuration

The receiver usually consists of an optical amplifier to amplify the optical power that is high enough to overcome thermal noise of receiver circuit, a photo diode that converts optical signal into electrical current, electrical amplifier, clock recovery circuit that provide timing signal into the decision circuit and a decision circuit to recover original digital data. The actual configuration of optical receivers depends on what kind of characteristics we used for data transmission including optical amplitude, optical phase, and so on.

Optical fibers for high-speed transmission

Optical fibers for optical communication are standardized in International Telecommunication Union (ITU). Typical characteristics of optical fibers are shown in Table 1-1.

Tab. 1-1 Examples of ITU-T standardized optical fibers

Specification	Fiber type	Maximum loss at 1550nm	Chromatic dispersion (ps/nm/km)	Max PMD (ps/√km)
G.652	Single mode optical fibers	0.3 dB/km	13.3(min)-18.6(max) at 1550 nm	0.20
G.655	Non-zero dispersion-shifted single mode optical fibers	0.35 dB/km	1(min)-10(max) in 1530-1565 nm	0.20

G.652 which is standard single mode fiber and G.655 which is non-zero dispersion-shifted fibers are widely installed in telecommunication network. Typically they have about 0.2-0.3 dB/km of loss. Therefore, optical power decreases by 1/100 (20-30 dB) after 100km transmission. Such a small loss realized long-haul optical transmission systems that support current information society. The group velocity dispersion (GVD) and polarization mode dispersion (PMD) degrade optical waveform transmit trough optical fibers and they limit optical reach of optical communication systems. So we need higher tolerance against these

impairments and/or compensation countermeasure to extend optical reach. Also, optical fibers have non-linear refractive index. Depending on the input optical power, refractive index of optical fiber has non-linear response [1], so optical signal transmit through optical fiber will suffer optical phase change, which means optical frequency chirp occurs. Such frequency chirp will be converted into waveform distortion through interaction with GVD and/or PMD mentioned above.

Optical amplifier and optical regenerator

Attenuation of optical fiber limits maximum optical reach of optical communication systems. To overcome the limit, we usually deploy optical amplifiers or optical regenerators. To be precise, we will have two types of limits; one is optical attenuation and another is OSNR. Optical amplifiers boost optical amplitude, so we can overcome the attenuation limit by deploying optical amplifiers, but they inherently generate amplified spontaneous noise (ASE). Thus the ASE noise will accumulate and limit the optical reach. Basically, the minimum noise figure of optical amplifiers is 3 dB. To recover OSNR, we need optical regenerator.

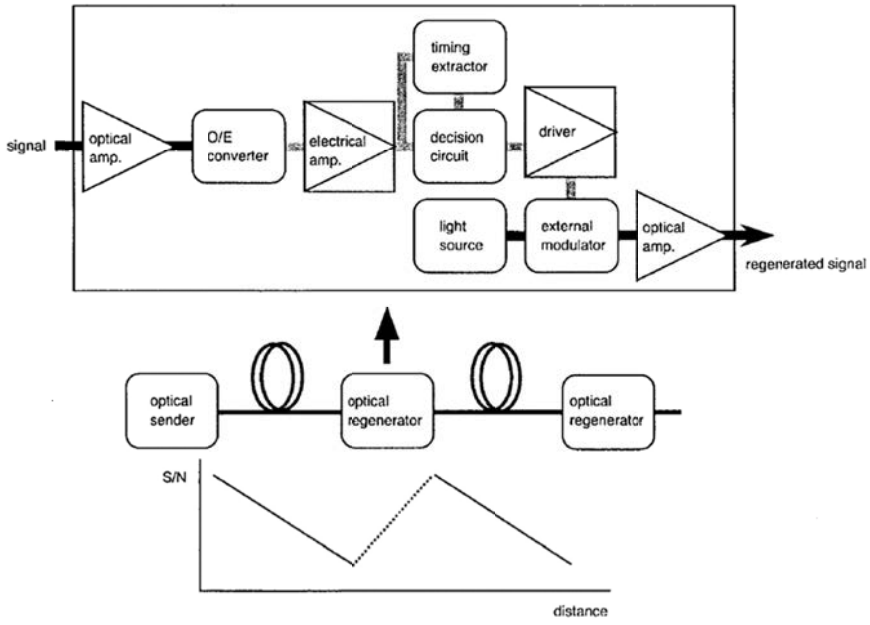

Fig. 1-4 Conventional regenerator configuration and SNR recovery

Figure 1-4 shows schematic configuration of optical regenerator. The optical regenerator usually consists of a pair of optical receiver and transmitter. In principle, optical regenerator recovers original digital data inside. Therefore, all the impairments including GVD, PMD,

optical loss, and OSNR degradation can be mitigated. Namely, optical signal is "regenerated," so all the impairments will be reset. So it is a very powerful tool for optical transmission. However, from the viewpoint of cost and power consumption, optical regenerator is less attractive since it doubles the number of transmitter and receiver in optical communication systems, and more, when needed. Thus, when we design cost-effective optical network for telecommunication, we usually try to minimize the number of regenerators.

We can categorize countermeasures against above mentioned impairments. Optical modulation formats that have higher tolerance against these impairments are effective to extend optical reach and capacity. In addition to that, compensation techniques for such impairments are also attractive. Usually, we use both to enhance transmission performance. Also, impairment evaluation such as GVD/PMD measurements is also essential to select appropriate modulation formats and/or compensation method. All-optical regeneration that does not need optical receiver and transmitter pair is a candidate for cost-effective optical transmission.

Major impairments (ISI and SNR degradation)

Group velocity dispersion (GVD)

Group velocity dispersion is one of the major inter symbol interference (ISI) impairments which limit the transmission performance of optical communication systems. Optical signal has some extent of optical bandwidth depending on its light source and modulation formats. In optical fibers, optical signal travels at different group velocity depending on its optical frequency.

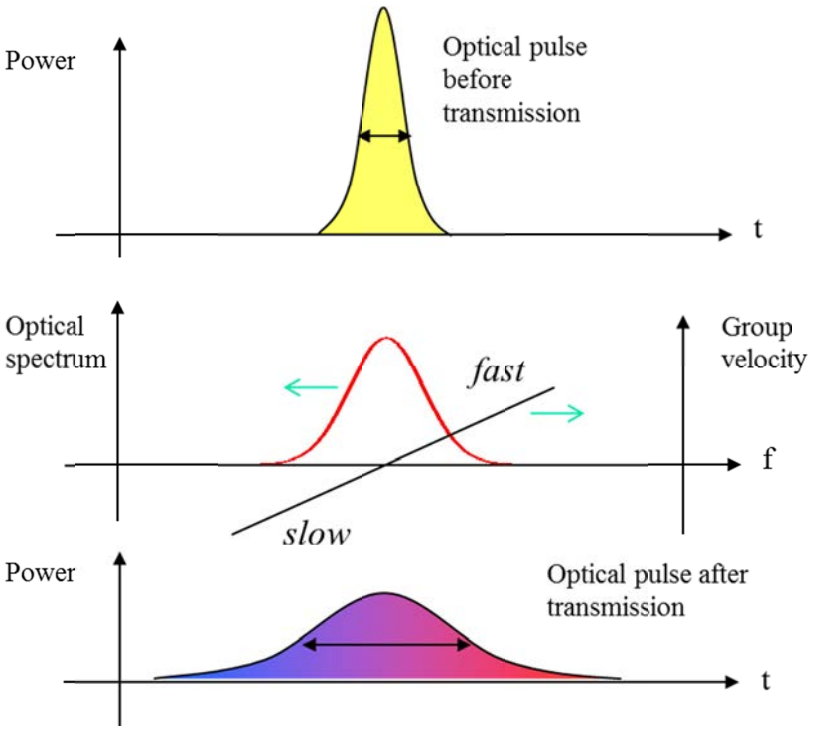

Fig. 1-5 Group velocity dispersion

Figure 1-5 shows optical pulse broadening caused by group velocity dispersion of optical fibers schematically. As shown in the middle of Fig 1-5, optical pulse has some extent of spectral bandwidth and the spectral component travel at different group velocity depending on its spectral frequency. Therefore, after transmission, the pulse will be broadened because some portion of the pulse travels faster and other portion travels slower. In this specific case, the spectral component of higher frequency travels faster and lower travels slower, respectively.

We can define group velocity dispersion D as follows. When the optical signals which have spectral difference of 1nm shows D ps of relative delay after 1km of transmission of optical

fiber, we define the fiber has D ps/nm/km of group velocity dispersion.

Maximum transmission can be estimated as the function of D. When we define the maximum transmission reach as the distance where the transmitted optical signal suffers 25% of pulse broadening, the maximum reach can be expressed by the following equation.

$$L(\max) = \frac{10^3 c}{4a\lambda^2 |D| f_c^2} \qquad \text{Eq. 1-1}$$

D : Group velocity dispersion [ps/nm/km]

f_c : Modulation bit rate [Gbit/s]

c : Speed of light [m/s]

a : Factor for modulation format

λ : Wavelength [nm]

Polarization mode dispersion (PMD)

Polarization mode dispersion is another important ISI impairment which limits transmission reach of optical communication systems. Optical fiber accepts two independent polarization modes which has two relatively perpendicular directions of electrical fields. When the optical fiber has fabricated in true circular symmetry, the fibber will shows no polarization mode dispersion at all. However, actual optical fibers have some asymmetry or deviation from true circle, so it will have relative delay between the two polarization modes, which means it will have birefringence. We can define fast and slow axis of optical fiber

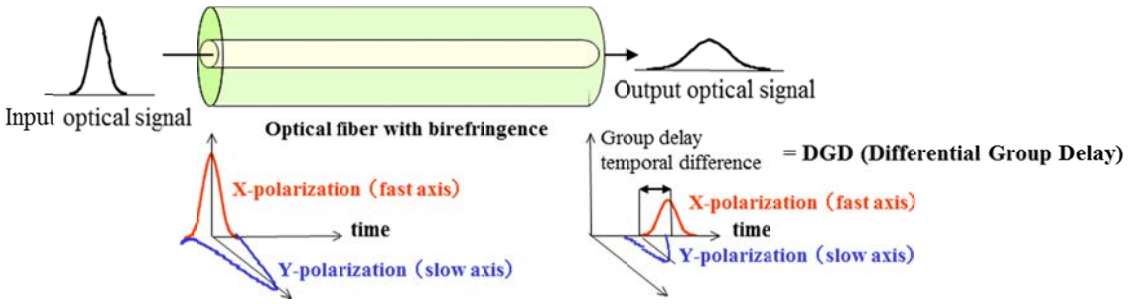

with birefringence as shown in Fig. 1-6.

Fig. 1-6 Polarization mode dispersion

When we launched optical pulse into the optical fiber, the pulse suffers different group delay depending on its initial polarization state into the optical fiber. We call the group delay difference as differential group delay (DGD). As a result, output optical pulse will be broadened as shown in the Fig 1-6. Provided that we launched into the fast or slow axis only, we will have no pulse broadening. We call such polarization state where no pulse broadening occur the principal state of polarization (PSP). Usually, the power ratio into these two axes has some finite value as shown in Fig. 1-7, the output pulse will be broadened after direct detection.

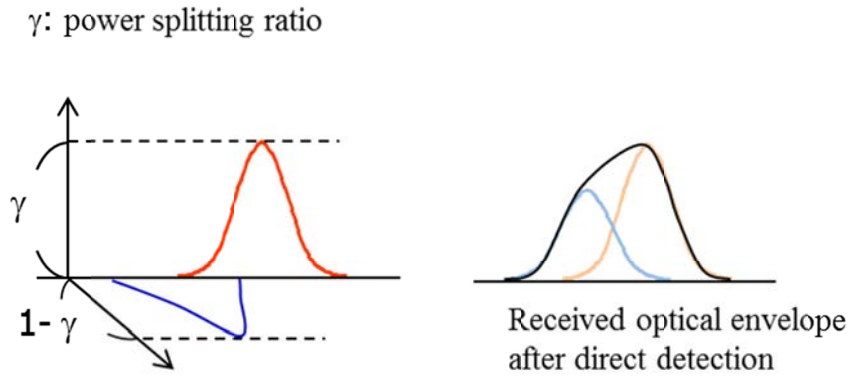

Fig. 1-7 Waveform impairment by polarization mode dispersion

In addition to that, the DGD also depends on signal wavelength. As I explained in discussion on GVD, each signal transmit trough fast or slow axis also suffers GVD, respectively. This is one component (wavelength dependence of DGD) of the higher order PMD. Moreover, the position of fast and slow axis on birefringence fiber also deviates depending on the signal wavelength. Thus, even when we launched the optical pulse into the fast axis, the pulse suffers broadening. This is the second component (PSP rotation) of higher order PMD.

Fiber nonlinearity-induced waveform distortion

Optical fibers have nonlinear refractive index intrinsically. Due to the nonlinear refractive index, optical signal transmitted through optical fibers suffers nonlinear phase rotation depending on the input power. Temporal phase rotation induces instant frequency shift in optical signal. This additional frequency shift will interact with group velocity dispersion and polarization mode dispersion as discussed, since the shifted frequency component will suffer different group velocity. As a result, the nonlinear phase rotation will induce additional waveform distortion. Thus we need to consider fiber nonlinearity to design large capacity optical transmission systems.

The simplest case of this phase rotation is called as Self Phase Modulation (SPM), where only single channel are transmitted through optical fibers. When we transmit multiple optical signals by using wavelength division multiplexing (WDM), optical signals suffers nonlinear phase shift induced by adjacent optical signals. This is called as Cross Phase Modulation (XPM). In addition to that, in a special case where a phase matching condition meets, additional optical signals will arise. This phenomenon is called as Four Wave Mixing (FWM). These are depicted in Fig. 8-1. I will discuss a novel limiter circuit using this effect in Section 5.1.

ASE noise accumulation (SNR degradation)

Signal to noise ratio is a fundamental parameter which determines transmission capacity and distance. In typical optical receivers which employs PIN-PD and TIA, signal to noise ratio can be determined by signal current, signal shot noise, and thermal noise. Each component can be expressed by the following equations.

$$I_{signal} = \frac{e\eta}{h\nu} P_s \qquad \text{Eq. 1-2}$$

$$N_{shot} = 2e\frac{e\eta}{h\nu} P_s \qquad \text{Eq. 1-3}$$

$$N_{thermal} = \frac{4k_B T_a}{R_L} \qquad \text{Eq. 1-4}$$

By using the above formulas, signal to noise ratio of the PIN-PD and TIA type receiver can be calculated as follows,

$$SNR = \frac{4\left(\frac{e\eta}{h\nu} P_s\right)^2}{\left(\sqrt{\left(2e\frac{e\eta}{h\nu} P_s + \frac{4k_B T_a}{R_L}\right)\frac{B}{2}} + \sqrt{\frac{4k_B T_a}{R_L}\frac{B}{2}}\right)^2} \qquad \text{Eq. 1-5}$$

e : Elementary charge
η : Quantum efficiency
h : Planck constant
ν : Optical frequency

P_s: Optical power

k_B: Boltzmann constant

B: Bit rate

T_a: Temperature

R_L: Electrical resistance

In low optical received power, the receiver sensitivity is limited by thermal noise, and in high received power, main noise component is signal shot noise.

In the optically pre-amplified receiver, we can achieve high input power into PIN-PD, thus, we can overcome the thermal noise in the electrical circuit with the help of large gain of optical pre-amplifier. Signal to noise ratio of such optically pre-amplified receiver can be given by the following equation.

$$SNR = \frac{4(GP_s)^2}{\left(\sqrt{(2GP_s p_{sp} + p_{sp}^2 B_o)B_e} + \sqrt{p_{sp}^2 B_o B_e}\right)^2} \quad \text{Eq. 1-6}$$

G : Gain of optical amplifier

P_s: Optical power

B_o: Bandwidth of optical filter

B_e: Bandwidth of electrical filter

p_{sp} : Power density of amplified spontaneous emission

$$p_{sp} = n_{sp}(G-1)h\nu \quad \text{Eq. 1-7}$$

n_{sp} : Spontaneous emission coefficient

G : Gain of optical amplifier

h: Planck constant

ν : Optical frequency

The numerator expresses the power of optical signal. The first and the second term in the denominator are signal-ASE beat noise and ASE-ASE beat noise, respectively.

When we supposed sufficiently large gain of optical pre-amplifier, main noise component will be signal-ASE beat noise as shown in the equation. Therefore, the signal-ASE beat noise is the main limitation of optical reach of optical communication systems with optical amplifiers.

Contributions and Structure of the Thesis

Figure 1-8 shows main contributions of my Thesis along with the evolution of optical transport systems. Evolution of optical transport systems can be divided into three phases as shown below.

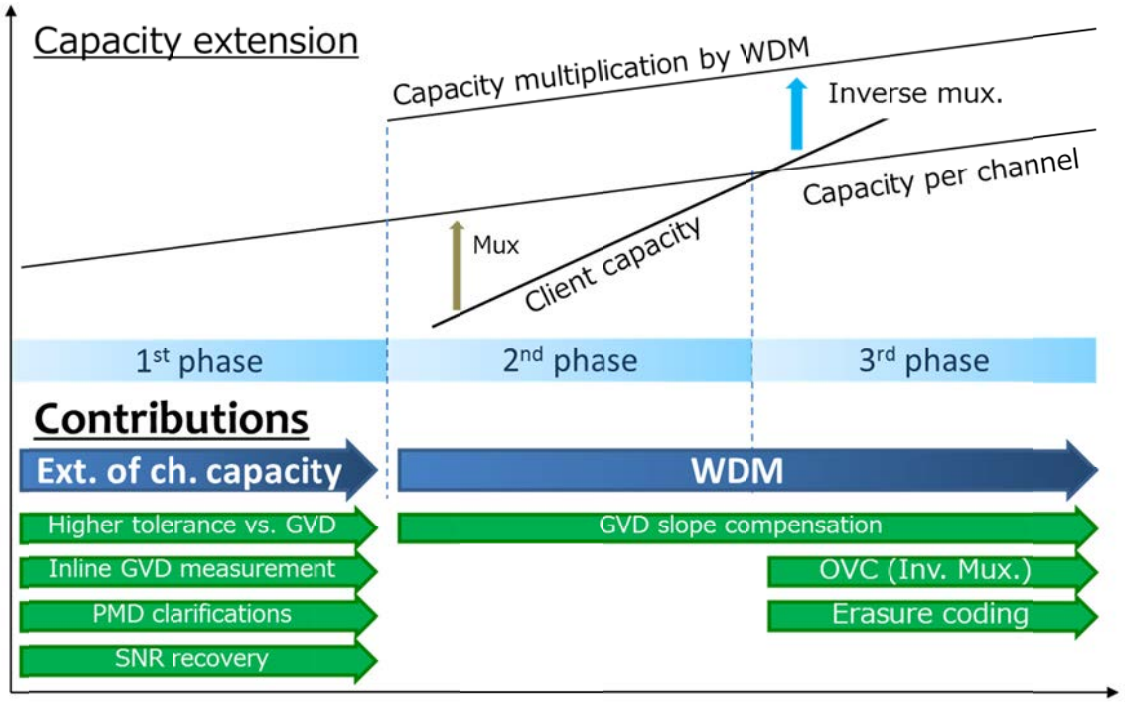

Fig. 1-8 Contributions of the Thesis

First phase of evolution is enhancement of single channel transmission speed. With the help of high speed optical devices and invention of stable laser light source together with low loss optical fibers, transmission speed of single channel expanded in this first phase. To further enhance the transmission speed, inter-symbol-interference mainly by group velocity dispersion (GVD) and polarization mode dispersion (PMD) are to be accommodated. For 10 Gbit/s/ch transmission. Simple intensity modulated and direct detection scheme can be applied with simple dispersion compensation fibers, since dispersion tolerance of this system extends over 1000 ps/nm/km. However, if we intend to extend to 40 Gbit/s/ch, dispersion tolerance will be 1/16 as schematically shown in Fig. 1-9 (a), so precise dispersion accommodation should be needed. One of the approaches is enhance dispersion tolerance of optical signal, and another is to compensate chromatic dispersion in more accuracy. Thus, I have proposed new modulation format which is discussed in section 2 where I controlled optical phase to increase inter symbol distance then realize higher tolerance as schematically shown in the left-hand side in Fig. 1-8 and 1-9 (a). Then I have proposed highly

accurate GVD measurement method which can be used in real operation as shown under the above proposal in Fig. 1-8 and 1-9 (a), which is discussed in section 3. As of PMD, we have similar circumstance with GVD at 10 Gbit/s/ch. But for 40 G bit/s/ch, there had been no guarantee of evidence of no outage from PMD as of 2004. So I have conducted a field experiment in collaboration with Deutche Telekom in Germany, to evaluate the actual impairment from PMD as schematically shown in Fig. 1-9 (b). At that time, Deutche Telekom has many high PMD installed fibers in Berlin area, and NTT has 40 Gbit/s/ch high speed transmission prototype systems. I have clarified actual power penalties resulted from PMD in installed fibers which is discussed in section 4 and confirmed statistical design against PMD as show in the bottom-left in Fig. 1-8. In addition to that, we need more SNR to realize 40 Gbit/s/ch systems, so I have proposed novel all-optical SNR recovery systems and confirmed effectiveness of this method by both numerically and experimentally as schematically shown in Fig. 1-9 (c), which is also shown in bottom-left in Fig. 1-8, which is discussed in section 5.

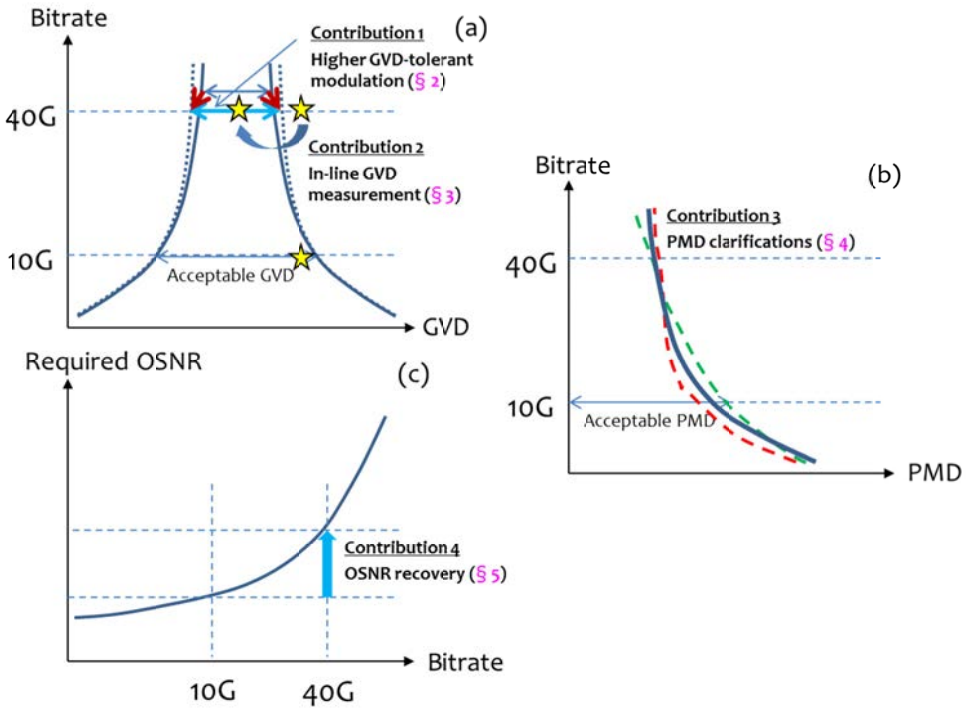

Fig. 1-9 Contributions in 1st and 2nd phases

Second phase of evolution is adoption of wavelength division multiplexing (WDM) with the help of wavelength multiplexing devices and optical fiber amplifiers as shown in the middle in Fig. 1-8. WDM multiplied transmission capacity by tens of times more than single channel approaches. However, WDM utilizes wide frequency bandwidth for transmission, so GVD variation among these WDM channels will be an issue as shown in Fig. 1-10 (a). I have proposed novel method to compensate the GVD variation by realizing GVD slope compensator which has GVD of the same value with opposite sign (where GVD has positive values, it has negative sign), which is discussed in section 6.1. With the help of the proposed techniques, all the WDM channels can be transmitted without GVD penalty as schematically shown in Fig. 1-10 (b).

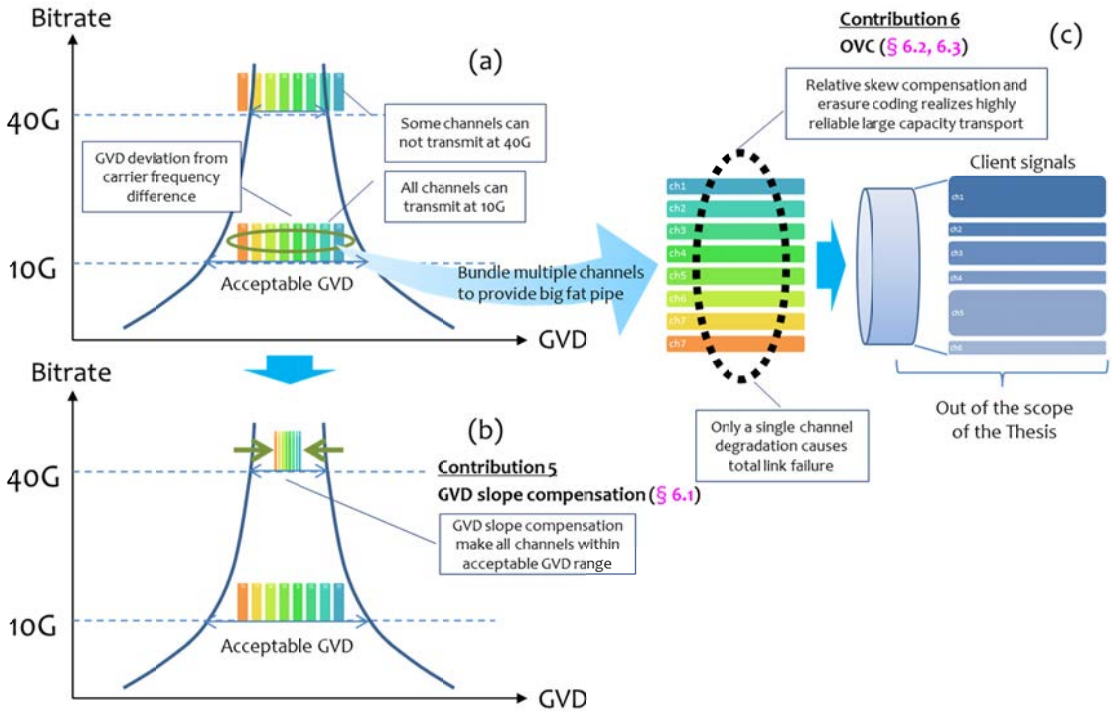

Fig. 1-10 Contributions in 3rd phase

The third phase of evolution is exceeding of client capacity beyond transmission capacity as shown in the right-hand side of Fig. 1-8. Traditionally, optical network had been serving to transport telephone services which have 64 kbit/s for each connection. So we need sophisticated aggregation mechanisms including SONET/SDH and OTN. But as high quality video and mobile data penetrate into public services, client capacity has been expanding rapidly and 100 and 400 GbE being standardized which exceed the speed of back-bone network which resides around 100 Gbit/s/ch. Therefore, we need novel mechanism which is

opposite to aggregation, something like inverse multiplexing. To meet the demands, I have proposed optical virtual concatenation (OVC) to provide big fat pipe concatenating multiple wavelengths as schematically shown in Fig. 1-10 (c), which is discussed in section 6.2, which is designated in the right-hand side of Fig. 8. When we rely on multiple wavelength to provide big fat pipe, we will suffer increased failure rate resulted from increase of number of devices and equipment consisting of the total system as schematically shown in Fig. 1-10 (c). So I have invented a novel mechanism that can realize higher robustness or resiliency with minimum number of redundant devices which is discussed in section 6.3. The advantage of the method will increase with increased number of parallel connections, so it will play an important role in the third phase of evolution.

In my Thesis, I used the term "impairment mitigation" in the broad sense of the term. In section 4, I used the term to recover errors caused by PMD by using FEC. In the latter section 6.3, I used the term to recover failures of a channel in multiple channels such as WDM channels by using FEC. So I define and use the term "impairment mitigation" to cover both use cases discussed here. In both cases, "impairment mitigation" realizes large capacity optical transmission.

In line with the above discussion, I have constructed my Thesis as the following structure.

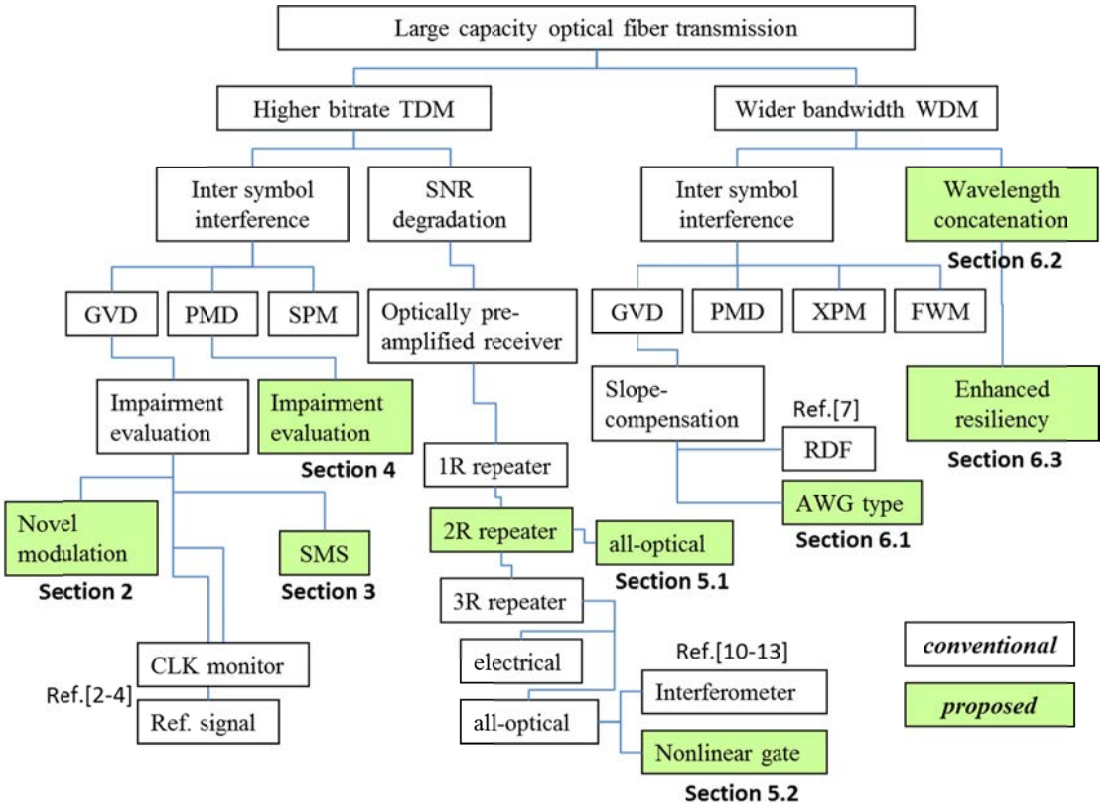

Fig. 1-11 Structure of the Thesis

The structure of this Thesis is provided in Fig. 1-11. As I have discussed in the preceding sections, toward optical transport with more capacity and longer reach, we need to overcome impairments in optical fiber transmission. The main issues involve GVD and PMD of optical fibers. So far, various approaches have been proposed aiming to mitigate GVD [2-4]. However, these methods require the use of dithering in order to detect signs of chromatic dispersion, because the clock level is almost symmetrical around zero dispersion. Also, one of them requires an additional reference signal for phase comparison, and it is essential to have bit-phase stabilization between the optical signals at the transmitter side.

Toward GVD mitigation, we have mainly two approaches including achieving optical modulation techniques with more tolerance against GVD and inventing measurement and compensation techniques of GVD to cancel the impairment induced.

To increase tolerance against GVD, I have proposed novel return-to-zero (RZ) based modulation techniques [5], which is discussed in the Section 2 in this Thesis. I have examined GVD tolerance by changing the relative optical phase and revealed that higher tolerance against GVD of 25 ps/nm at 80 Gbit/s in the out-of-the phase condition, where relative phase difference between adjacent time-slot is π. The achieve tolerance was 1.7 times larger than the conventional format where relative phase difference is 0.

Then I have proposed novel spectral manipulation techniques to measure the GVD value with its sign and sufficient accuracy based on the novel modulation scheme discussed in the Section 3 [6]. Various reports have proposed GVD measurement techniques [2-4]. However these methods cannot be applied to in-line applications, where we can measure the GVD value in real-time without disturbing transport services. Also detection of sign of GVD has been a remaining issue. The method of monitoring clock power can be applied to in-service applications, but it suffers some accuracy issue and cannot detect sign of GVD. The method I proposed can be applied to in-service applications and can detect sign and GVD value with sufficient accuracy. I have actually implemented this method with the modulation format I have proposed and confirmed sufficient sensitivity of 0.16 ps/nm/mV in the comparator output voltage. I have discussed this method in the Section 3 in this Thesis.

Another important and essential obstacle to realize high speed and long reach optical transmission should be PMD. So far, we have limited information and knowledge on PMD in the viewpoint of impairment in optical transmission. Especially we are lacking of experimental value of PMD-related impairments including the first and second-order PMD in the field environment. Thus I have conducted field experiment to evaluate such impairment in actual deployed environment in Deutsch Telekom in Germany [7]. In the field trial I have evaluated precise impairment induced by 1^{st} and 2^{nd}-order PMD, tolerance of novel modulation formats and FEC performance against PMD for the first time as of Aug. 2004. Then I have confirmed good agreement of 2^{nd} order PMD component between the measured and theoretical estimation, higher and comparable tolerance of RZ-based format against 1^{st} and 2^{nd} order PMD, respectively and effective performance of FEC in the field environment. These results are discussed in the Section 4 in this Thesis.

As I discussed in the preceding section, in the optically pre-amplified receivers, signal-ASE beat noise is a dominant noise source. Usually, such SNR degradation can be mitigated by electrical 3R regenerator as discussed above. However such 3R regenerators are expensive and consume much electrical power. Therefore, all-optical and/or opt-electrical approaches

have some potential to realize cost-effective and green (power-efficient) repeaters. Some reports discussed all-optical approaches to regenerate optical signals [8-11], but they suffer complicated configuration to operate. Most of those proposals rely on nonlinearity resulted from interferometric effect of Lightwave. Intrinsically, optical interferometer is sensitive to optical phase, therefore, it suffers severe instability that comes from optical phase deviation by vibration, tension, temperature change and so on. In contrast to these approaches, I have examined a simple approach including a method utilizing fiber four wave mixing (FWM) and achieved successful suppression of signal-ASE beat noise [12, 13]. I have explained those evaluations in the Section 5.1 in this Thesis. This approach is based on 2R function which includes reshaping and regeneration.

As the next step, I have proposed all-optical 3R regenerator based on nonlinear optical gate [14]. It has re-timing function in addition to the 2R repeaters. Again, this approach does not rely on interferometric nonlinearity discussed above, but rather utilize nonlinear transmittance of optical gate. Thus I can achieve compact and stable implementation. When I applied nonlinear optical gate, probability density function (PDF) of output signal would be somewhat different from Gaussian shape. I have estimated such PDF profile and revealed that I can get quasi Gaussian shape after optical amplification. Thus I have found that I can apply usual treatment of SNR calculation even in the case where I utilize nonlinear optical gate for the first time as of 1999. These discussions have been provided in the Section 5.2 in this Thesis.

To expand the transmission capacity, we need to use wider optical bandwidth such as wavelength division multiplexing (WDM) where we multiplex optical signals in wavelength domain. For WDM transmission, ITU-T standardized frequency grid for wavelength assignment of each optical signal. In typical case, we multiplex about tens of channels on 100 GHz grid, for example. In such application, total frequency bandwidth extends to over 1 THz or around 10 nm. Optical fibers have deviation of GVD depending on the wavelength, namely, dispersion slope. Typical value of such slope is around 0.07 ps/nm^2/km. When we suppose that we transmit WDM signal which has 10 nm of bandwidth and 100 km of fiber length, we expect about 70 ps/nm of GVD deviation between shortest and longest wavelength channels. Such deviation could be additional impairment on optical signal. As for the standard single mode fibers, some special fibers have been fabricated and tested [15]. However, there had been no means to compensate such deviation for dispersion shifted fibers, so far. I have proposed novel dispersion slope compensator fabricated on planar light wave circuits (PLC) and confirmed successful mitigation of such impairment

experimentally [16]. I have realized 25-nm bandwidth dispersion slope compensator which has -7.1 ps/nm^2 of dispersion slope that can compensate the dispersion slope of 100 km of DSF. I have described this approach in the Section 6.1 in this Thesis.

To further upgrade transmission capacity, we need parallel transport of multiple optical wavelengths, since single channel capacity is approaching its theoretical limit [17]. One of the obstacles to be overcome is compensation of dispersion slope as discussed above for Section 6.1. Traditionally, each WDM channel is independent and carries traffic from different client or applications. However, high-end applications (such as large visualization) are expected to push traffic exceeding a single channel capacity. Thus, some wavelength concatenation technique will be essential for such purpose. I have proposed such scheme for parallel transport [18]. Then I have implemented the proposed scheme with de-skewing circuit that compensate latency deviations among multiple parallel channels and demonstrated the total function withlarge capacity applications which will be expected in the near future. The high-end large capacity applications can be accommodated and transported seamlessly in real-time as discussed in Section 6.2.

Then I have extended the approach to support programmable resiliency [19]. As we increase the number of wavelength channels, the total number of components that consist of transport systems will also expand. Thus failure rate of total transmission systems will increase accordingly. To avoid this issue, I have proposed novel transmission architecture that supports programmable resiliency and achieves higher robustness (lower failure rate) with minimum resource. In addition to that, at the beginning of 21st century, aging society and low birthrate have been becoming inevitable issue where we are gradually suffering lacking of labor power. So the next generation transport system should meet such issues. The proposed architecture can realize enhanced resiliency or robustness against failures with minimized additional expense. This will help to reduce track-roll for maintenance operation for network. These approaches are discussed in Section 6.3 in this Thesis.

The main concerns, proposals, and results discussed in this Thesis are summarized in the following table.

Tab. 1-2 Abstracts of each section

Section 2	Purpose	To realize higher bitrate Time-Division-Multiplexing (TDM) transmission
	Issue	Mitigation (in-service measurement and compensation) of Inter symbol interference (ISI) of group velocity dispersion (GVD)
	Proposal	Novel optical modulation format by precise manipulation of optical phase
	Achievement	Maximum GVD tolerance of 25 ps for 80 Gbit/s Return-to-Zero (RZ) optical signal is achieved in out-of-phase condition. The achieve tolerance was 1.7 times larger than the conventional format where relative phase difference is 0.
Section 3	Purpose	To realize higher bitrate Time-Division-Multiplexing (TDM) transmission
	Issue	Mitigation (in-service measurement and compensation) of Inter symbol interference (ISI) of group velocity dispersion (GVD)
	Proposal	New GVD measurement method based on spectral structure of optical signal.
	Achievement	GVD measurement method which can both determine and evaluate the sign of dispersion and the value, respectively, is confirmed by both numerical estimation and experiment. Sufficient sensitivity of 0.16 ps/nm/mV was achieved in the comparator output voltage
Section 4	Purpose	To realize higher bitrate Time-Division-Multiplexing (TDM) transmission
	Issue	Mitigation (in-service measurement and compensation) of Inter symbol interference (ISI) of polarization mode dispersion (PMD)
	Proposal	Experimental verification of PMD-induced impairments in actual field environment.
	Achievement	Good agreement of 2^{nd} order PMD component between the measured and theoretical estimation, higher and

		comparable tolerance of RZ-based format against 1st and 2nd order PMD, respectively and effective performance of FEC in the field environment
Section 5	Purpose	To realize higher bitrate Time-Division-Multiplexing (TDM) transmission
	Issue	Recovery of SNR degradation by Signal (S) -Amplified Spontaneous Emission (ASE) beat noise
	Proposal	Fiber Four-Wave-Mixing (FWM) type optical limiter with enhanced nonlinear response and all-optical 3R (Reshaping, retiming, and regenerating) regenerator using ultra high speed optical gate with nonlinear response
	Achievement	More than 2 dB suppression of S-ASE beat noise by the proposed FWM type optical limiter Successful all-optical regeneration and SNR recovery of up to 5 dB by the propose 3R regenerator by experimental evaluation Generated precise model for nonlinear optical gate and evaluated the regeneration performance quantitatively
Section 6	Purpose	To realize wider bandwidth Wavelength-Division-Multiplexing (WDM) transmission
	Issue	Mitigation of chromatic dispersion slope (GVD deviation over wide wavelength range) Consolidation mechanism of plural WDM channels to accommodate large capacity client traffic Reliability enhancement with minimum resource against disasters
	Proposal	Space-time conversion type dispersion slope compensator for L-band transmission in G.653 fibers Optical virtual concatenation (OVC) concept and demonstration in global field environment Novel transmission architecture to realize higher reliability with minimum network resource
	Achievement	Successful compensation of dispersion slope of G.653 fibers through 25 nm bandwidth in L-band and transmission over 100 km of optical fibers

		Successful demonstration of dual channel concatenation in global field environment and presentation to academic and industrial community in real-time demo Achieved programmable resiliency with minimized network resource via erasure-encoding over plural optical channels

2. Optical phase and GVD tolerance

Optical-Time-Division Multiplexing (OTDM) with optical phase control

The OTDM technique is one attractive means for upgrading channel speed to achieve a level in excess of 40-Gbit/s [20-22]. Some issues still remain to be solved, however, if high-speed OTDM systems are to be successfully developed. One of these is chromatic dispersion of the transmission fibers, which limits network scale and interferes with network stability and robustness. To increase dispersion tolerance, it will be necessary to minimize the spectral bandwidth. To achieve this, it is essential to optimize the optical phase difference and duty ratio of optical pulses. One means to achieve this is through optical phase control, which is an effective technique for reducing spectral bandwidth. The adoption of the phase inversion technique into optical duo-binary code has achieved bandwidth one-half that of conventional NRZ code [22]. Another effective way of reducing bandwidth is controlling the duty ratio of signal pulses. An OTDM coder with optical phase control has been previously reported [23], but its duty ratio was neither variable nor optimized.

In this work, I did the first-ever research as of 2002 on power penalty as a function of duty ratio and the relative optical phase difference between two optical signals optically time-division-multiplexed at a channel speed of 80-Gbit/s. In this section, I show that the dispersion tolerance of multiplexed signals depends on the relative optical phase difference for a duty ratio above 0.5. By optimizing duty ratio and optical phase control, I obtained high dispersion tolerance for the out-of-phase conditions where the relative optical phase difference and duty ratio were π and 0.5, respectively. Under these conditions, the central carrier component in the optical spectrum was suppressed by optical phase inversion between adjacent time slots. Furthermore, I was able to achieve a wide dispersion tolerance of 25 ps/nm for an 80-Gbit/s optical signal by fabricating a monolithic 80-Gbit/s OTDM transmitter [5].

Numerical estimation of optical phase dependency

To estimate the dispersion tolerance of carrier-suppressed return-to-zero (CS-RZ) format based on OTDM technique, I numerically calculated the dispersion tolerance in a 2-to-1 (40 x 2) type 80-Gbit/s OTDM for three duty ratios, as shown in Fig. 2-1.

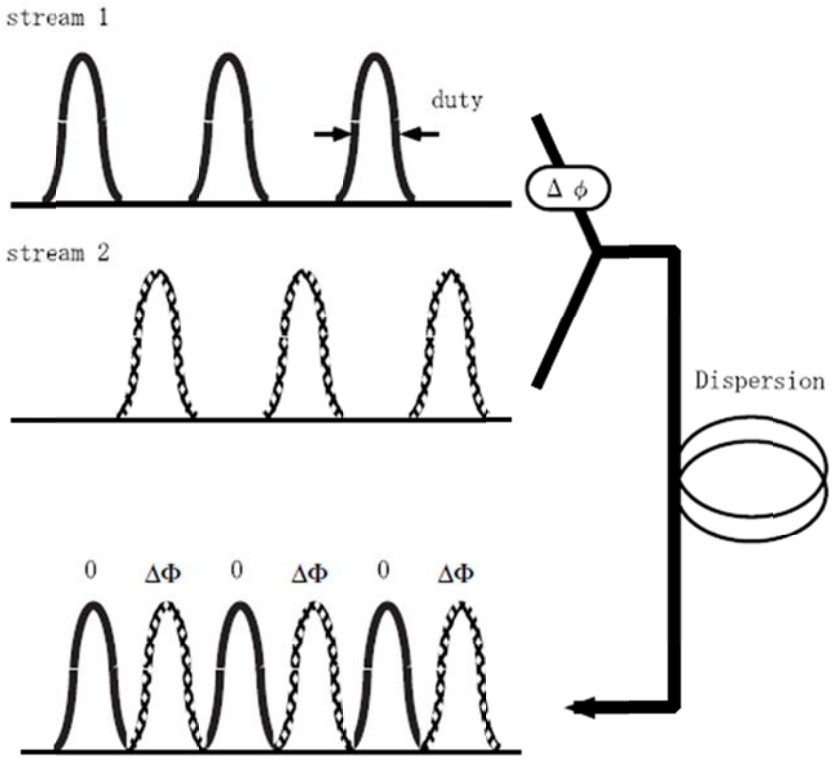

Fig. 2-1 Numerically estimated the dispersion tolerance

I multiplexed two 40-Gbit/s pulse-streams of a Gaussian shape. Two 40-GHz pulse streams were individually encoded by a seventh-stage pseudo random binary sequence (PRBS). One 40-Gbit/s pulse-stream was shifted by a quarter of the total length of PRBS to suppress pattern dependence. The multiplexing delay between these streams was set to half the time-slot (12.5 ps) to obtain an ideal 80-Gbit/s optical pulse stream. I evaluated dispersion tolerance by using two key parameters: the duty ratio of the optical pulse and the relative optical phase difference between two neighboring pulses. The multiplexing phase difference was set to 0 (in-phase), π /2 (middle-phase), and π (out-of-phase).

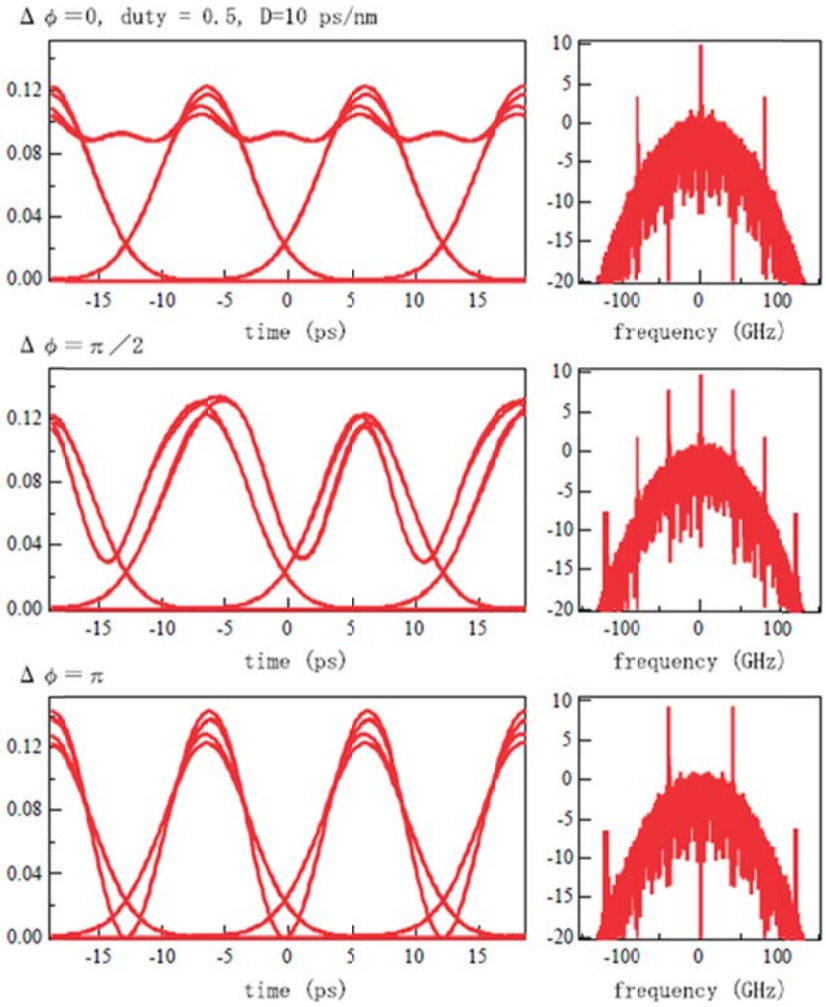

Fig. 2-2 Simulated eye diagrams

Simulated eye diagrams at 10 ps/nm of chromatic dispersion are shown in Fig. 2-2 with the corresponding optical spectrum. In the in-phase condition, inter-symbol-interference (ISI) was additive at the intermediate point between adjacent time slots, thus, severely distorting the eye diagram. On the other hand, in the out-of-phase condition, the ISI was destructive at the middle point between the time slots. Therefore, the electrical field intensity at the point becomes null and the ISI was effectively suppressed. The suppression of ISI will also be effective to reduce nonlinearity-induced waveform distortion.

From the viewpoint of an optical spectrum, NRZ code has a simple double side-banded spectrum and thus has 2B bandwidth (B: bit rate). In contrast, conventional RZ code (in-phase condition) that mainly consists of three line components in its optical spectrum

has 4B bandwidth, and CS-RZ code that needs only two line components has 3B bandwidth. Therefore, dispersion tolerance of CS-RZ code can be expected to expand more than conventional RZ code, and eye diagram distortion will be diminished.

I found 40-GHz oscillation in the middle-phase condition. When optical pulses are broadened by chromatic dispersion, the electrical field in the intermediate region between neighboring pulses will be superposed in $\pi/2$ phase-difference in the middle-phase condition, and the optical phase in the superposed region will shift from its original position. Consequently, the optical pulses can be looked upon as alternately chirped pulses. The resultant chirp is expected to induce intensity modulation by chromatic dispersion [24]

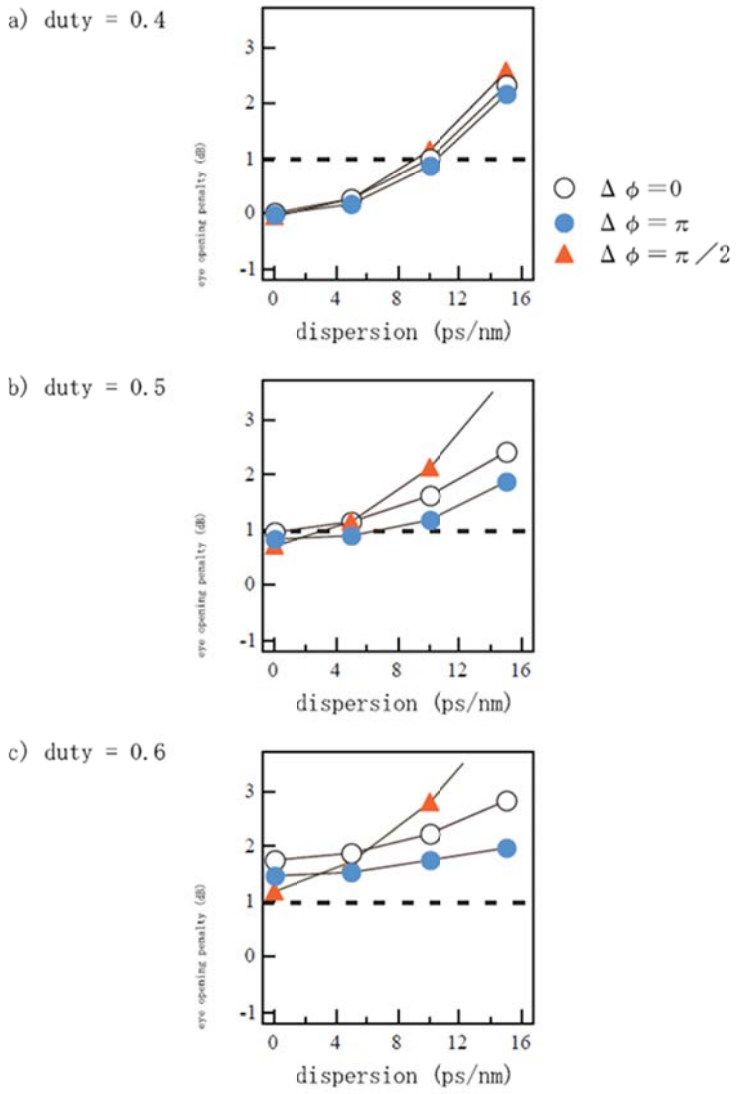

Fig. 2-3 Simulated dispersion tolerance

Figure 2-3 shows simulated dispersion tolerance for three phase conditions: in-phase, out-of-phase, and middle-phase, where relative optical phase difference were equal to zero, π, and half of π, respectively. The top, middle, and bottom are the tolerances in duty ratios of 0.4, 0.5, and 0.6, respectively. In the calculations, I set the chirp parameter to zero. Therefore, the tolerance is symmetrical in the sign of the dispersion.

For a duty ratio of 0.4, the dispersion tolerance was as small as 10-ps/nm at an eye opening penalty of 1 dB, and no significant phase dependence was observed. I obtained almost the same performance in all three phase conditions. As I increased the duty ratio, the dispersion tolerance improved and the phase dependence increased. For a duty ratio of 0.5, I obtained a tolerance of 16-ps/nm in the out-of-phase condition. The power penalty at zero dispersion was less than 1 dB relative to the value obtained for a duty ratio of 0.4. There was a significant degradation of the tolerance in the middle-phase condition. For a duty ratio of 0.6, the tolerance increased further. But power penalty also increased and exceeded 1 dB at zero dispersion. Therefore, I adopted a duty ratio of 0.5 for the experimental investigation.

For a small duty ratio of 0.4, there is little phase dependence was found, but for a duty ratio of 0.6, the phase dependence became clear. I also found the out-of-phase condition achieved the best dispersion tolerance performance.

80-Gbit/s OTDM transmitter

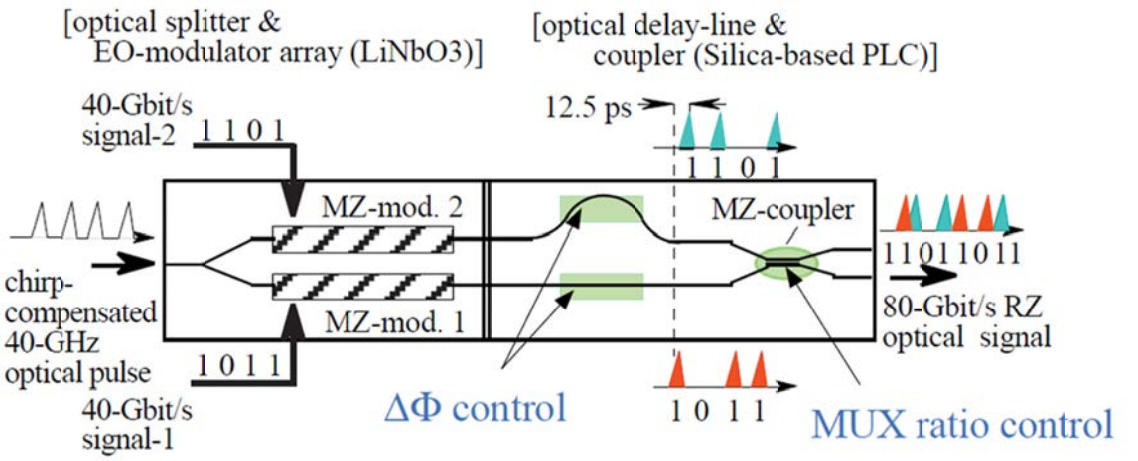

Fig. 2-4 Configuration of 80-Gbit/s OTDM CS-RZ transmitter

Figure 2-4 shows the configuration of novel 80-Gbit/s OTDM CS-RZ transmitter. The transmitter consists of two low driving voltage Lithium Niobate (LN) 40-Gbit/s

Mach-Zehnder modulators [25] and a planar-lightwave-circuit (PLC) optical multiplexer with a phase and amplitude controller. The half wavelength voltage and the extinction ratio of the LN modulators are 3.4-V and more than 19-dB, respectively. A 40-GHz repetition pulse stream generated by a chirp-compensated semiconductor mode-locked laser diode (MLLD) monolithically integrated with an electro-absorption (EA) modulator [26] was externally supplied. The pulse width was tuned by changing the bias voltage of the EA modulator. I set the pulse width at 6.5-ps at full-width at half-maximum (FWHM), for which the duty ratio was 0.5. The center wavelength was 1551.6-nm. Encoded signals were split and fed into two LN Mach-Zehnder intensity modulators, then individually encoded by a 40-Gbit/s electrical signal that was multiplexed by InP HEMT MUX ICs [27]. One of the encoded signals was delayed by a time slot (12.5-ps), and multiplexed into an 80-Gbit/s signal. I was able to control the relative phase difference of the multiplexing signal by using the phase shifter on the PLC. The final MZ coupler adjusted the multiplexing ratio and minimized the pulse height fluctuation.

Experimental setup for evaluation

I conducted an experiment to evaluate the dispersion tolerance dependence on the relative phase difference. The eye diagram of an 80-Gbit/s signals generated by the OTDM transmitter was measured with an optical sampling oscilloscope having a temporal resolution of 0.9-ps [28]. The measured eye diagram is shown in Fig. 2-5.

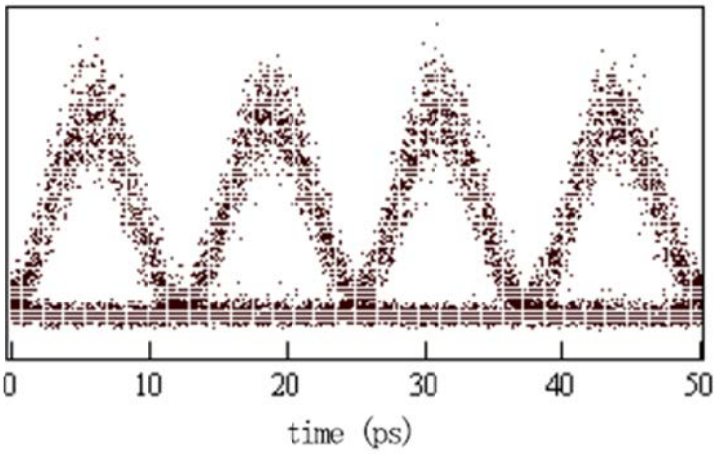

Fig. 2-5 Measured eye diagram

I obtained the same eye diagram for all three phase conditions, meaning that in the duty ratio of 0.5 that I adopted, ISI between adjacent time slots was negligible at chromatic dispersion of 0-ps/nm. The optical signal was then launched into dispersive fibers and received. A block diagram of the optical receiver employed in the investigation is shown in Fig. 2-6.

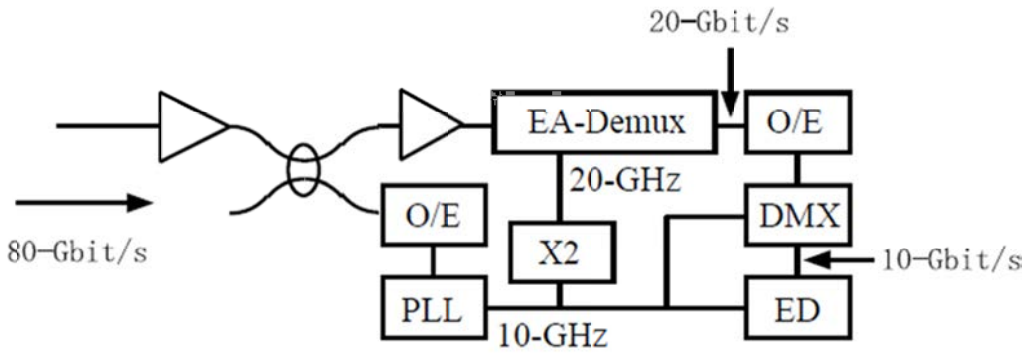

Fig. 2-6 Block diagram of the optical receiver

The received optical signals were amplified, divided and sent to an optical demultiplexer that used an EA modulator for optical gating and a timing extraction circuit. Each optically demultiplexed 20-Gbit/s signal was detected by a photo diode (PD) and electrically demultiplexed into eight 10-Gbit/s signals. I measured error rates for all eight individual 10-Gbit/s channels and chose the one with an 80-Gbit/s error rate as the worst one.

Results

I measured the 80-Gbit/s eye diagrams and corresponding optical spectrum at the chromatic dispersion of 10-ps/nm and back-to-back using an optical sampling oscilloscope for the three optical phase conditions shown in Fig. 2-7.

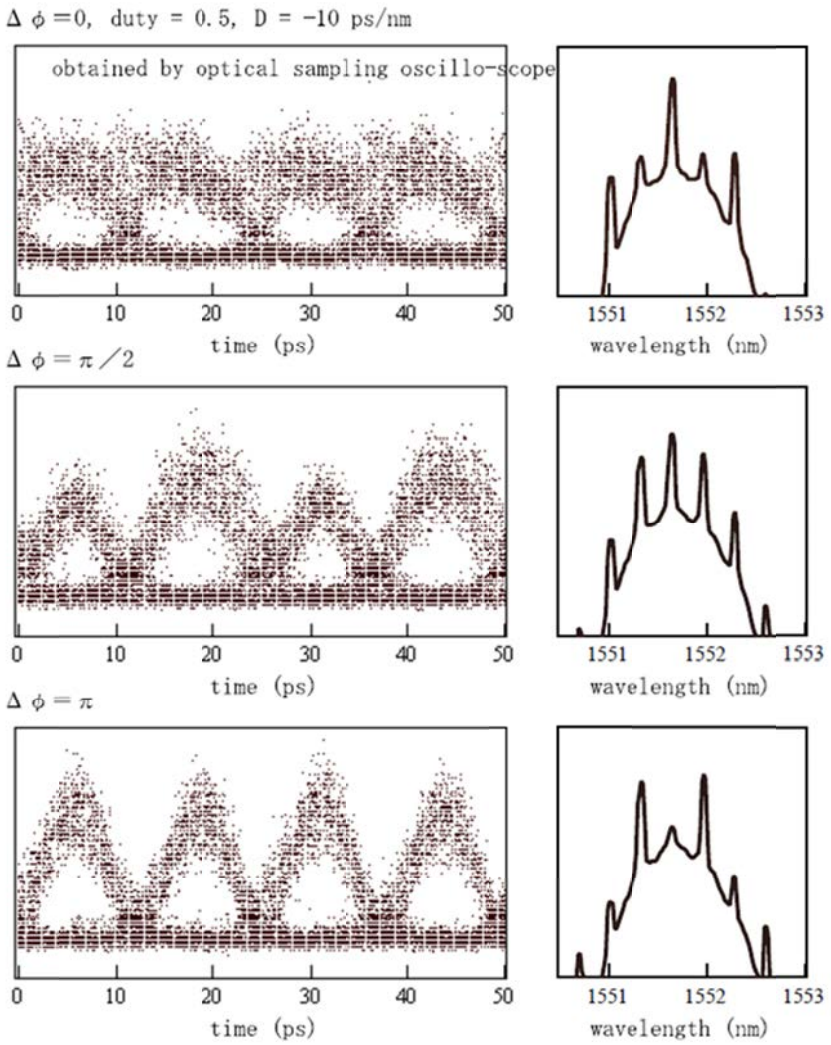

Fig. 2-7 Eye diagrams and corresponding optical spectrum

For the in-phase condition, I obtained a distorted eye diagram similar to the diagram obtained in the numerical simulations. As in the simulations, 40-GHz amplitude fluctuation was observed in the middle-phase condition. The optical spectrum was also consistent with that obtained by simulation. I obtained a clear eye opening for the out-of-phase condition as predicted in the simulation. In the optical spectrum, the central carrier component was effectively suppressed. The residual 40-GHz spaced component might have been caused by a slight imbalance between either the two MZ modulators or the two driving electrical waveforms.

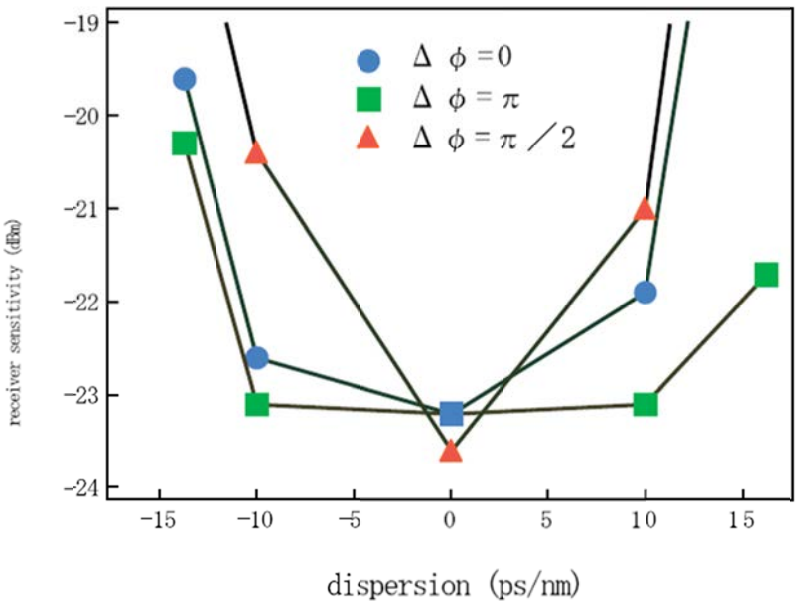

Fig. 2-8 Measured dispersion tolerance

The measured dispersion tolerance is shown in Fig. 2-8. The receiver sensitivity was plotted against chromatic dispersion for the three optical phase conditions. A wide dispersion tolerance of 25-ps/nm at 1-dB of receiver sensitivity degradation was achieved for the out-of-phase condition. For the middle-phase condition, the tolerance was severely decreased. The decrease resulted from the 40-GHz amplitude fluctuation, which was observed in both the numerical simulations and the experiments. The slight asymmetry in measured dispersion tolerance can be attributed to residual frequency chirp that may have been caused by a slight imbalance between the two driving electrical signals supplied to the two MZ modulators.

DSF transmission experiment

I conducted a DSF transmission experiment to confirm the wide dispersion tolerance of the out-of-phase condition (CS-RZ). With the exception of dispersive fibers, which were substituted for by a 60-km DSF, the experimental setup for the transmission was the same as that used for the dispersion tolerance evaluation. Measured bit error rates are shown in Fig. 2-9.

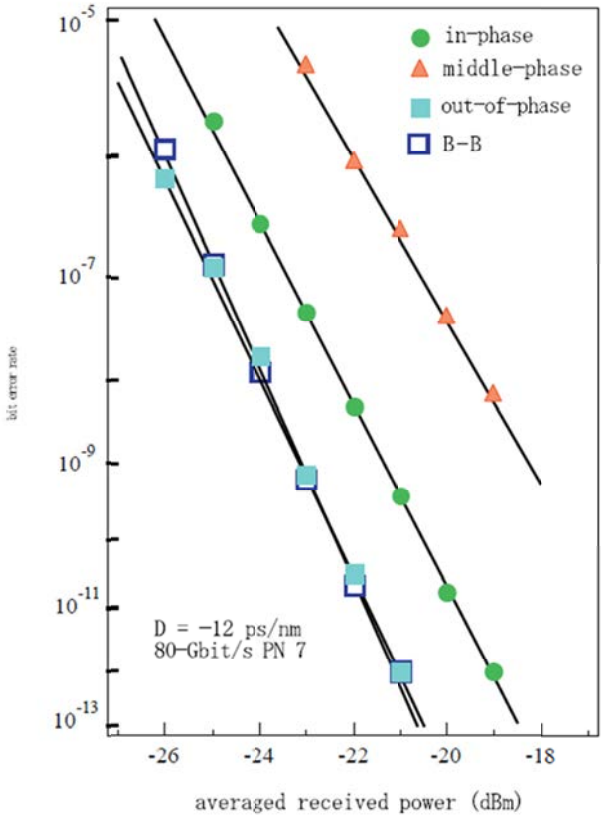

Fig. 2-9 Measured bit error rates

The residual dispersion was 12-ps/nm. No receiver sensitivity degradation was observed in the out-of-phase condition; thus, no dispersion-compensating component was needed. But there was a significant penalty for the middle-phase condition.

These experimental results I obtained confirm the superior tolerance of the out-of-phase condition (CS-RZ format).

Discussion

Dispersion tolerance has an inverse square dependence versus the bit rate. The reported tolerance for 40-Gbit/s non-return-to-zero (NRZ) systems is about 95-ps/nm [29]. Therefore, a tolerance of 25-ps/nm is wide for an 80-Gbit/s return-to-zero (RZ) system. This is comparable to the value of 1700-ps/nm obtained for a 10-Gbit/s RZ system using baseband differential code [30] where the ISI from the adjacent mark bit was suppressed. Since my proposed technique only reduced the ISI from the adjacent time slot, I can deduce that the ISI from two or more time slots would be negligible.

I found that a large penalty appears in the middle-phase condition. In short, the dispersion tolerance strongly depended on the relative phase at a duty ratio of 0.5. This shows that stabilizing the transmitter is essential for developing a reliable OTDM system. This requirement could only be identified with the very stable OTDM system that I fabricated.

Section summary

In this section, I have investigated the dispersion tolerance of 80-Gbit/s OTDM signals as a function of duty ratio and multiplexing optical phase difference. By fabricating and using a stable LN-PLC integrated OTDM transmitter with a channel speed of 80-Gbit/s, I experimentally achieved a wide dispersion tolerance of 25-ps/nm in the out-of-phase condition at a duty ratio of 0.5 for the first time as of Feb. 2002. I also demonstrated dispersion-compensation-free 80-Gbit/s 60-km DSF linear transmission and confirmed the superior tolerance of the out-of-phase condition (CS-RZ format) for 80-Gbit/s OTDM signals.

Up to the time of this work, optical transmission systems have used on/off keying only, in commercial systems. This work opened new horizon of phase-shift keying in optical communication systems to reduce symbol rate and overcome ISI from group velocity dispersion and polarization mode dispersion. The proposed signal format has three symbol points without degradation of inter symbol distance, so symbol rate was decreased by 2/3 and improved tolerance against above impairments. After this invention, one more symbol was added and implemented for 40 Gbit/s commercial systems. Thus, this work pioneered phase shift keying in optical transmission systems and bridged to current multi-level, multi-phase shift keying modulation techniques.

3. Spectral Mode Splitting

Background

Technologies enabling 40-Gbit/s/ch WDM network applications have been extensively studied for various application areas, such as very-short-reach (VSR), metropolitan, and long-haul transmission. For VSR applications, the main interest of technologies is how to achieve lower costs. Accordingly, preference is given to simple modulation formats such as non-return-to-zero (NRZ).

On the other hand, in metropolitan or long-haul applications, it is critical to accommodate several impairments resulting from transmission fibers. These include group-velocity-dispersion (GVD), polarization-mode-dispersion (PMD), nonlinear effects such as self-phase-modulation (SPM), cross-phase-modulation (XPM), and four-wave-mixing (FWM), as well as their interaction with each other. To mitigate these impairments resulting from GVD and fiber-nonlinearity, it is necessary to study transmission performance, which clearly depends on the modulation formats used. In this respect, RZ and several RZ-related formats have notable advantages against fiber-nonlinearity [31-34]. In these RZ-type formats, carrier-suppressed (CS) RZ and duo-binary-carrier-suppressed (DCS) RZ [5, 35] have many advantages resulting from their intrinsic spectral structure.

In this section, I will describe and address the superior two-mode spectral characteristics that enabled novel detection schemes; including one called "mode-splitting detection". Then I will propose the latter detection scheme and its outstanding features, including expansion of chromatic dispersion tolerance [36] and automatic dispersion compensation [37] that can detect signs of chromatic dispersion without using a dithering technique.

Spectral redundancy in carrier-suppressed RZ formats

Generation method and spectral structure of CS-RZ and its related RZ formats [5, 35] are summarized in Fig. 3-1. These spectra are measured at the carrier wavelength of 1552.52 nm for three RZ formats.

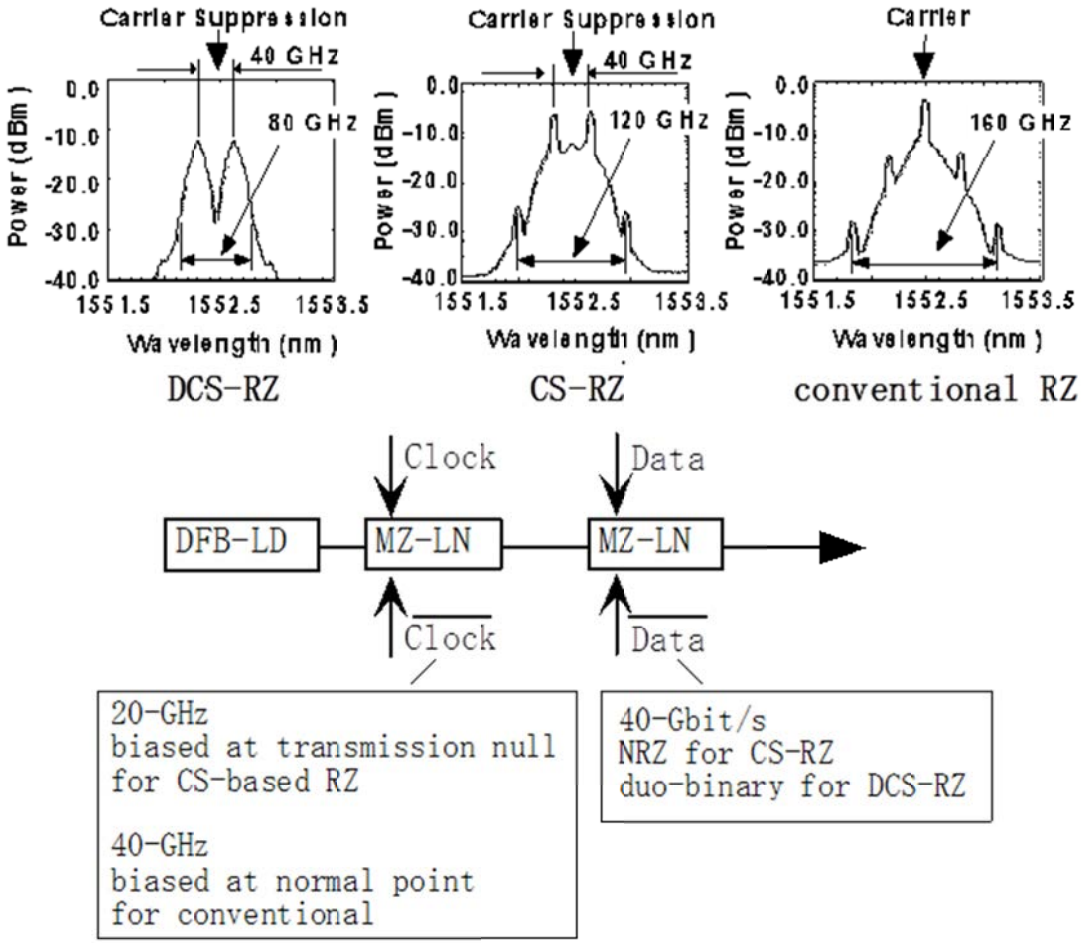

Fig. 3-1 Optical spectrum comparison

To generate conventional RZ format, the conventional in-phase clock pulse signal generated by the 1st Mach-Zehnder intensity modulator is intensity-modulated by the NRZ signal in the 2nd modulator. The word "in-phase" means that there is no phase inversion between adjacent time-slot in the optical signal. Thus, carrier and double side band components appear in the modulation spectra. The modulation bandwidth defined as full-width at -20 dB is approximately 160 GHz, and corresponds to 4B (B = 40 GHz), where B is line rate frequency.

For the CS-RZ format generation, two-mode beat clock pulse signals generated by the 1st modulator bias at the transmission null point and driven by half clock (20-GHz) are intensity-modulated by the NRZ data signal in the 2nd modulator. The word "two-mode beat clock" means that the RZ clock pulse is generated by coherent beat between two mode-locked line components. The two-mode beat clock signals can also be generated by a semi-conductor mode-locked laser-diode [38]. Since each longitudinal mode is modulated

by the NRZ format, the modulation bandwidth is reduced to 120 GHz, which corresponds to 3B (120 GHz). The bandwidth reduction is realized by the fact that we need only two modes to generate RZ pulse in CS-RZ. On the other hand, we need at least three modes for RZ pulse generation without phase inversion. The alternation in phase reversal realizes the carrier-suppressed spectral feature.

In the DCS-RZ format, the two mode beat clock pulse is intensity and is phase modulated by the duo-binary data format. The three-level electrical duo-binary signal was prepared by 5th order Bessel-Thomson low-pass filter of B/4 bandwidth. Since each longitudinal mode of the two mode beat clock pulse is intensity and phase modulated by the duo-binary data format, the modulation bandwidth becomes 80 GHz, which corresponds to 2B (80 GHz). The carrier component is completely suppressed in the format, because of its narrow modulation bandwidth in the duo-binary data format. The modulation bandwidth of the DCS-RZ format is the narrowest as modulated without any optical filters among all reported RZ formats to my knowledge as of 2002. The bandwidth is comparable to the NRZ format and is quite appropriate to high spectrally efficient DWDM transmission applications.

CS-RZ and DCS-RZ signals have two individual longitudinal modes in their optical spectrum as shown in Fig. 3-1. The two individual modes have identical information. In the case of the 40-Gbit/s CS-RZ format, the optical spectrum consists of two 40-Gbit/s NRZ spectral components. The frequency separation between these components corresponds to the bit rate frequency that is B (40-GHz). The separation frequency is determined by 2 x (modulation frequency) applied to the MZ modulator in its generation. Since the NRZ format has 2B bandwidth (80 GHz), the two NRZ spectral components superpose each other in the central carrier frequency region. Therefore, the central carrier component is suppressed, but does not vanish.

Accordingly, the DCS-RZ format consists of two identical optical duo-binary spectral components. The frequency separation is also B, but optical duo-binary signals have the modulation bandwidth of B. Thus, the two duo-binary spectral components are not superposed in the central carrier frequency region, and the carrier component vanishes.
I showed with experimental evaluation, for the first time to the best of my knowledge as of 2002, that we can divide these modes by using spectral mode-splitters and can extract two constituent data signals individually [36]. By the spectral mode-splitting of CS-RZ format, optical waveform will change to NRZ format. In the same way, waveform of DCS-RZ format will change to optical duo-binary. The mode-splitting detection scheme that I have proposed is completely different from the detection schemes where we need to regenerate optical carrier to recover waveforms, such as for single-sideband (SSB) signal without optical carrier component. In my detection scheme, I can recover NRZ waveform by simple

direct-detection scheme and need no optical phase information. The fundamental difference between these detection schemes is that the split NRZ signal has optical carrier component and we do not have to regenerate it to recover waveform. The mode-splitting technique brings about various advantageous applications, such as the expansion of dispersion tolerance, automatic dispersion compensation [37], and bit error rate (BER) improvement [39].

Expansion of dispersion tolerance by spectral mode splitting

A GVD accommodation of transmission fibers is one of the key issues for achieving a 40-Gbit/s/ch transmission system. An optical duo-binary format [40] expands GVD tolerance, because of its narrow spectral width. However, fiber nonlinearity-induced impairments such as self-phase modulation (SPM) and cross-phase modulation (XPM) limit the transmission capacity and distance. In terms of accommodating these impairments, RZ-shaped transmission formats have a number of advantages over NRZ-shaped formats, including optical duo-binary ones. However, RZ pulses have a relatively broad spectral width in comparison with optical duo-binary or NRZ formats, and thus have smaller dispersion tolerance. Namely, I find a trade-off between dispersion tolerance and allowance for fiber nonlinearity. Thus, a transmission scheme that can achieve both wide dispersion tolerance and sufficient allowance for fiber nonlinearity-induced waveform distortion is desirable.

One attractive application of the mode-splitting detection scheme is for DCS-RZ [36]. The transmission format in this scheme is DCS-RZ, whereas the detection format is optical duo-binary that is converted from the DCS-RZ format by mode-splitting in the receiver. Dispersion tolerance is strongly dependent on a spectral bandwidth at the detector. Since the spectral bandwidth at the detection was reduced by mode-splitting, we can expect expansion of dispersion tolerance.

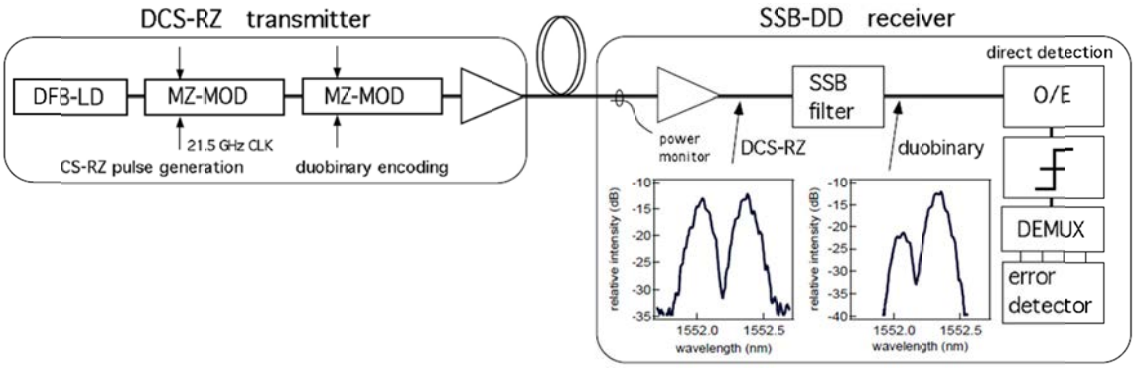

Fig. 3-2 Proposed transmission scheme

The proposed receiver configuration and its experimental setup are shown in Fig. 3-2. The experimentally obtained eye-diagrams and spectra are also shown as insets of the figure. The first push-pull Mach-Zehnder modulator [25] driven by a 21.5-GHz sinusoidal clock generated carrier-suppressed RZ pulses. The second modulator biased at transmission null point encoded the pulses into a 43-Gbit/s DCS-RZ format. The driving three-level electrical duo-binary signal was prepared by InP HFET ICs [27] with 5th order Bessel-Thomson low-pass filter of B/4 bandwidth. The generated DCS-RZ signal transits the optical fiber, and is detected by the mode-splitting receiver. To avoid fiber nonlinearity, I set the fiber launched optical power to -5 dBm. I can select each optical duo-binary spectral component of the DCS-RZ signal by narrow band-pass filtering. A typical optical spectrum before and after mode-splitting is shown in the figure. The shape of the filter that has 0.35-nm of half-width at -20 dB of maximum can be modeled as a 1.6th-order super Gaussian filter. I employed low-dispersion flat-top AWG filter for mode-splitting which has less than 5 ps/nm of group velocity dispersion. The cross talk from the neighboring spectral component was measured as less than -10 dB. Figure 2 shows the measured eye diagrams with and without a mode-splitting filter, and I obtained NRZ-like diagrams with the mode-splitting filter. The small oscillation observed at the "mark" level can result from optical coherent interference from an adjacent residual spectral component that should be filtered out. The back-to-back receiver sensitivity with and without mode-splitting filter was -20.6 dBm and -24.3 dBm, respectively. The 3.7-dB penalty of receiver sensitivity can be resulted not from mode-splitting detection scheme itself, but from insufficient receiver configuration optimization, such as base-band bandwidth of the receiver [41].

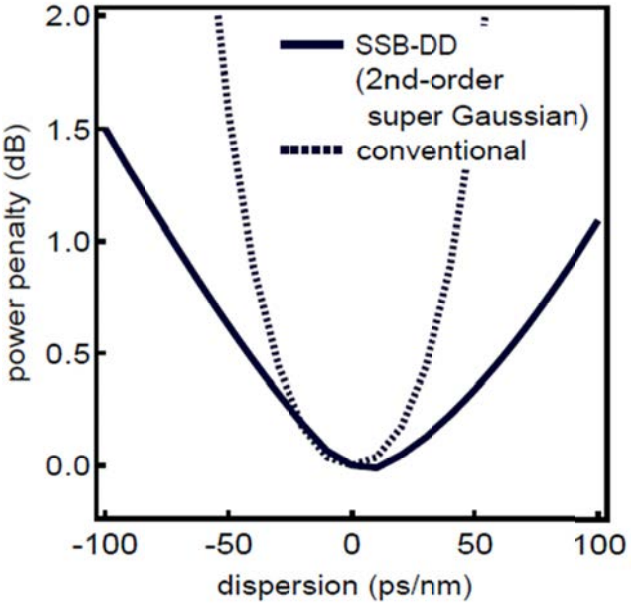

Fig. 3-3 Simulated dispersion tolerance

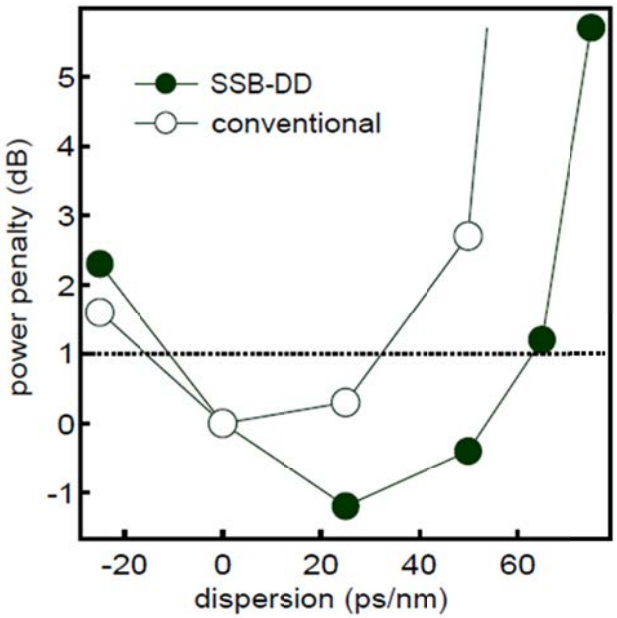

Fig. 3-4 Measured dispersion tolerance for DCS-RZ

Figures 3-3 and 3-4 show simulated and measured dispersion tolerance with and without a mode-splitting filter. By using a 2nd-order super Gaussian filter, I can double the dispersion tolerance in the simulation. In the numerical simulation, the optimum chromatic dispersion slightly moved toward the positive dispersion region when I selected the low

frequency component (longer wavelength component). When I selected the counterpart in the split two modes in the optical spectrum, optimum shift direction inverted. Since I have generated chirp-less DCS-RZ signals in my simulation, I can deduce that the optimum shift did not result from frequency chirp, and instead could have originated from insufficient mode-splitting of the DCS-RZ signal.

The dispersion tolerance defined at 1-dB power-penalty was 75 ps/nm for 43-Gbit/s signal with the mode-splitting filter, which was 1.6 times wider than the value without the mode-splitting filter in my experiment. To generate DCS-RZ signals, I adopted push-pull modulation to realize chirp-less modulation both in duo-binary encoding and CS-pulse generation. Thus, the observed shift of optimum chromatic dispersion can result from mode-splitting of DCS-RZ signals, as I pointed out in the numerical simulation.

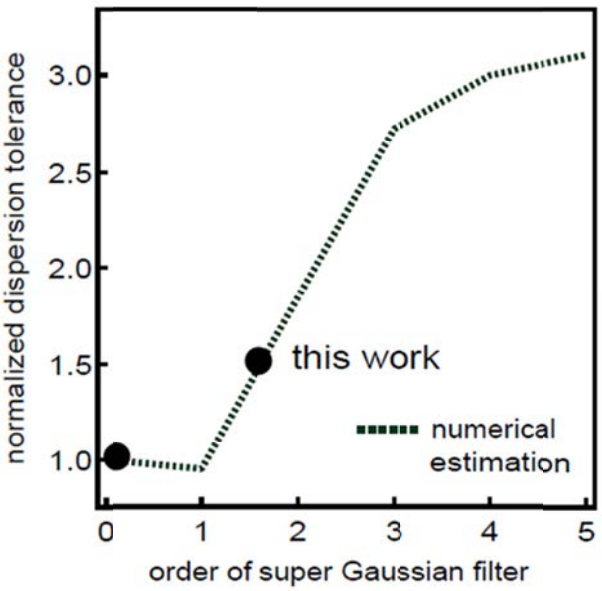

Fig. 3-5 Dispersion tolerance normalized by the value without SSB-filtering

Figure 3-5 shows the normalized dispersion tolerance defined at 1-dB eye-opening penalty I have achieved in my numerical simulation by changing the shape of the mode-splitting filter. I also plotted my result of the experiments in the figure, supposing that eye-opening penalty approximately corresponded to power-penalty. The normalization factor was the dispersion tolerance without a mode-splitting filter. As the figure shows, excellent consistency between numerical and experimental results was obtained. The normalized dispersion tolerance enlarged as I increased the order of the super Gaussian mode-splitting optical filer, finally reaching three times the original value. Thus, I can expect that using

steeper filters will produce more drastic expansion of the dispersion tolerance. The split signal from DCS-RZ signal has similar spectrum with optical duo-binary. In principle, I can expect four time enhancement of dispersion tolerance. The limitation of three time enhancement I have obtained in my estimation can be resulted from residual spectral component from neighboring mode.

I next conducted a 43-Gbit/s 100-km DSF transmission experiment to demonstrate the effect of dispersion tolerance expansion and its tolerance against fiber nonlinearity. The fiber launched optical power was set at +10 dBm, and the residual chromatic dispersion was set at +70 ps/nm.

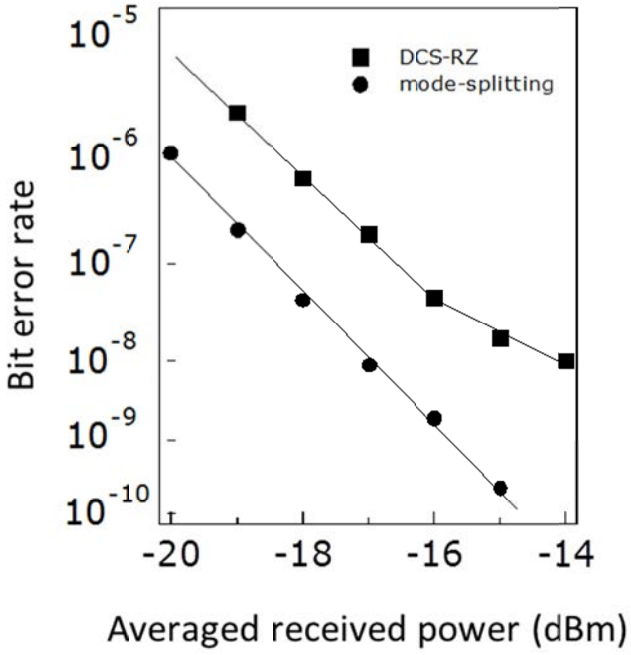

Fig. 3-6 Bit error rate performances with and without a mode-splitting filter

Figure 3-6 shows the bit error rate performance with and without a mode-splitting filter. The dispersion induced power penalty was clearly reduced by using the mode-splitting filter even in a high-power (+10 dBm) transmission. Thus, the proposed mode-splitting detection scheme realizes both high fiber-nonlinearity tolerance that is inherent to RZ pulse transmission and wide dispersion tolerance at the receiver. The mode-splitting scheme can be applied to a wide variety of transmission formats that have multiple modes in their optical spectra such as CS-RZ and DCS-RZ.

Automatic dispersion compensation by spectral mode splitting

Automatic chromatic dispersion deviation resulting from changes in ambient temperature or changes in fiber length due to fiber repairs is an important issue to accommodate for implementing 40-Gbit/s/ch WDM networks and operating them in a stable manner. A number of automatic dispersion equalization techniques have heretofore been reported. These include a zero dispersion detection technique based on clock level monitoring [2, 3] that requires the use of dithering in order to detect signs of chromatic dispersion, because the clock level is almost symmetrical around zero dispersion. Another proposed scheme is one of automatic dispersion equalization using spacing-fixed WDM signals to monitor relative phase shift [4]. This scheme, however, requires an additional reference signal for phase comparison, and it is essential to have bit-phase stabilization between the optical signals at the transmitter side.

Mode-splitting detection can be applied to CS-RZ signals, and it achieves a highly accurate automatic dispersion compensation scheme that can detect any sign of GVD without any dithering operation. Each CS-RZ signal consists of two identical NRZ signals superposed coherently with frequency separation that corresponds to the bit rate as pointed out in Fig. 3-7. Therefore, I can divide a CS-RZ signal into two identical NRZ signals (USB and LSB components) by spectral mode-splitting.

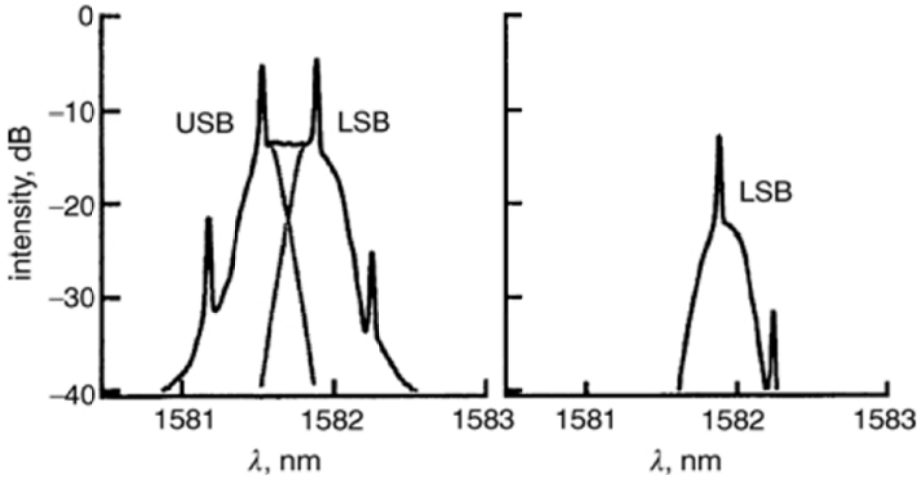

Fig. 3-7 Optical spectrum structure of CS-RZ signal

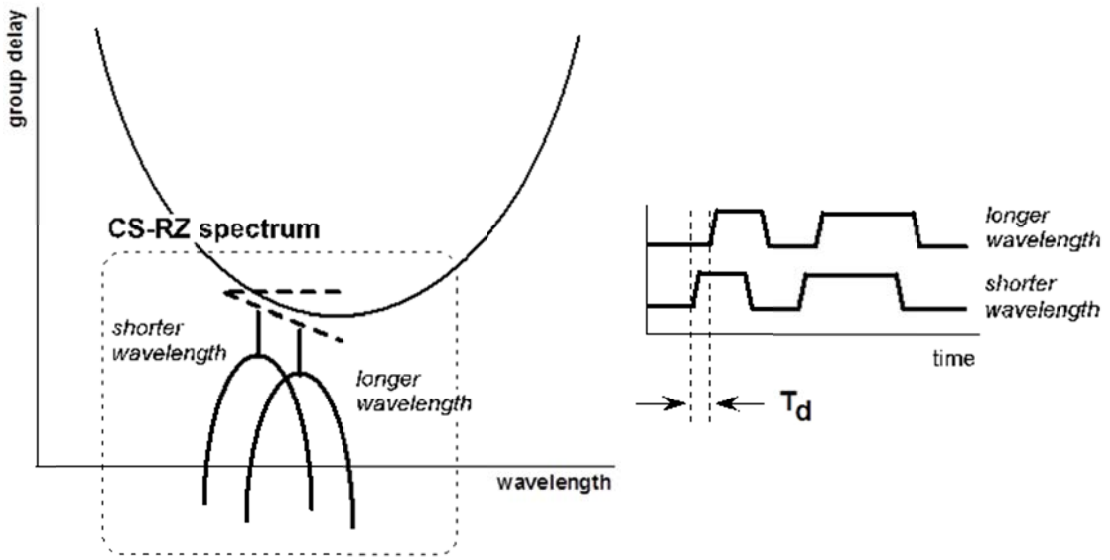

Fig. 3-8 Conceptual mechanism of dispersion detection

Figure 3-8 shows the conceptual mechanism of my dispersion compensation scheme [37]. Since GVD in transmission fibers generates group delay in accordance with signal wavelength, the two constituent longitudinal modes incur different group delay levels depending on their wavelengths. Thus, I can measure the chromatic dispersion by comparing the two constituent longitudinal modes. Assuming that D, T_d, $F_{carrier}$, $F_{separation}$, and c are chromatic dispersion, relative bit-phase shift induced by group delay of optical fibers, optical carrier frequency, frequency separation of two modes to be split, and speed of light, respectively, I can derive D as the following simple equation,

$$D = -\frac{T_d F_{carrier}^2}{cF_{separation}} \qquad \text{Eq. 3-1}$$

In this proposed scheme, I can detect signs of GVD by measuring the direction of relative bit-phase shift induced by group delay of optical fibers as shown in Fig. 3-9.

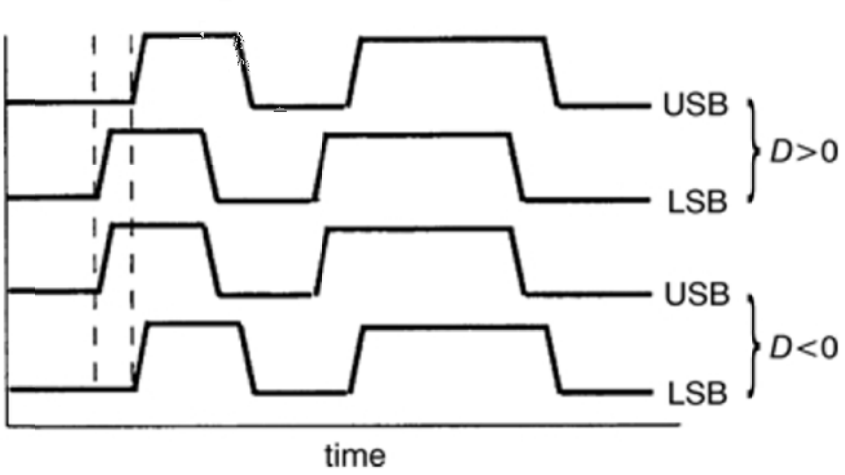

Fig. 3-9 Mechanisms to detect the sign of GVD

I conducted a transmission experiment to evaluate the newly proposed dispersion compensation scheme; the experimental setup is shown in Fig. 3-10.

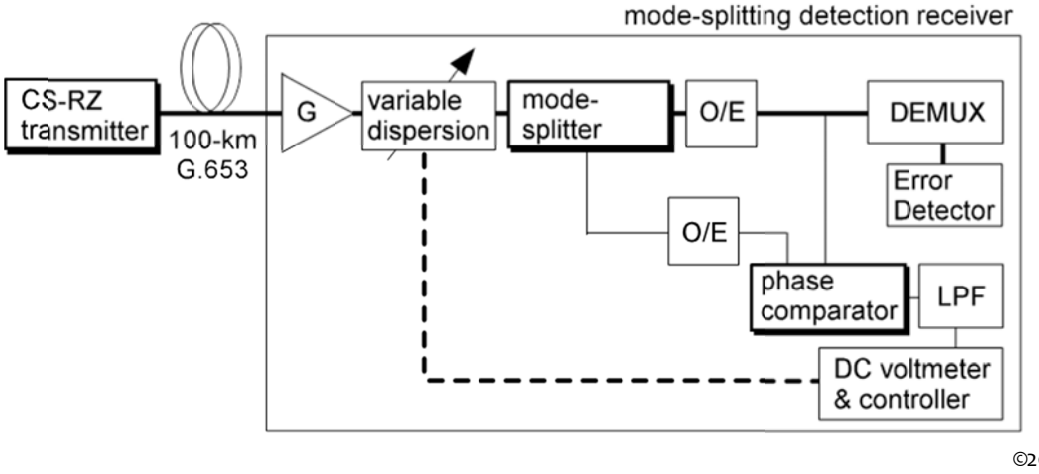

Fig. 3-10 Experimental setup for evaluation

A 43-Gbit/s CS-RZ signal encoded with a 23rd order PRBS was launched into a 100-km DSF. The wavelength used was the 1582.018 nm that was in the L-band of the DSF. The transmitted signal was divided into two NRZ spectral components that were detected individually, and the two divided signals were tapped and inputted to a 43-Gbit/s comparator circuit comprising InP-based HEMT ICs [42]. The measured eye diagrams and optical spectra obtained before and after the mode-splitter are shown in Fig. 3-11.

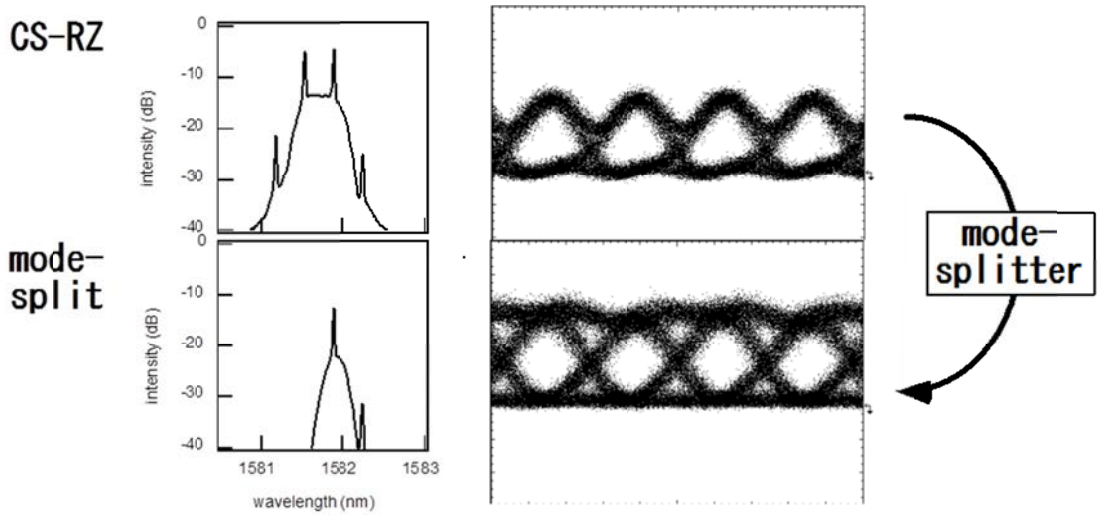

Fig. 3-11 Measured eye diagrams and optical spectra

For the first time to my knowledge as of 2002, the CS-RZ waveform was successfully converted into its constituent NRZ components that showed a clear eye opening by mode-splitting [37]. The relative phase difference between these two NRZ signals was converted into DC voltage by a comparator circuit and a low-pass-filter (LPF). I measured the DC voltage by using a conventional voltmeter.

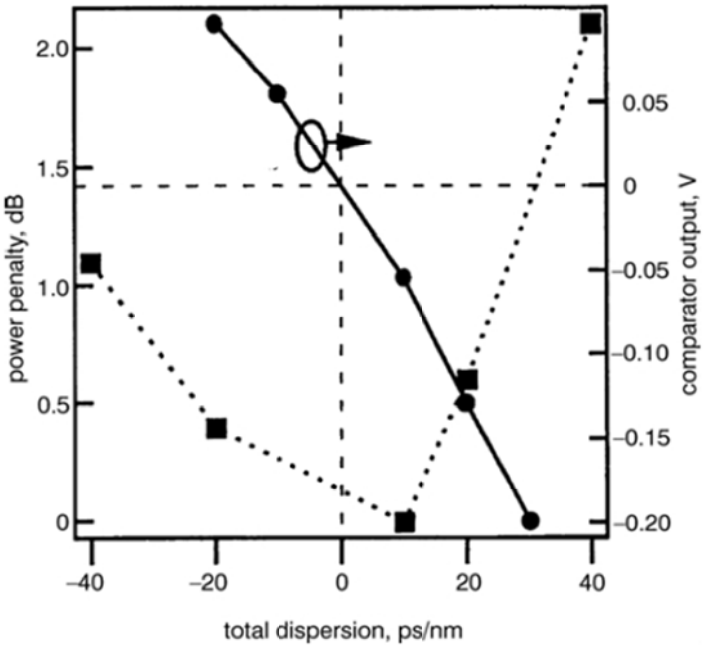

Fig. 3-12 Measured dispersion tolerance

I also evaluated the dispersion tolerance after 100-km DSF transmission. The split 43-Gbit/s electrical signal was de-multiplexed into four 10.7-Gbit/s signals by InP-based HEMT DEMUX ICs [27]. The receiver sensitivity for all four 10.7-Gbit/s signals was evaluated and I adopted the worst one. The measured dispersion tolerance after 100-km DSF transmission and corresponding comparator output DC voltage after LPF are shown in Fig. 3-12. The sign and its value of GVD were clearly measured as the comparator output voltage. The sensitivity of 0.16 ps/nm/mV was high enough to detect dispersion induced power penalty as shown in the figure. I also achieved 65 ps/nm of dispersion tolerance, which was wider than that of conventional CS-RZ signal. Similarly, the proposed GVD detection scheme can be applied to DCS-RZ signal in the same configuration.

Discussion

The proposed dispersion compensation scheme successfully detected signs of chromatic dispersion with its GVD value without any dithering in signal wavelength or dispersion value of dispersion compensation fibers (DCF). In my proposed scheme, data transmission and dispersion compensation work simultaneously, meaning that the scheme can be applied to adaptive dispersion equalization using a variable dispersion compensator without any additional reference signal. Furthermore, since relative bit phases between the constituent longitudinal modes are strictly fixed at the transmitter side, I need no stabilization mechanism in the transmitter.

The maximum dispersion range that the proposed GVD measurement method can cover is determined by an approximate 0.5 time-slot of the relative bit phase difference induced by GVD. Therefore, the maximum dispersion range was about 40-ps/nm of the chromatic dispersion that will give rise to 12.5-ps of relative bit shift. Provided that the dispersion exceeds the maximum value, the comparator output will degrade and not maintain sufficient accuracy. To extend the measuring range, I can use tone signals modulated on each longitudinal mode and extract tone components at the receiver side. One term period of a 1-GHz tone signal is 1000-ps. Thus, I can expect a 40 times wider measurable chromatic dispersion range [43].

The mode-splitting scheme can be applied to a wide variety of transmission formats including NRZ. For optical signals that contain multiple longitudinal modes, I can simply split each longitudinal mode. Even for a single mode signal such as an NRZ signal, I can split it by using the vestigial side band (VSB) filtering technique [44]. In VSB filtering, I can use two optical frequency signals at two optimum filter displacement points for phase comparison and so on.

One advanced application of the proposed mode-splitting technique is in a frequency

diversity detection receiver (F-DDR) [39]. Since two constituent longitudinal modes have slightly different optical frequencies, these two components will have independent noise levels through amplified transmission in optical fiber. Thus, I can deduce that these two frequency components have different error statistics, depending on their optical frequency. Accordingly, I can expect error correction independent from forward error correction (FEC) code based on the independent error statistics. Along this line, the combination of mode-splitting and "consensus" logic gate realized total 9-dB gain (3-dB for F-DDR and 6-dB for FEC) with forward error correction (FEC).

Section summary

I have proposed a novel mode-splitting detection scheme of CS-RZ and DCS-RZ transmission formats and its applications. In my numerical simulation and experimental investigations, I confirmed that CS-RZ and DCS-RZ signals could be converted into two NRZ and duo-binary signals, respectively. The mode-splitting detection can be realized by a redundancy in the optical spectrum of these transmission formats, resulting in the achievement of expanded dispersion tolerance, automatic GVD compensation, and BER improvement in a novel frequency diversity detection receiver.

I achieved 1.6 times expansion of dispersion tolerance of 43-Gbit/s DCS-RZ signals by introducing the mode-splitting detection in the receiver. The enhancement of dispersion tolerance was quantified by numerical simulation as a function of sharpness of the mode-splitting filter. In my numerical investigation, threefold expansion of GVD tolerance could be expected in a 3rd order super Gaussian-shaped mode-splitter. I also realized precise chromatic dispersion measurement with its sign detection without any dithering operation and demonstrated its application to automatic dispersion compensation in 43-Gbit/s CS-RZ transmission by employing the mode-splitting detection receiver for CS-RZ signals. I experimentally confirmed that the scheme had high enough sensitivity to compensate for the GVD-induced power penalty in 43-Gbit/s CS-RZ signal transmission.

Spectral mode splitting which I have proposed is based on spectral mode orthogonality. We can split spectral components which is orthogonal to each other. In my work, I have used this characteristic to detect the sign and magnitude of group velocity dispersion. Thus they are redundant and can be used for multiplexing. The basic understanding of spectral mode orthogonality has been used for further upgrade of wavelength multiplexing, such as optical orthogonal frequency division multiplexing (O-OFDM) toward realizing more capacity.

As for group velocity dispersion accommodation, cutting edge digital coherent transmission systems implemented automatic dispersion detection mechanism, which is

based on the work in this section for automatic compensation by digital coherent signal processor. In actual implementation, such spectral splitting is realized in digital circuits after analogue to digital (A/D) conversion.

4. PMD-impairment evaluation

The need for PMD mitigation

Polarization Mode Dispersion (PMD) is one of the key issues to be accommodated for implementation of 43-Gbit/s/ch or over optical transport systems in Optical Transport Network (OTN) [45-47]. In recent years, a number of reports considering various kinds of PMD compensators, or comparison in modulation formats [48, 49] were presented. Many previous reports have discussed based on Differential Group Delay (DGD, 1st-order PMD) only or including higher-order by using PMD emulators or numerical simulations. To the best of my knowledge, there is no report on PMD tolerance of 43-Gbit/s/ch CS-RZ in actual field fiber in combination with ITU-T standard FEC Reed-Solomon (RS) (255,239) [45].

In this section, I evaluated PMD tolerance of CS-RZ [31] in comparison with conventional NRZ signal against all-order PMD in buried fiber cables in DT(Deutsche Telekom)'s field for the first time as of Aug. 2004 at the data rate of 43-Gbit/s and got wider tolerance for CS-RZ. Furthermore, I evaluate tolerance against higher-order PMD in Principal State of Polarization (PSP) transmission. I achieved significant expansion of PMD tolerance and almost the same performance for CS-RZ and NRZ. Furthermore, I confirmed the impact of standard (RS) (255,239) FEC against all-order PMD.

Field trial configurations

Figure 4-1 shows experimental setup of the field trial. The transmitter in our Optical Transport Network (OTN) system generates both 43-Gbit/s CS-RZ and NRZ signals. The OTN system can accommodate four 10-Gbit/s tributaries and can generate OTU3 signal introducing the RS (255,239) FEC in its frame. I controlled input state of polarization by inserting the polarization controller. To exclude undesirable penalties except for PMD, I adopted 7.5 dBm of launched optical power to avoid both fiber nonlinearity effect- and SNR degradation-induced penalty. Chromatic dispersion was also completely compensated by using variable chromatic dispersion compensator to an accuracy of less than 5 ps/nm.

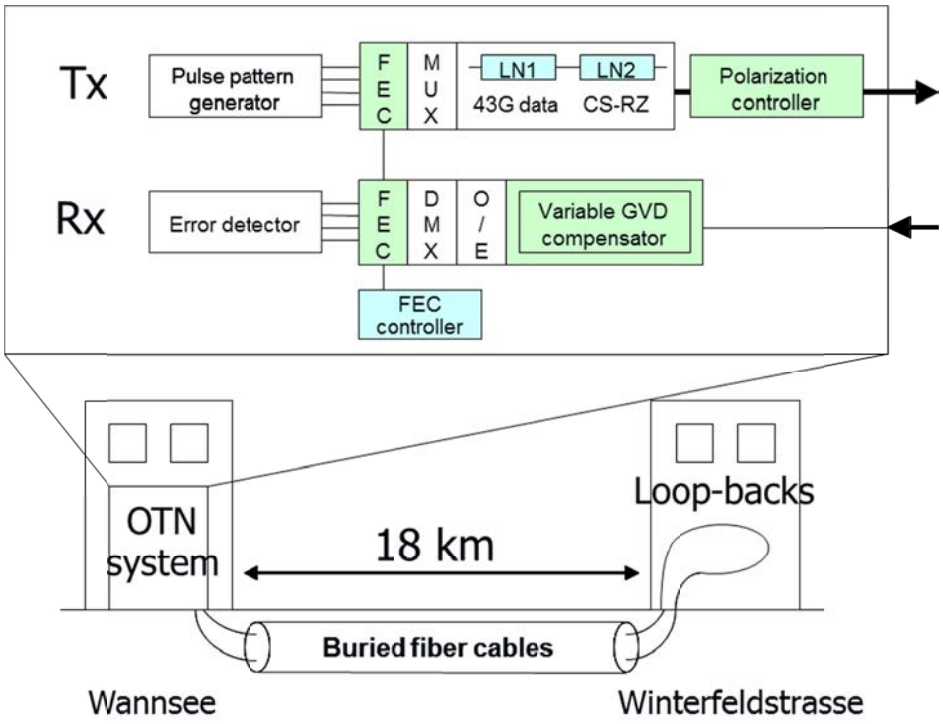

Fig. 4-1 Experimental setup for the field trial

We prepared 9 fiber pairs installed in downtown Berlin which had different DGD values ranged from about 1 to 20 ps. CS-RZ and NRZ has about 1 nm spectral bandwidth, so I evaluated PMD values at 1 nm of bandwidth centered at the signal wavelength of 1592.1 nm. These values had changed about 10% in a day and were consistent with previous reports [46, 50]. Typical time period to complete a power penalty measurement will be less than half an hour. Thus, I can measure transmission performance at a static PMD value as a snapshot of PMD variation. Furthermore, I measured 2^{nd}-order PMD for each fiber spans by U-parameter method. Fig. 4-2 shows measured total 2^{nd}-order components for each fiber spans. The solid line designates 2^{nd}-order component which was theoretically estimated by the following equation: $2^{nd}\text{-order} = DGD^2/3^{0.5}$[51], assuming that the fiber length is long with respect to the mean coupling length. They showed good agreement and I can deduce that these fiber spans would meet the above assumption. The condition is no strict one-to-one functional relation but only an expression for the statistical mean of the correlation of 1^{st}- and 2^{nd}-order PMD.

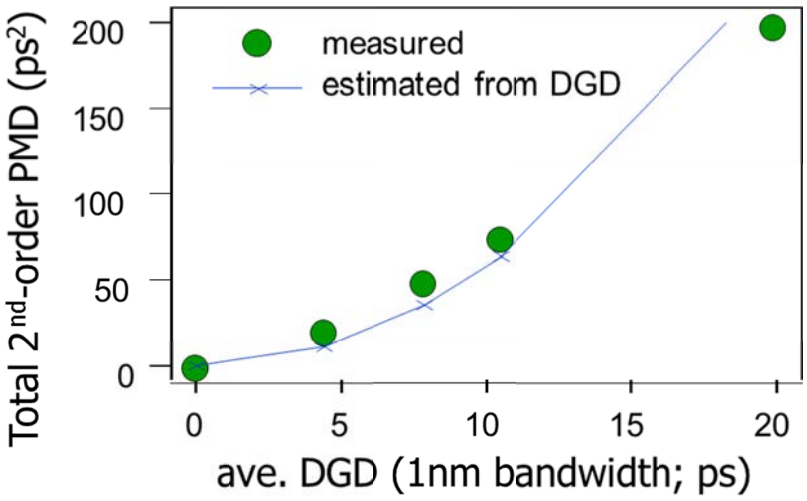

Fig. 4-2 Measured total 2nd-order components for each fiber spans

Tolerance against all-order and 2nd-order PMD

Figure 4-3 shows measured power penalties. The horizontal axis shows 1st-order PMD component in the buried fibers.

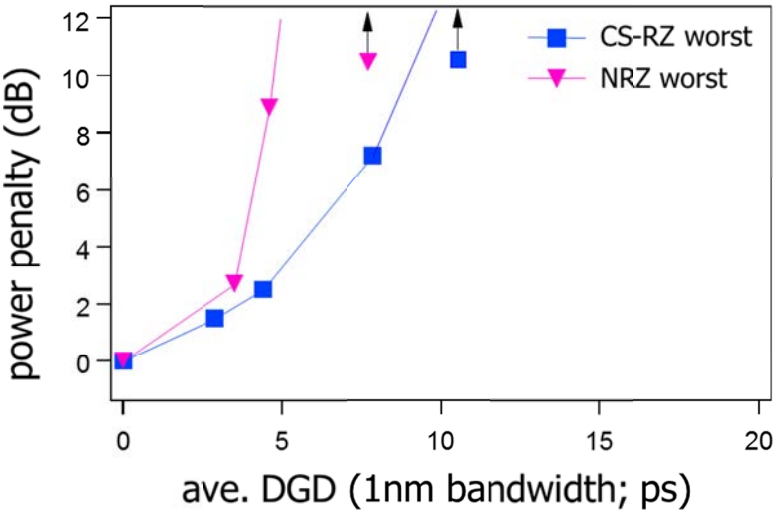

Fig. 4-3 Measured power penalty after transmission

The plots designated as "worst" were obtained by adjusting the input state of polarization so that I could get the worst bit error ratio. With the adjustment, I aimed to set input state of polarization at γ=0.5 where I can expect the worst performance. As a result, I

achieved better tolerance for CS-RZ signal against all-order PMD as shown in Fig. 4-3. Here, I would like to address that these penalties were resulted not only from 1st-order PMD but also from all higher-order PMD. The plots designated as "Principal State of Polarization (PSP)" in Fig. 4-4 were obtained as I optimized the input state of polarization so that I could get minimum bit error ratio.

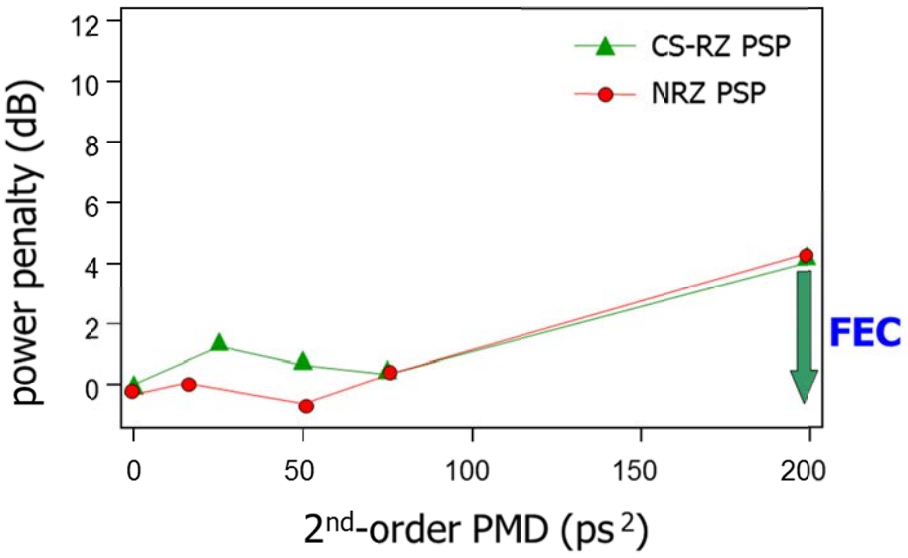

Fig. 4-4 Measured power penalty after transmission

By the optimization, I can expect to launch into PSP of each fiber span [52]. In PSP transmission, 1st-order PMD would be effectively suppressed. As a result, I achieved significant expansion of tolerable PMD. I successfully suppressed the power penalty resulted from high 2nd-order PMD of 200ps^2 with FEC decoding. I would like to notify that CS-RZ and NRZ had showed almost the same performance against 2nd-order PMD. The observed convergence could be explained by their similar spectral bandwidth. From these result, I can say that CS-RZ will have more robustness against all-order PMD compared with conventional NRZ without any PMD compensators. With 1st-order compensator, I can expect similar performance for these formats.

FEC performance against all-order PMD

I evaluated error correction performance of standard FEC RS (255,239) in high PMD field environment. The input state of polarization was set at the worst state to evaluate error correction performance against all-order PMD. The measured receiver sensitivities defined at bit error rate of 10^{-9} were plotted in Fig. 4-5.

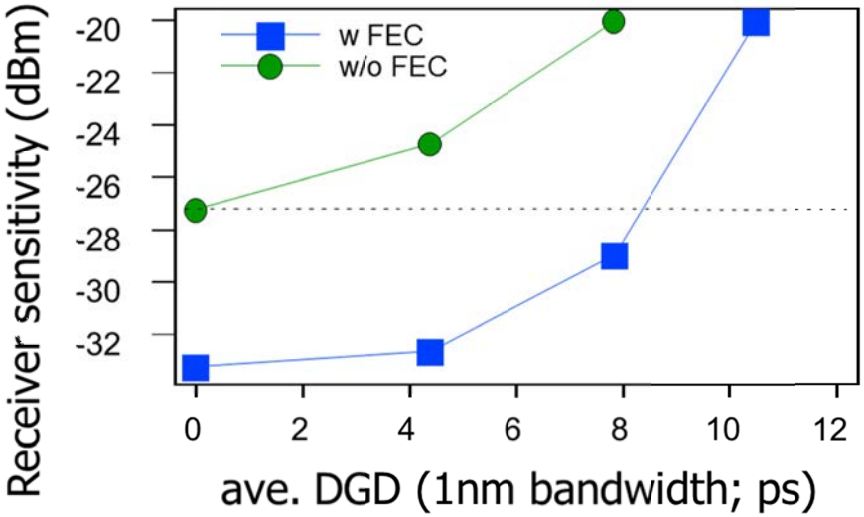

Fig. 4-5 Measured receiver sensitivities defined at bit error rate of 10^{-9}

The back-to-back receiver sensitivity without FEC decoding was -27.2 dBm and I achieved 6-dB coding gain. As I increased the PMD by changing fiber spans, the receiver sensitivities degraded. But I confirmed that G.709 standard FEC kept its coding gain constant against all-order PMD. The coding gain did not fluctuate during two weeks in this field experiment. Thus I can expect that random error statistics up to 10.5 ps of high averaged DGD in this field experiment. The result suggests that G.709 standard FEC will be applicable to PMD mitigation in actual 40G transport system.

Section summary

In this section, I clarified the impact of CS-RZ modulation format and G.709 standard FEC against all-order PMD under actual PMD-limited field environment, in the joint field trail of NTT and DT, for the first time as of Aug. 2004. Against all order PMD, CS-RZ format outperformed NRZ. CS-RZ and NRZ had similar tolerance against 2^{nd}-order PMD. G.709 standard FEC worked well against all-order PMD and also accommodated high 2^{nd}-order PMD of $200ps^2$ in my field trial.

Up to the time of this work, signal degradation resulted from ISI by PMD has been investigated only in laboratories and/or some limited works for 1^{st} order PMD in field environment have been reported [45-49]. However, for actual design of 40 Gbit/s optical transport systems, PMD must be considered to avoid unexpected system failure.

The work in this section provided basic understanding for system design considering PMD. Based on the tolerance measured in this field experiment, actual 40 Gbit/s system had

been designed and adopted differential quadrature phase shifted keying (DQPSK) signal format for the system to avoid system outage caused by temporal change of 1^{st} and 2^{nd} order PMD. Since lowering the symbol rate was critical to reduce outage probability resulted from PMD. In addition to that, ITU-T standard G.709 FEC has been also adopted for commercial transport systems being deployed worldwide.

5. SNR recovery toward higher bitrate TDM

5.1 All-optical 2R (Reshaping and Regeneration) repeater

Signal-ASE beat noise suppression

Amplified spontaneous emission ASE noise generated by erbium doped fiber amplifiers (EDFA) gives the Signal-to-Noise Ratio (SNR) limit for maximum transmission distance without regenerative repeaters in high-speed optical transmission links [53]. ASE-ASE beat noise that appears in"0"-level ("space") in digital signal can significantly be suppressed by using a narrow optical band pass filter at the output of EDFA. However, ASE-signal beats that appears mainly in "1"-level ("mark") cannot be removed by such a filter. A new approach is required for the reduction. Four wave mixing (FWM) in optical fibers has been applied to such optical circuits as wavelength converters [54], optical de-multiplexers [55], and optical phase conjugators [56]. I propose a novel all-optical limiter circuit that can suppress the noise on the "mark" level using non-linear pump depletion in the FWM process and investigate its performance experimentally.

Non-linear FWM Limiter

In the four wave mixing process in optical fibers, optical pumping power is converted to Stokes and anti-Stokes light waves [57]. The conversion efficiency is a function of pumping power and an optical phase matching condition that depends on the difference between the pumping wavelength and the zero dispersion wavelength of the optical fiber. At low pumping powers, where self phase modulation (SPM) of the pumping light itself is negligible, the conversion efficiency depends on square of the pumping power. However, high pumping power causes SPM of the pumping light wave and changes the pumping wavelength for maximum efficiency to a shorter zero dispersion wavelengths [57]. Provided that I detune the zero dispersion wavelength of the fibers to slightly longer than that of the pumping light waves as shown in Fig. 5-1-1, effective phase matching will be obtained abruptly at a particular pumping power. Therefore, conversion efficiency will increase abruptly, as illustrated in Fig. 5-1-2, and the transmitted power will saturate at the pumping power and act as all-optical limiter as illustrated in Fig. 5-1-3.

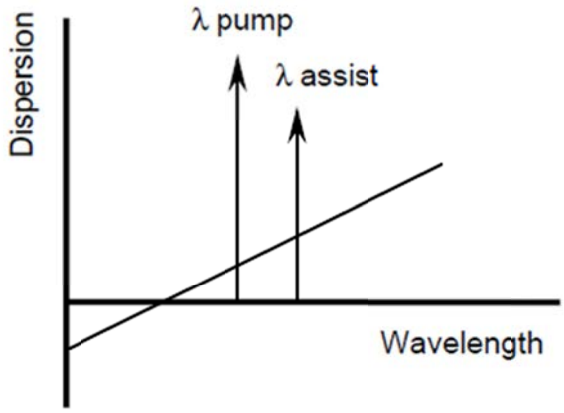

Fig. 5-1-1 Pumping light configuration for limiter function

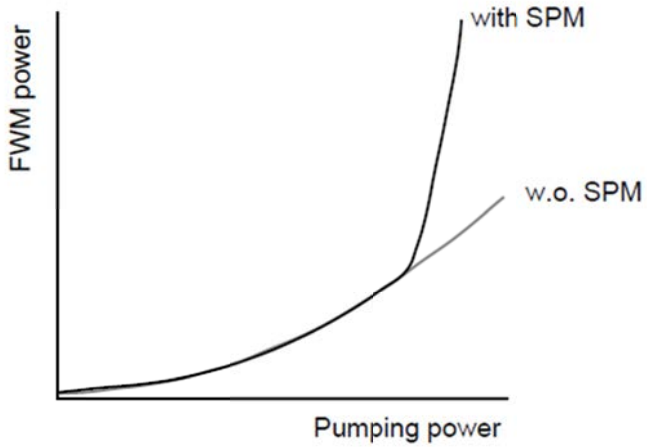

Fig. 5-1-2 Conversion efficiency w./wo. SPM

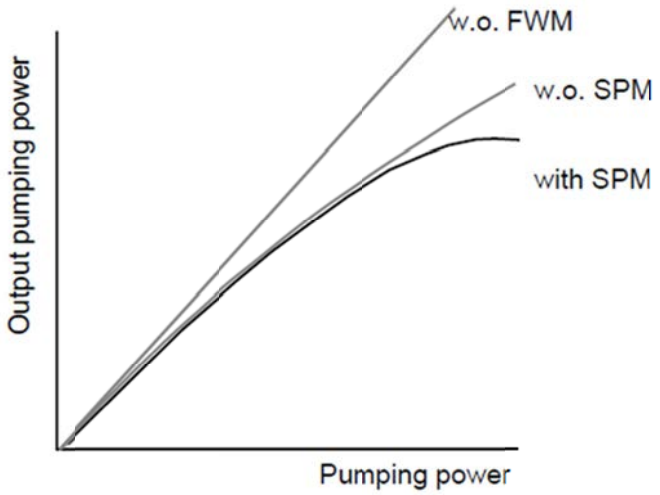

Fig. 5-1-3 Pumping power characteristics

Optical pumping power is converted to Stokes and anti-Stokes light waves [57] in the four wave mixing process in optical fibers. The conversion efficiency is a function of pumping power and an optical phase-matching condition that depends on the difference between the pumping wavelength and the zero dispersion wavelength of the optical fiber. Phase-mismatch κ can be expressed as,

$$\kappa = \Delta k + 2\gamma P_0 \qquad \text{Eq. 5-1-1}$$

$$\Delta k = \frac{2\pi c \lambda_0^3}{\lambda_p^3 \lambda_a^2} \frac{dD}{d\lambda} (\lambda_0 - \lambda_p)(\lambda_a - \lambda_p)^2 \qquad \text{Eq. 5-1-2}$$

where $\Delta\kappa M$ and $\Delta\kappa\Omega$ are phase-mismatch resulted from material and waveguide dispersion, respectively, g is the nonlinearity coefficient, P_o is the degenerated pumping power [57]. The conversion efficiency is proportional to square of the pumping power at low pumping powers, where self phase modulation (SPM) of the pumping light itself is negligible. Since $\Delta\kappa$ is negative in the anomalous-Group Velocity Dispersion (GVD) regime, it is possible to compensate it by the nonlinear contribution $2\gamma P_o$. In other word, high pumping power causes SPM of the pumping light wave and changes the pumping wavelength for maximum conversion efficiency to a shorter zero dispersion wavelengths [57]. Therefore, effective phase-matching will be obtained abruptly at a particular pumping power, provided that I detune the zero dispersion wavelengths of the fibers to slightly longer than that of the

pumping light waves. Therefore, conversion efficiency will increase abruptly and the transmitted pumping power will saturate at the power and act as all-optical limiter.

Experimental Setup

Figure 5-1-4 shows the experimental setup of the FWM limiter circuit. Wavelengths of pumping and assist light waves were 1552.4 nm and 1553.8 nm, respectively. A polarization-maintaining 3-dB coupler combines amplified pumping and assist light wave. I launched these light waves into 12.5-km single mode optical fibers whose zero dispersion wavelengths was set at 1551.0 nm. Optical powers of the launched pumping and assist light wave were 30 mW and 7 mW, respectively. The transmitted pumping light wave was isolated from the assist light wave and generated FWM light wave (Stokes and anti-Stokes components) by two cascaded optical band-pass filters (1 nm at full width at half maximum (FWHM)).

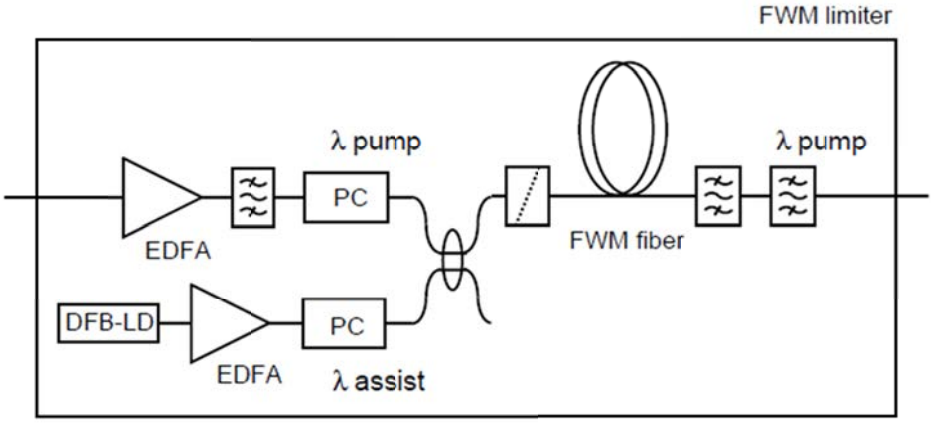

Fig. 5-1-4 Experimental setup of the FWM limiter

Results and Discussion

I measured the transmitted optical power of the pumping light wave by changing launched pumping power. Transmitted power saturated abruptly above 30 mW of pumping power as shown in Fig. 5-1-5.

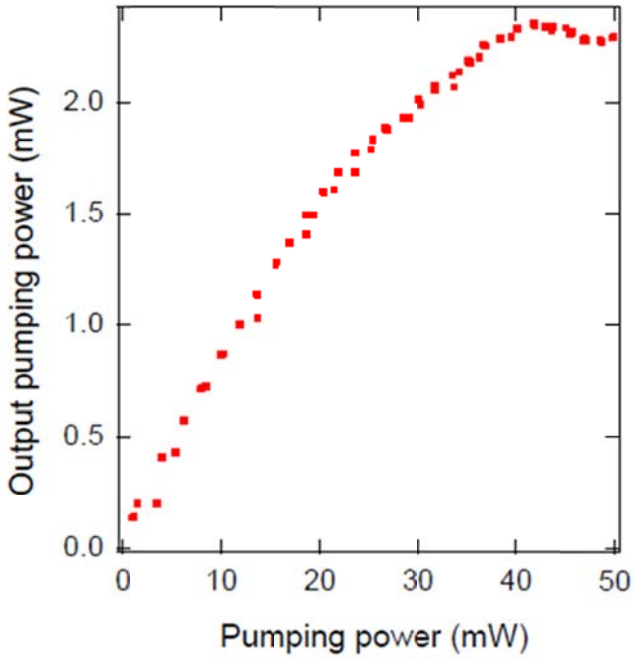

Fig. 5-1-5 Transmitted power as a function of pumping power

Next, I employed the limiter circuit for suppression of ASE noise imposed on a 20-Gbit/s non return to zero (NRZ) signal. I imposed ASE noise by attenuating the input optical power to an Erbium doped fiber amplifier (EDFA) down to -25 dBm. I used an optical band pass filter (1 nm FWHM) at the output of the EDFA to suppress the "space" level noise which resulted from ASE-ASE beat noise. The eye diagrams before and after optical limiter application are shown in Fig. 5-1-6 with their histograms at the midpoint of the eye diagrams.

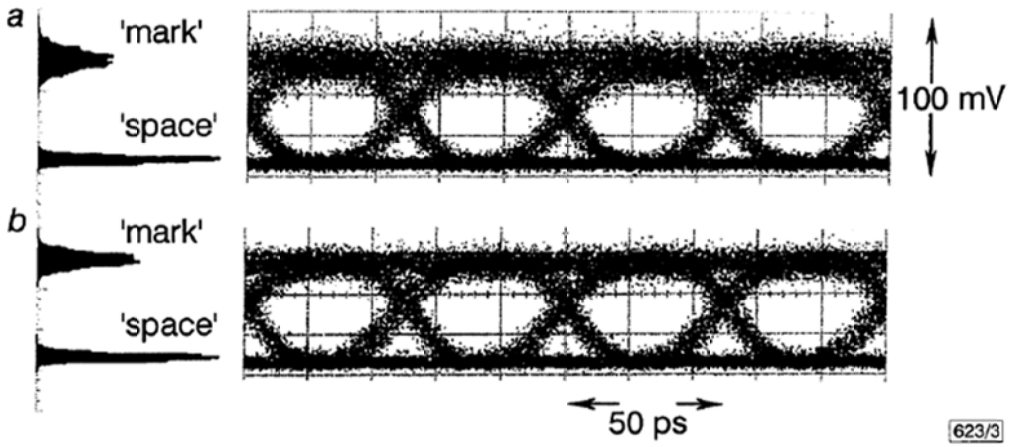

Fig. 5-1-6a,b Rye diagrams before and after optical limiter

The "space" level noise was effectively suppressed by the 1-nm FWHM optical filter, as shown in Fig. 5-1-6a. However, ASE-signal beat noise was clearly observed on the "mark" level. The variance of the "mark" level which resulted from ASE-signal beat noise was successfully suppressed by optical limiting, as shown in Fig. 5-1-6b. The bit error rate (BER) performances before and after optical limiter application is shown in Fig. 5-1-7. ASE-induced power penalty of more than 2 dB were effectively suppressed and no error floors were observed after the all-optical limiter.

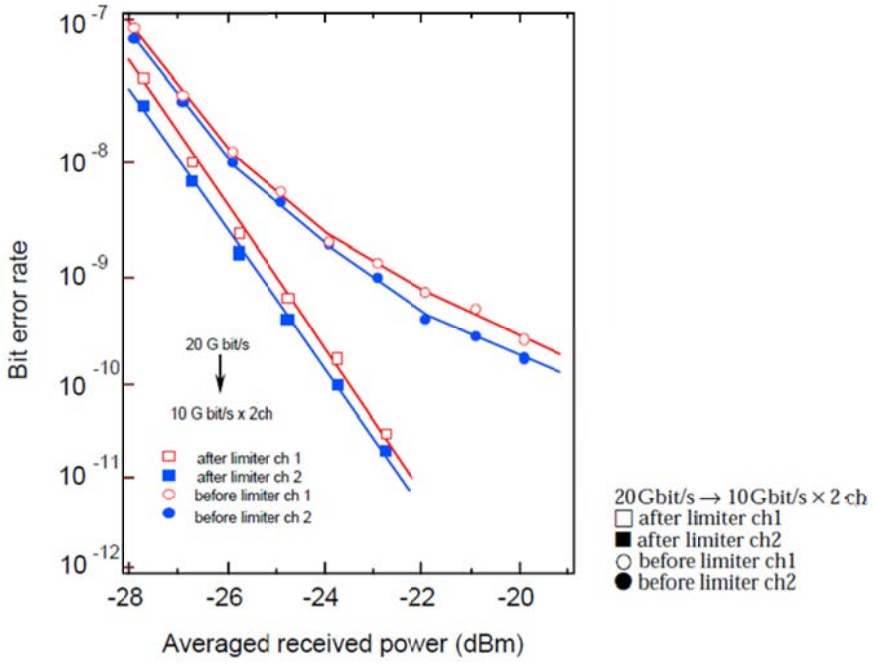

Fig. 5-1-7 Bit error rate performances

Section summary

In this section, I have proposed a novel all-optical limiter circuit based on non-linear limiting input/output response of a pumping light wave in FWM in optical fibers. I achieved the limiting feature by evaluation of the transmission response as a function of pumping power by setting the zero dispersion wavelengths of the fibers to slightly shorter wavelength than the pumping light wave. Then I confirmed the effectiveness of my approach by applying the limiter circuit to the suppression of ASE-signal beat noise.

5.2 All-optical 3R (Retiming, Reshaping, and Regeneration) regenerator

All-optical approach for ASE noise suppression

The emerging demands for more transmission capacity driven by progress in multi-media services and computer networks will become more intense in the near future. Time division multiplexing is a key technique to meet the demands. In order to increase the transmission capacity of time division multiplexed system, operating speed has to be boosted beyond the bandwidth limit of electronic circuits. All-optical processing circuits are suitable for such high-speed processing because they have the potential for ultra fast response time.

In such high-speed transmission systems, accumulated amplified spontaneous emission (ASE) noise generated by erbium doped fiber amplifiers (EDFA) determines the signal to noise ratio (SNR) limit for the maximum transmission distance, if no regenerative repeaters are used. Regenerators regain the SNR.

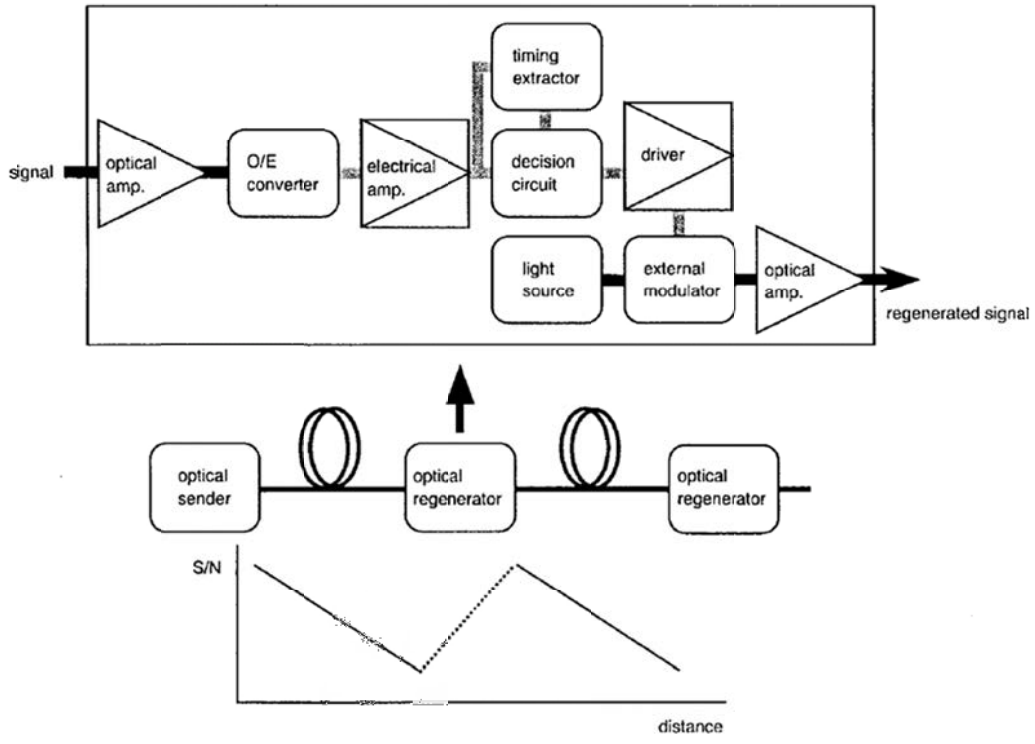

Fig. 5-2-1 Conventional regenerator configuration and SNR recovery
(the same figure with Fig. 1-4)

The conventional regenerator shown in Fig. 5-2-1 consists of an optical amplifier, an O/E converter, electrical amplifiers, an electrical timing extractor, an electrical decision circuit, a driver amplifier, a light source, an optical intensity modulator, and an optical booster amplifier. Among these components, the key ones are the amplifier, decision circuit, and timing extractor. The decision circuit discriminates incoming data stream into the "1" and "0" level.

To achieve ultra fast all-optical regenerators, there are several optical gates [8-11] candidates for the optical discrimination circuits, and optical mode-locking [58] or optical PLL circuits [59] are expected to be used as timing extractors. In this work, I focus on optical discrimination.

Optical discriminators using an interferometric switch based on semiconductor optical amplifiers (SOA) or a nonlinear fiber-loop mirror (NOLM) switch have been presented as of 1999 [8-11]. These devices can be categorized into resonant and non-resonant types. NOLM-based switches are non-resonant types. Resonant means that optical switching is realized by the generation of actual carriers which means the operating speed is limited by the relaxation time of the carriers. On the other hand, no actual carriers are involved in non-resonant switching. Operating speed is determined by ultra fast Kerr nonlinearity, which provides the response time of several fs. In general, non-resonant-type circuits such as NOLM have relatively large latency due to its long switching fibers. In contrast, resonant-type circuits have relatively small dimensions owing to the large nonlinearity induced from carrier excitations and relaxation. Our low-temperature-grown optical switch (LOTOS) [60-62] is a compact resonant-type optical gate that has ultra fast carrier relaxation time.

Our target is the realization of an all-optical high-speed regeneration circuit without any optical detectors, electrical amplifiers, electrical decision circuits, or electro-optical modulators. Such a regenerator would overcome the SNR limit and suppress the penalty caused by waveform distortion without the bandwidth limitation of electrical, E/O, and O/E circuits. The all-optical discriminator (ODSC) [63-65] enables high-speed, simple, and compact all-optical regenerator.

In this section, I report on a simplified evaluation of the discrimination performance of these optical gates with the introduction of performance parameters for their transmittance. I demonstrate all-optical discrimination performance utilizing LOTOS.

Optical discrimination

The conceptual model of the ODSC is shown in Fig. 5-2-2. The discriminator consists of an optical amplifier, optical gate, and a local clock pulse source. The optical amplifier controls the "optical" decision level by changing its gain. The local clock pulse source generates low-noise optical clock pulses which are synchronized with the input signal pulses. The optical gate discriminates the input degraded optical signal pulses. The clock pulses are encoded by the signal pulses via nonlinear gating by the optical gate. Nonlinear change in the transmittance of the optical gate caused by amplified signal pulses encodes optical clock pulses, which are simultaneously input to the gate. Accumulated noise on the "1" and "0" level in incoming signal pulses transmitted through optical fiber links can be suppressed by the nonlinear gating, and the SNR of discriminated optical pulses have almost the same value as the SNR before transmission. I will discuss discrimination performance in the next section.

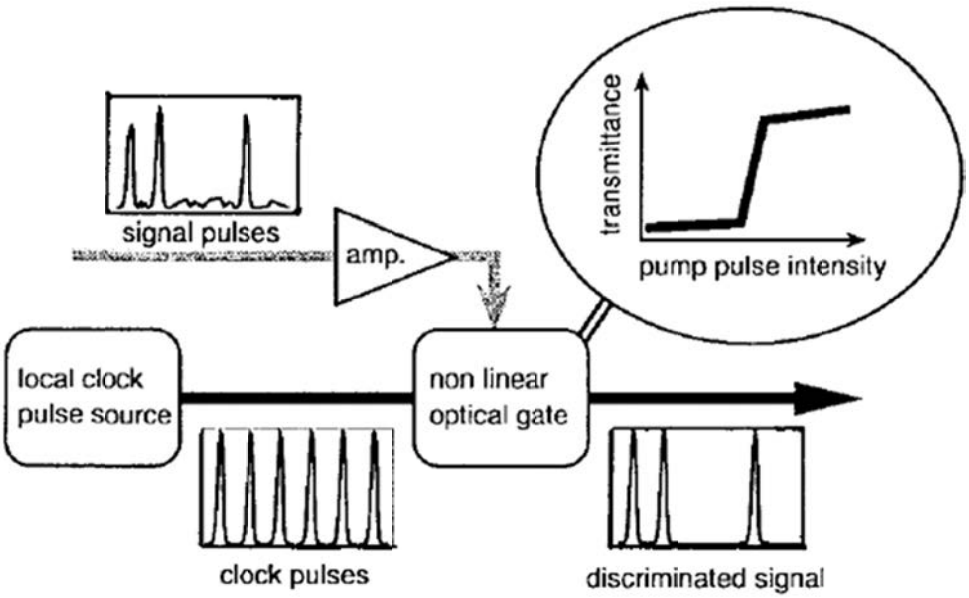

Fig. 5-2-2 Conceptual model of the ODSC

Estimation of discrimination performance

A. Model

I used the simple model shown in Fig. 5-2-3 to evaluate the discrimination performance. The optical sender generates optical signal pulses that have shot noise only. The loss medium acts as a pure absorber and adds no additional noise. Optical amplifier α amplifies optical signal pulses and has a noise figure of 3 dB, which means inverse population factor

n_{sp} is unity. I assume that the nonlinear optical gate has no loss at maximum transmittance for simplicity. Discriminated signal is received by the optical receiver, which contains an optical pre-amplifier β. The bit error rate was estimated for the detected signal.

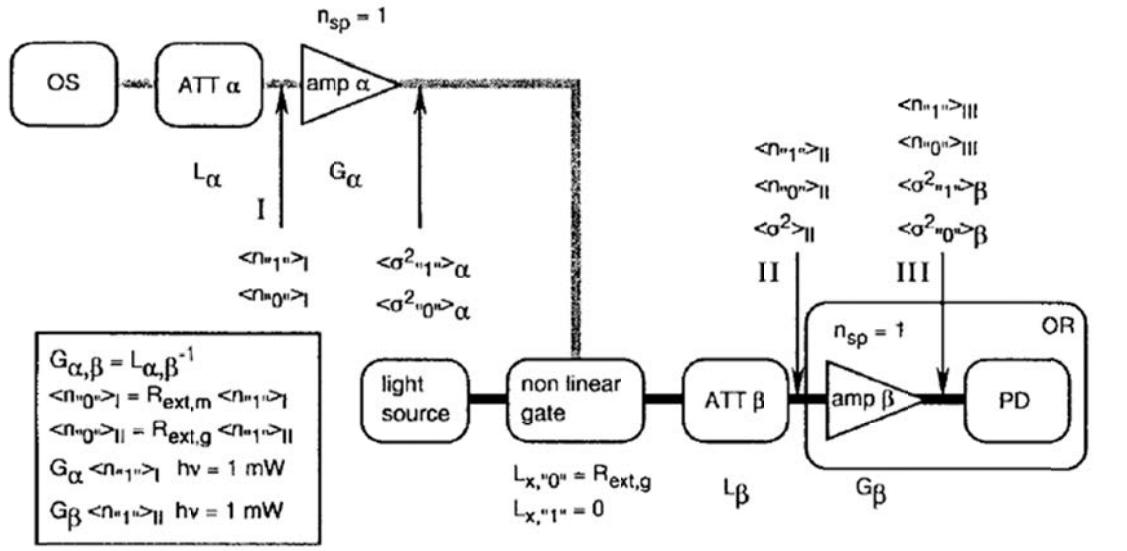

Fig. 5-2-3 Model to evaluate the discrimination performance

B. Ideal Nonlinear Transmittance of Optical Gates

The ODSC uses optical gates that have nonlinear transmittance as a function of inputted pump pulse intensity. Transmittance is primarily determined by pump pulse energy in a resonant-type switch and by pumping peak power in a non-resonant-type. Ideal nonlinear transmittance characteristics are shown in Fig. 5-2-4.

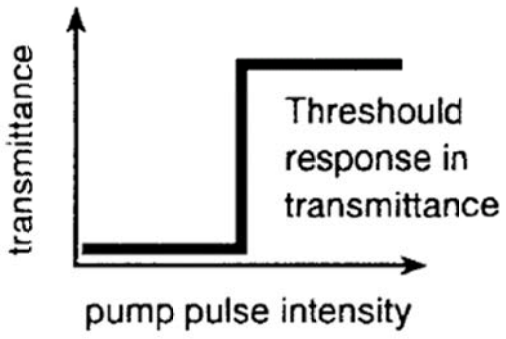

Fig. 5-2-4 Ideal nonlinear transmittance characteristics

The transmittance abruptly increases at a threshold pump pulse intensity. For lower pumping intensity, the gate shows a high extinction ratio, and high flat transmittance for higher pumping intensity. I call the threshold intensity the "optical decision level". I optimize the "optical decision level" to one that gives the lowest bit error probabilities.

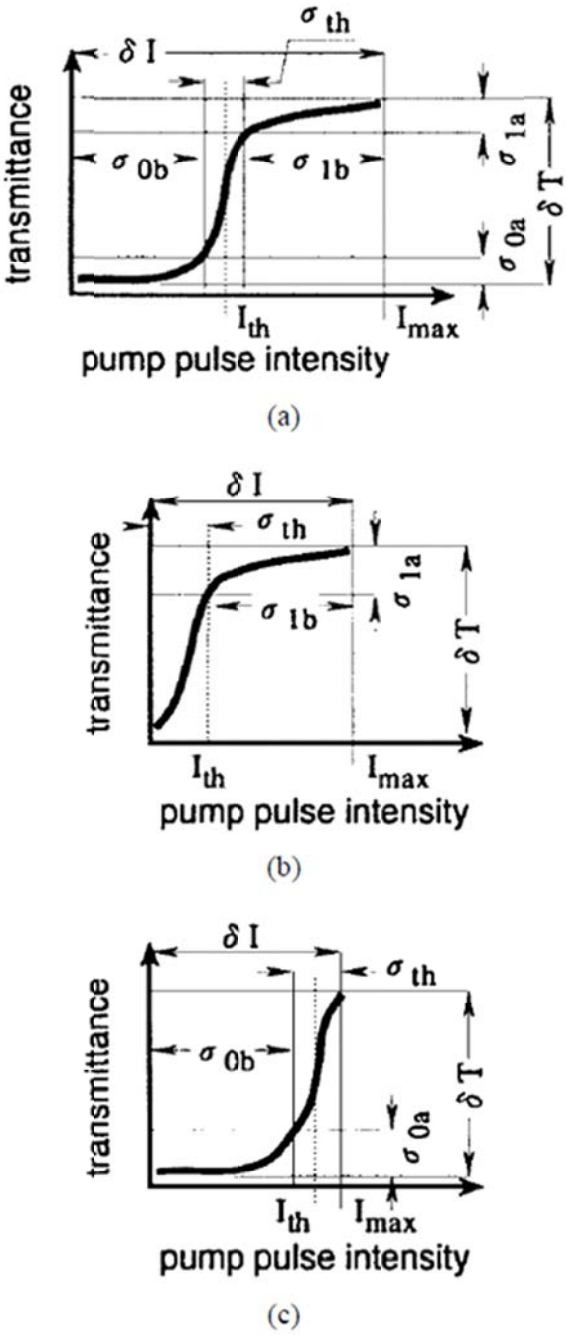

Fig. 5-2-5 Parameters definitions

C. Performance Parameters for Optical Gates

For the calculation of discrimination performance, I defined the performance parameters for optical gates. Each parameter is defined as shown in Fig. 5-2-5(a), where I_{max} means the maximum pumping intensity and δI is the allowable pumping dynamic range for discrimination. $\sigma_{(0,1)a}$ and $\sigma_{(0,1)b}$ are the variances of transmittance and pumping intensity range for the (0,1) level. I define I_{th} as the pumping intensity where the deferential coefficient of transmittance reaches maximum. σ_{th} is an ambiguity region for discrimination, which I define as the range of pumping intensity in which the transmittance of the gates is 20-80 % of their maximum. δT means the total dynamic range in transmittance. For simplicity, I assume the maximum transmittance is unity. Among these parameters, σ_{1b} normalized by I_{max} is important for discrimination. At discrimination, the tail of the probability distribution function over σ_{1b} will not be clamped and will cause errors. Therefore, the optical gates should have σ_{1b} that is large enough ensure the bit error rate is lower than the requirements for the transmission link. Typical requirement for the BER is less than 10^{-15}. η_1, the second parameter is the σ_{1a} (normalized by δT) divided by σ_{1b} (normalized by I_{max}). The η_1 expresses the clamping parameter for the fluctuation of "1" level. The η_1 should be zero for ideal discrimination, which means no fluctuation will transmit to the discriminated signal. In the ideal case, discriminated signal has only the fluctuation of the clock light source, which should have shot noise only. The η_1 of unity means no reduction of fluctuation of the "1" level. These two parameters can be determined for the "0" level in a similar manner.

I cannot determine the parameters for the "0" level when the gate has only limiting characteristics, as shown in Fig. 5-2-5(b). On the contrary, I cannot define these parameters for the "1" level when the gate has thresholding characteristics only, as shown in Fig. 5-2-5(c).

The third parameter is the extinction ratio ($R_{ext,g}$) of the optical gate. $R_{ext,g}$ is the ratio of the transmittance of the "0" level to "1" level. More than 10 dB of $R_{ext,g}$ is required for sufficient discrimination.

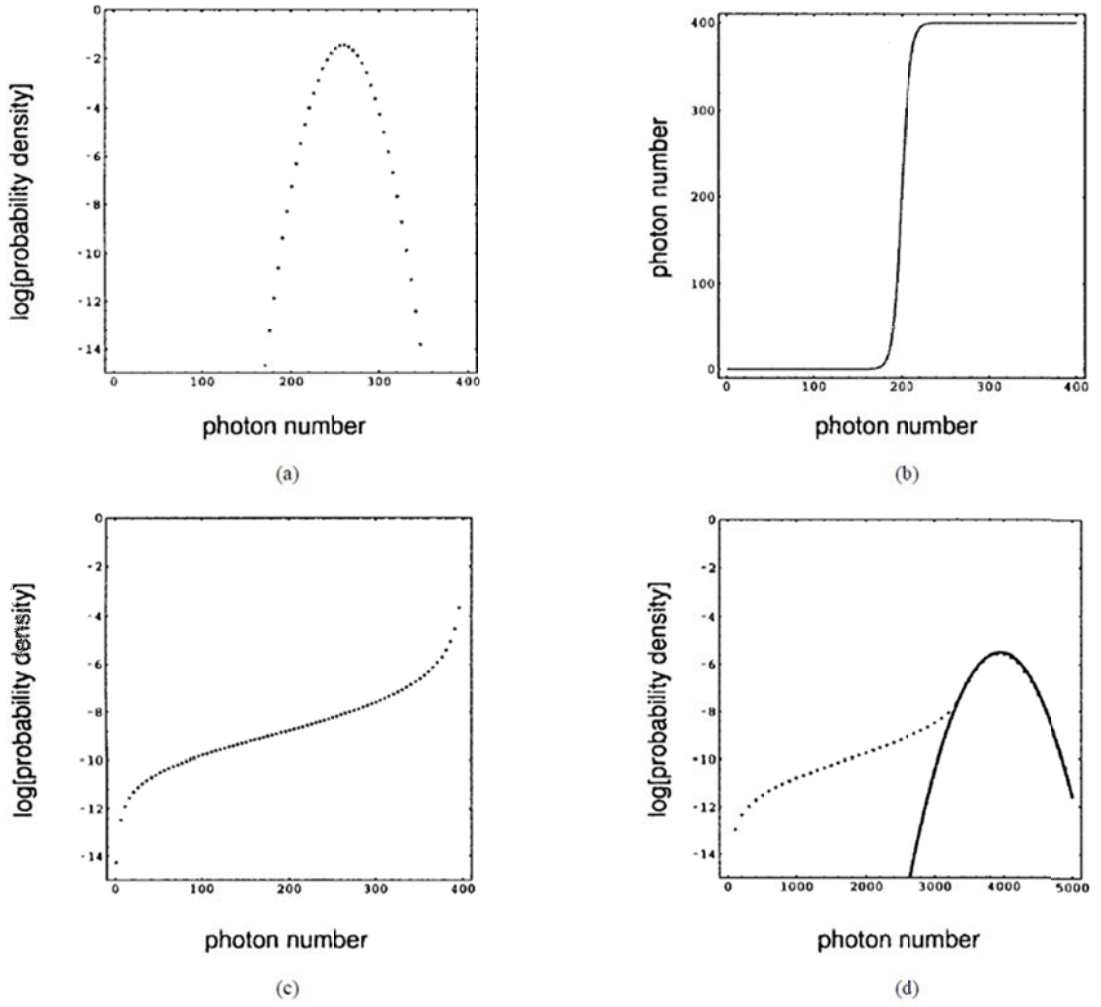

Fig. 5-2-6 Transmittance of optical gate

D. Calculation of Probability Density Functions (PDF)

In general, the probability density function (PDFs) of "0" and "1" for signal pulses can be expressed

$$P_{"0"}(n) = \frac{1}{\sigma_0 \sqrt{\pi}} e^{-\left(\frac{n-n_0}{\sigma_0}\right)^2} \qquad \text{Eq. 5-2-1}$$

$$P_{"1"}(n) = \frac{1}{\sigma_1 \sqrt{\pi}} e^{-\left(\frac{n-n_1}{\sigma_1}\right)^2} \qquad \text{Eq. 5-2-2}$$

The parameters are summarized in Table 5-2-1.

Tab. 5-2-1 Parameter descriptions for PDF calculations

symbol	*meaning*
n_0	mean photon number in "0" level
n_1	mean photon number in "1" level
σ_0	variance of photon number in "0" level
σ_1	variance of photon number in "1" level

In the case of amplification by an optical amplifier, the mean number of amplified photons and its variance can be expressed as,

$$\langle n_{out} \rangle = G \langle n_{in} \rangle + 2\,(G-1)\; n_{sp}\; B_{opt} \qquad \text{Eq. 5-2-3}$$

$$\sigma^2 = G \langle n_{in} \rangle + 2\,(G-1)\, n_{sp}\, B_{opt} + 2\,G\,(G-1)\, n_{sp} \langle n_{in} \rangle + 2\,(G-1)^2\, n_{sp}^2\, B_{opt} \qquad \text{Eq. 5-2-4}$$

The parameters are summarized in Table 5-2-2.

Tab. 5-2-2 Parameter descriptions for PDF calculations

symbol	*meaning*
n_{out}	amplified photon number
n_{in}	input photon number
G	amplifier gain
n_{sp}	inverse population factor
B_{opt}	optical bandwidth of EDFA
σ	variance of amplified photon number

The first term in Equation 7-3 is an amplified signal, and the second term is the spontaneous emission component. The first two terms in Equation 7-4 express shot noise. The remaining two terms are signal-ASE beat noise and ASE-ASE beat noise components, respectively. By all-optical discrimination, PDFs will be modified depending on the nonlinear threshold response of the optical gate. I assume transmittance T (n) of the gate as the shape shown in Fig. 5-2-6(b). The function has a nonlinear threshold change in transmittance.

As a result, PDFs of the discriminated "0" and "1" level can be expressed as,

$$P_{"0"}^{out}(n) = P_{"0"}^{in}\left(T^{-1}(n)\right) \quad \text{Eq. 5-2-5}$$

$$P_{"1"}^{out}(n) = P_{"1"}^{in}\left(T^{-1}(n)\right) \quad \text{Eq. 5-2-6}$$

In this way, I can calculate the change of PDFs by all-optical discrimination.

I have solved the master equation for discriminated non-Gaussian PDFs, and obtained non-Gaussian amplified PDFs [66]. The PDFs for the "1" level before and after discrimination and after amplification by the EDFA are shown in Fig. 5-2-6 with the response of nonlinear optical gate. Because the discriminated PDFs do not have a Gaussian distribution, I cannot characterize the PDFs after discrimination by a mean and variance, which is valid in the case of Gaussian PDFs. In the amplification, the shape of the PDFs are modified and become more Gaussian in shape. This modification can be interpreted as a coherent linear amplification of input PDFs and the addition of Gaussian noise [67, 68]. The main source of this Gaussian noise can be attributed to the well-known signal-ASE beat noise. For simplification of analysis, I only consider the condition where the integrated non-Gaussian tail of PDFs generated by discrimination below the threshold level is less enough than a required bit error probability. Accordingly, the contribution to signal-ASE beat noise caused by the non-Gaussian tale of PDFs is small enough to be neglected. In ordinary electrical decision circuits, the detected electrical signal at certain SNR is discriminated and the bit error rate fixed at a value that is small enough not to degrade the BER more than the required level at final termination of fiber link. Similarly, I assume the condition where the fixed or discriminated errors can be neglected. Under these assumptions, I can formulate the mean photon number and its variance for the "1" and "0" level in front of the final detector.

At the output of optical amplifier α in Fig. 5-2-3, I can express the variance of photon number as,

$$\left\langle \sigma^2_{"1"} \right\rangle_\alpha = \left(G_\alpha \langle n_{"1"} \rangle_I + 2\,(G_\alpha - 1)\, n_{sp}\, B_{opt} + 2\,(G_\alpha - 1)\, n_{sp}\, G_\alpha \langle n_{"1"} \rangle_I + 2\,(G_\alpha - 1)^2\, n_{sp}^2\, B_{opt} \right) \quad \text{Eq. 5-2-7}$$

$$\left\langle \sigma^2_{"0"} \right\rangle_\alpha = \left(G_\alpha \langle n_{"0"} \rangle_I + 2\,(G_\alpha - 1)\, n_{sp}\, B_{opt} + 2\,(G_\alpha - 1)\, n_{sp}\, G_\alpha \langle n_{"0"} \rangle_I + 2\,(G_\alpha - 1)^2\, n_{sp}^2\, B_{opt} \right) \quad \text{Eq. 5-2-8}$$

where the mean photon number on the "0" level can be written as,

$$\langle n_{"0"} \rangle_I = R_{ext,\,m} \langle n_{"1"} \rangle_I. \quad \text{Eq. 5-2-9}$$

The parameters are summarized in Table 5-2-3.

Tab. 5-2-3 Parameter descriptions for PDF calculations

symbol	*meaning*
$\langle \sigma^2_{\text{"1" or "0"}} \rangle_\alpha$	variance of photon number at the output of amplifier α
$\langle n_{\text{"1" or "0"}} \rangle_I$	the mean photon number at the input of amplifier α
G_α	gain of amplifier α
n_{sp}	inverse population factor
B_{opt}	optical bandwidth in optical amplifier
$R_{ext,\,m}$	extinction ratio of modulation in OS
$\langle n_{\text{"1" or "0"}} \rangle_{II}$	the mean photon number at the input of amplifier β
$R_{ext,\,g}$	extinction ratio of optical gate
$\langle n_{\text{"1" or "0"}} \rangle_{III}$	the mean photon number at the output of amplifier β
$\langle \sigma^2_{\text{"1" or "0"}} \rangle_\beta$	variance of photon number at the output of amplifier β
G_β	gain of amplifier β
$\eta_{\text{"1" or "0"}}$	clamping parameter of optical gate
B	electrical bandwidth of optical detector
erfc	complementary Gaussian error function

I assume the loss of the optical gate at the "1" level ($L_{x,\text{"1"}}$) is zero for simplicity. Therefore, the mean photon number at point II can be written as,

$$\langle n_{\text{"0"}} \rangle_{II} = R_{ext,\,g}\ \langle n_{\text{"1"}} \rangle_{II}. \qquad \text{Eq. 5-2-10}$$

In this calculation, I assume that the optical output power of each amplifier is equal and the gain of each amplifier is the inverse of the loss of the attenuator such that,

$$G_\alpha \langle n_{\text{"1"}} \rangle_I h\nu = G_\beta \langle n_{\text{"1"}} \rangle_{II} h\nu = 1\ \text{mW} \qquad \text{Eq. 5-2-11}$$

$$G_{\alpha,\,\beta} = 1 / L_{\alpha,\,\beta} \qquad \text{Eq. 5-2-12}$$

In this case, I assume the launched optical power for a nonlinear optical gate is 1 mW. Finally, I can estimate the mean photon number and variance at the point III in Fig. 5-2-3 as,

$$\langle n_{"1"} \rangle_{III} = G_\beta \langle n_{"1"} \rangle_{II} + 2 (G_\beta - 1) n_{sp} B_{opt} \quad \text{Eq. 5-2-13}$$

$$\langle n_{"0"} \rangle_{III} = G_\beta \langle n_{"0"} \rangle_{II} + 2 (G_\beta - 1) n_{sp} B_{opt} \quad \text{Eq. 5-2-14}$$

$$\langle \sigma^2_{"1"} \rangle_\beta = G_\beta \langle n_{"1"} \rangle_{II} + 2 (G_\beta - 1) n_{sp} B_{opt} + 2 (G_\beta - 1)^2 n_{sp}^2 B_{opt} + G_\beta \left\{ \frac{\eta^2_{"1"}}{G_\beta} \langle \sigma^2_{"1"} \rangle_\alpha - G_\beta \langle n_{"1"} \rangle_{II} \right\} \quad \text{Eq. 5-2-15}$$

$$\langle \sigma^2_{"0"} \rangle_\beta = G_\beta \langle n_{"0"} \rangle_{II} + 2 (G_\beta - 1) n_{sp} B_{opt} + 2 (G_\beta - 1) n_{sp} G_\beta \langle n_{"0"} \rangle_{II} + 2 (G_\beta - 1)^2 n_{sp}^2 B_{opt} + G_\beta \left\{ \frac{\eta^2_{"0"}}{G_\beta} \langle \sigma^2_{"0"} \rangle_\alpha - G_\beta \langle n_{"0"} \rangle_{II} \right\} \quad \text{Eq. 5-2-16}$$

The first four terms in Equation 7-15 and Equation 7-16 resulted from there being an optical amplifier in the receiver. The remaining terms are excess noise components imposed by the optical amplifier before discriminator. The derivation of those terms is described in Appendix. Under normal conditions, there is no squeezing in the quantum state. Therefore, I assume that the excess noise components must be positive or zero.

Assuming the quantum efficiency is unity, I can evaluate the Q factor at final detection as follows:

$$Q = \frac{\langle n_{"1"} \rangle_{III}^{elec} - \langle n_{"0"} \rangle_{III}^{elec}}{\langle \sigma_{"1"} \rangle_\beta^{elec} + \langle \sigma_{"0"} \rangle_\beta^{elec}}. \quad \text{Eq. 5-2-17}$$

$$\langle n_{"1", "0"} \rangle_{III}^{elec} = \langle n_{"1", "0"} \rangle_{III} \quad \text{Eq. 5-2-18}$$

$$\langle \sigma_{"1", "0"} \rangle_\beta^{elec} = \sqrt{2B} \langle \sigma_{"1", "0"} \rangle_\beta \quad \text{Eq. 5-2-19}$$

Provided that I set the decision level to an optimum value determined by

$$\langle n_{th} \rangle^{elec} = \frac{\langle \sigma_{"0"} \rangle_\beta^{elec} \langle n_{"1"} \rangle_{III}^{elec} + \langle \sigma_{"1"} \rangle_\beta^{elec} \langle n_{"0"} \rangle_{III}^{elec}}{\langle \sigma_{"0"} \rangle_\beta^{elec} + \langle \sigma_{"1"} \rangle_\beta^{elec}} \quad \text{Eq. 5-2-20}$$

The bit error rates can be calculated by the Q values easily as,

$$\mathrm{BER} = \frac{1}{2}\,\mathrm{erfc}\left(\frac{Q}{\sqrt{2}}\right)$$ Eq. 5-2-21

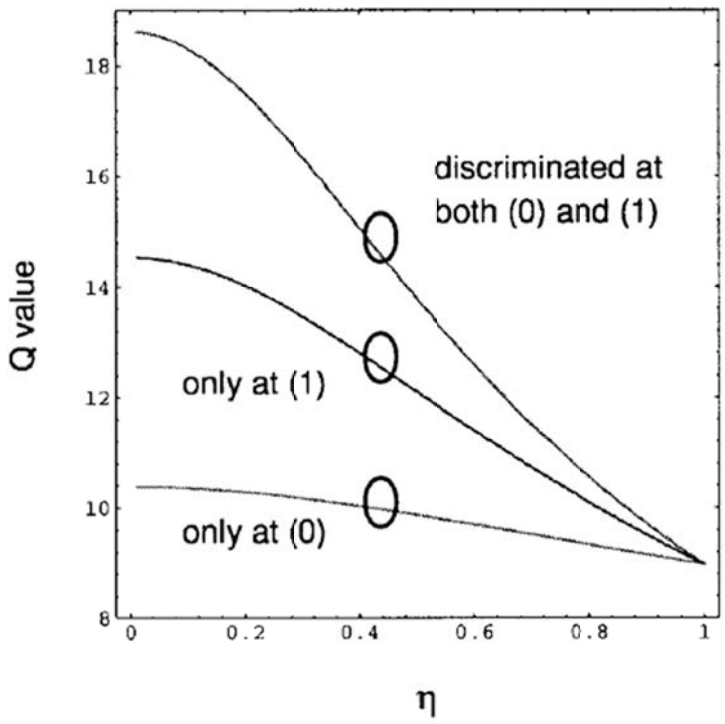

Fig. 5-2-7 Calculated Q values

E. Results of Estimation

According to the model and conditions, I calculated the Q values and the bit error rate of discriminated and amplified signal. Fig. 5-2-7 shows calculated Q values as a function of η. Assumed parameters are summarized in Table 5-2-4.

Tab. 5-2-4 Parameter descriptions for Q-value estimations

parameter	*value*
bitrate	10 GHz
Optical band-pass filter bandwidth	100 GHz
n_{sp}	1
gain of optical amplifier	32 dB
extinction ratio of modulator	10 dB
extinction ratio of optical gate	10 dB
optical input power for optical receivers rereceiver	- 27 dBm

When η is unity, optical discrimination has no effect and ASE noise generated by the first amplification contributes to the degradation of the Q values as a whole. But the contribution is reduced for small η. When η equals zero discrimination is complete, and any contribution to the degradation from amplifier α is completely eliminated. The resulting Q values stay high for small η. Naturally, both "1" and "0" level clamping is the most effective. As shown clearly in Fig. 5-2-7, clamping at "1" level only is more effective than at "0" level only. This difference can be attributed to the fact that the dominant noise source is a signal-ASE beat noise component, which is mainly imposed on the "1" level distribution. The Q value converges to a constant at η of around 0.4. At this value, the excess noise terms in Equation 7-15 and Equation 7-16 vanish. Fig. 5-2-8 shows the calculated bit error rate performances by optical discrimination. Assumed parameters are the same as the calculation in Fig. 5-2-7, but the optical input power to the OR is changed. The power penalty is effectively reduced by optical discrimination. I have carried out all-optical discrimination experiment to confirm these qualitative estimations.

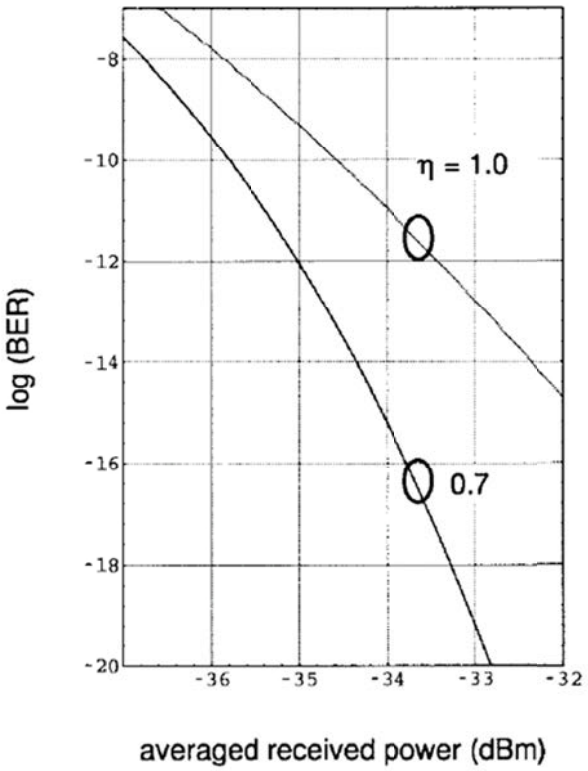

Fig. 5-2-8 Calculated bit error rate performances by optical discrimination

Ultra-fast nonlinear gate: LOTOS

A. Structure

Figure 5-2-9 shows the schematic structure of the LOTOS. The LOTOS comprises an anti-reflection film layer, an InP substrate, an InGaAsP/InP distributed Bragg reflector (DBR) layer, a Be-doped low-temperature-grown strained InGaAs/InAlAs multiple quantum well (MQW) layer, and an Au mirror layer. The reflectivity of the DBR mirror layer is set so that light leaking from the MQW layer in the OFF state is canceled. The optical phase of light reflected by the DBR is adjusted to have relative difference of π against the phase of leaked light. Consequently, the leaked light destructively interferes with the light reflected by the DBR mirror. Therefore, the extinction ratio can be improved by the interference effect. I will discuss the effect of the DBR mirror in Chap. VI.

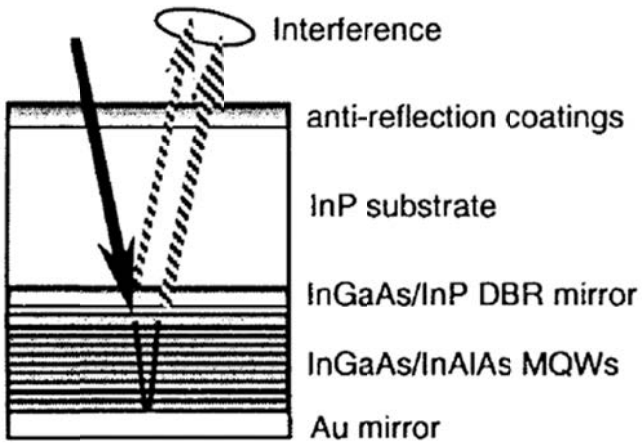

Fig. 5-2-9 Schematic structure of the LOTOS

B. Advantages and Disadvantages of LOTOS

The advantages of LOTOS are transmittance nonlinearity suitable for discrimination, ultra-short carrier lifetime, and a wide wavelength range for operation. LOTOS has ultra short carrier relaxation time, which can be controlled from several hundred femto seconds to tens of pico seconds, and a nonlinear change in transmittance due to the saturation of exciton absorption. Moreover, a high extinction ratio was achieved by using the DBR mirror layer. The operating wavelength range is as wide as 30 nm as a result of the bandwidth of the exciton absorption.

The LOTOS has a polarization dependence originating from the switching mechanism. The relaxation time between two excited spin states which correspond to two circular polarization states of pumping pulse, is several tens of ps. This is substantially longer than the carrier relaxation time of several ps. Therefore, the switching characteristics depend on the polarization state of pump pulses. One way to avoid this dependence is to pump with linearly polarized light. A linearly polarized light is equivalent to circularly polarized light in 50 % of clockwise and counterclockwise directions. Accordingly, there is no polarization dependency for the probe light.

C. Evaluation of LOTOS switching characteristics

Pump and probe pulses were coupled by a wavelength division multiplexing (WDM) coupler and focused on LOTOS by a lens with a numerical aperture (NA) of 0.7. The temporal transmission response of the optical gate was observed with a streak camera having resolution of 2 ps. I used a mode-locked laser diode (MLLD)[69] monolithically integrated with electro-absorption optical intensity modulator to generate pump pulses with 3-6 ps pulse width and gain switched laser to generate pulses with 10 ps width. Wavelengths were 1534.5 and 1565.0 nm for pump and 1530-1570 nm for probe. Probe pulse sources were a 1553-nm gain switched laser diode or a 1552-nm mode-locked laser diode that has the same structure as the pump pulse sources. The experimental setup is shown in Fig. 5-2-10.

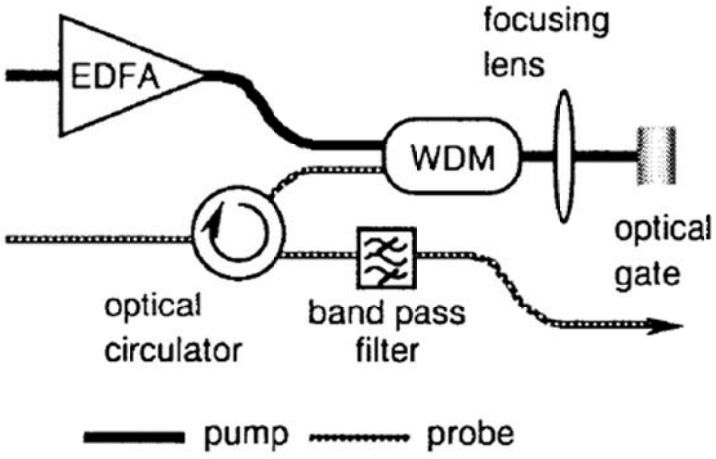

Fig. 5-2-10 Experimental setup

For the measurement of temporal transmittance, I used a 1552-nm continuous wave (CW) light source as the probe light. The extinction ratio of the gate was estimated by the

ratio of the intensity of the gated pulse in the OFF state to their intensity in the ON state, which were measured by a streak camera. The linearity of the response of the streak camera was calibrated by measuring the response count for optical pulses of known intensity. The maximum extinction ratio that can be measured by the method is about 15 dB. Transmittance was obtained by calculating the ratios of the intensity of the reflected probe pulses to the intensity of input probe pulses measured by an optical power meter. Isolation of probe light from pump light was more than 30 dB due to the use of an optical band pass filter.

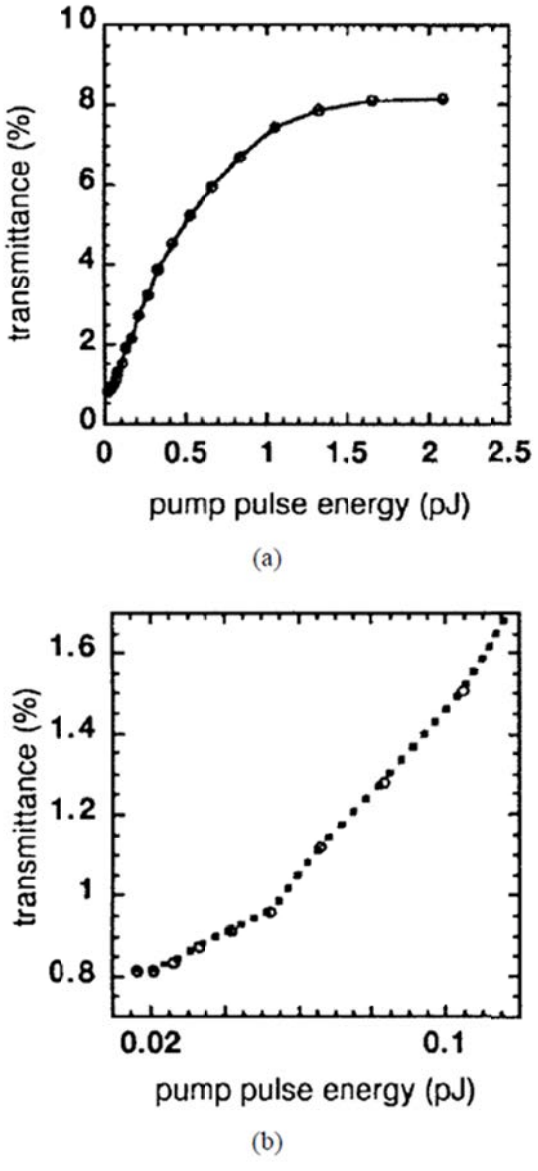

Fig. 5-2-11 Transmittance of the gate

Figure 5-2-11(a) and (b) show transmittance and extinction ratio of the gate against pump pulse energy, respectively. Both the transmittance and extinction ratio increase with increasing pump pulse energy. Transmittance has nonlinearity and abruptly increases at the threshold pump pulse energy. Saturation of transmittance was observed at high pump pulse energies. The estimated value of η is 0.57 for the 2-μm thick LOTOS. Therefore, effective discrimination performance can be expected.

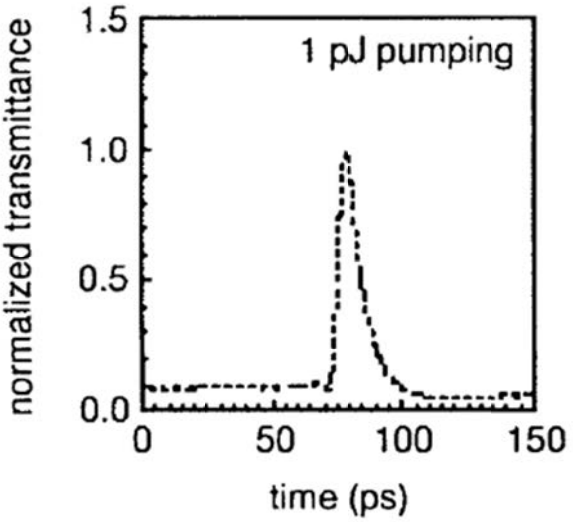

Fig. 5-2-12 Streak camera trace of measured temporal transmittance

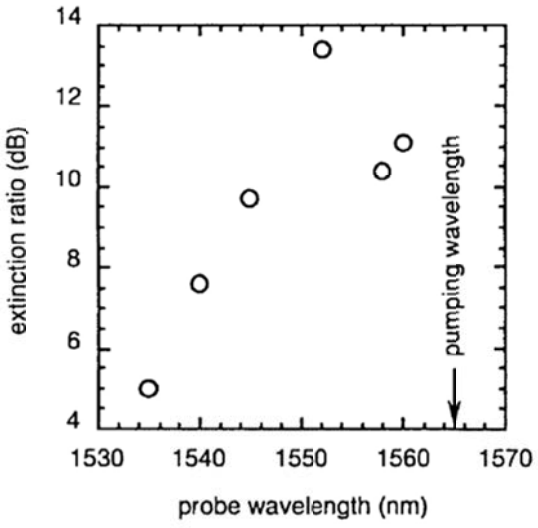

Fig. 5-2-13 Probe wavelength dependence of the extinction ratio

Fig. 5-2-12 shows a streak camera trace of measured temporal transmittance. I have obtained a short response time of 14 ps. The probe wavelength dependence of the extinction ratio was measured by changing the wavelength of the CW light source, and the results are shown in Fig. 5-2-13. The extinction ratio stayed at 10 dB under a wide wavelength range of about 10 nm and reached the maximum at 1552 nm. Therefore, I set the pump and probe wavelengths to 1565 and 1552 nm respectively in the optical discrimination experiments, which will be discussed later.

Experimental results

A. Experimental Setup for Discrimination

The experimental setup is shown in Fig. 5-2-14. I generated optical signal pulses encoded in a 31-stage pseudo random binary sequence (PRBS) by MLLD and lithium niobate (LN) optical intensity modulator. Local clock pulses were generated by another MLLD, which was synchronized with signal pulses using the same reference oscillator. Wavelengths of the signal pulses and the clock pulses are 1565 and 1552 nm, respectively. Pulse widths measured by the streak camera are 6 ps full-width at half-maximum (FWHM) for both. I set the optical pump pulse energy to 1-2 pJ for pumping and 1 x 10^2 fJ for the probe pulse to prevent gating by the energy of the probe pulse. That is, optical gating was achieved solely by pump pulses.

Discriminated signal pulses are separated by the same WDM coupler used at combining, and an additional optical band-pass filter of 3 nm FWHM was used to increase isolation from reflected pump pulses. No less than 30 dB isolation was achieved.

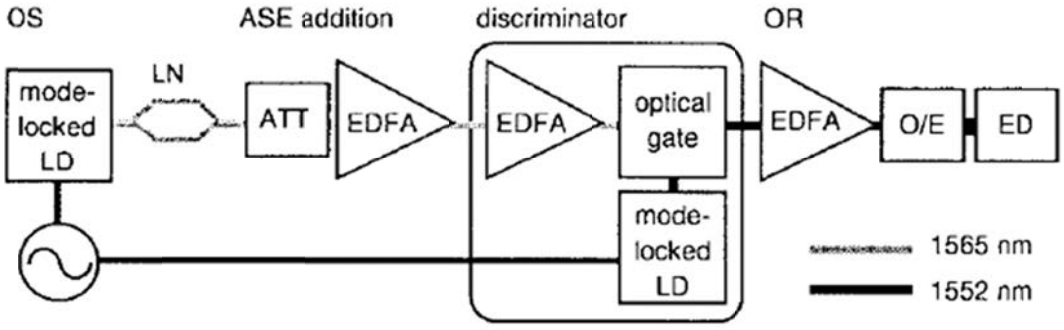

Fig. 5-2-14 Experimental setup

B. Discrimination performance for ASE noise

I examined the optical discriminator's tolerance against ASE noise by changing the amount of ASE noise added to the optical signal. Measured repetition frequencies were 0.6, 2.4, and 10 GHz. Thickness of the MQW layer in the LOTOS were 4, 2, and 1.2 μm.

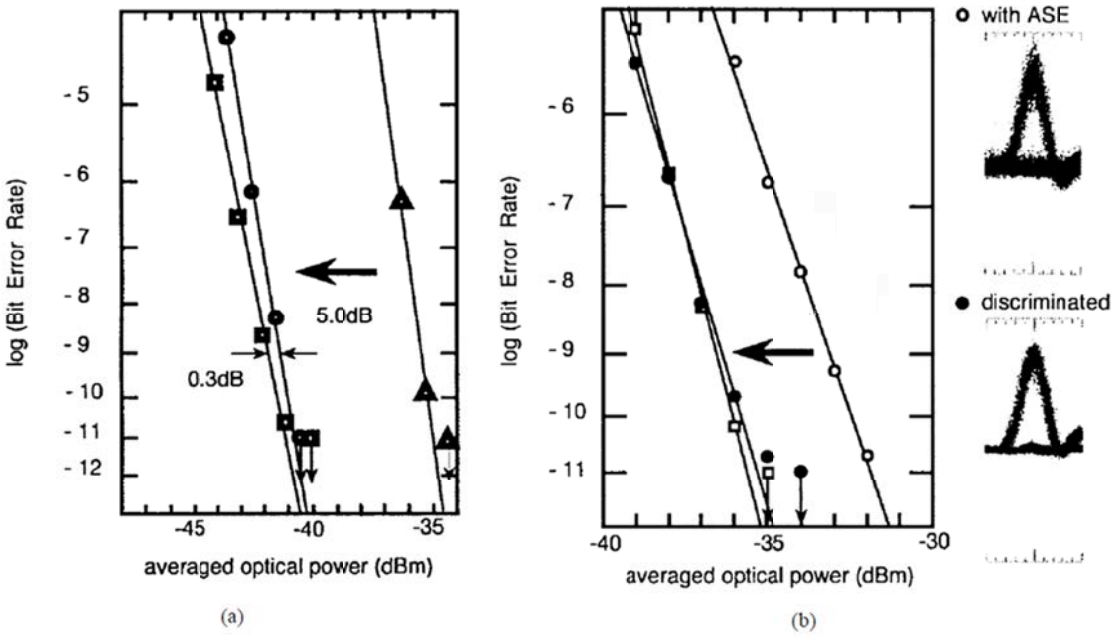

Fig. 5-2-15 Bit error rate at 0.6 and 2.4 Gbit/s and eye diagrams

Figure 5-2-15 shows the bit error rate at 0.6 and 2.4 Gbit/s and eye diagrams before and after discrimination at 2.4 Gbit/s. I measured bit error rates for optical signal pulses generated by the clock pulse source and LN modulator, for ASE added optical signal pulses, and for the discriminated signal pulses, which were ASE added in advance. The receiver sensitivity for the bit error rate of 10^{-9} after discrimination was 3 dB higher than before. The eye diagrams clearly indicate a reduction of ASE originated noise before and after discrimination. These results confirm the qualitative estimation of optical discriminator. Dependence of the sensitivity on pattern length of the PRBS in the range of 7 - 23 stages was not observed in discrimination experiment. Fig. 5-2-16 shows the result of an equivalent experiment at 10 Gbit/s using a 1-μm thick MQW. The regeneration of the S/N ratio by optical discrimination was confirmed at 10 Gbit/s.

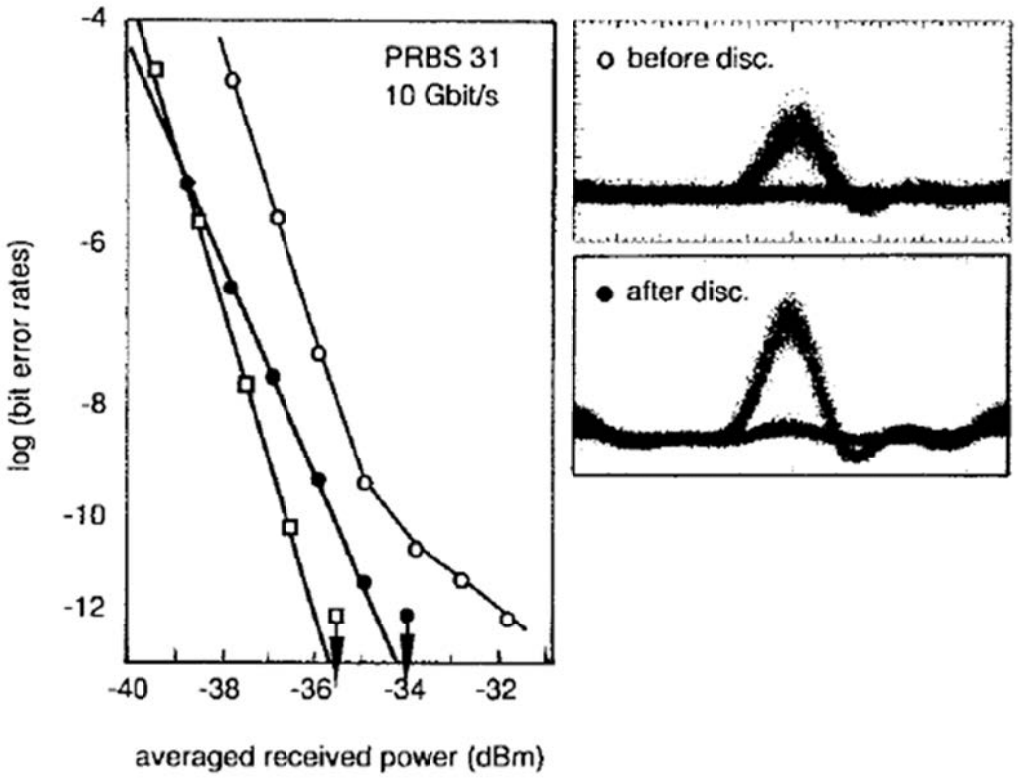

Fig. 5-2-16 Result of an equivalent experiment at 10 Gbit/s

Discussion

A. Nonlinearity and Other Optical Gates

The nonlinearity of optical gates is the key characteristic as I have pointed out in sec. III. As for LOTOS, I have obtained an η value of 0.57, which is effective for all-optical discrimination. Other optical gates, such as SOA-based interferometric optical gates or NOLM-based gates [8-11], have a cosine-like profile in principle. If I apply the same definition of η to those gates, the estimate η value is 0.54. Therefore, I can expect similar discrimination performances for these gates from the viewpoint of the nonlinearity of optical transmittance. The switching energy for LOTOS is around 1 pJ, which was less the value for NOLM or SOA optical gates. The gating window of LOTOS is 14 ps, but the value can be reduced to several hundred fs by controlling of the Be doping level. The intrinsic response time of Kerr nonlinearity, which governs the response time of NOLM-based optical gates is several fs. In SOA-based interferometric gates, the gating window is determined by the relative delay of the set/reset pumping pulse. Therefore, the size of the gating window depends on the pumping pulse width under pumping by pico-second pulses.

The operating wavelength range is about 30-nm for LOTOS. SOA or NOLM gates suffer severe restrictions on operating wavelength in principle. (Maximum repetition frequency will be discussed in sec. VI. B.) The actual size of LOTOS and SOA gates are about several cm, including the focusing optics. In comparison, NOLM are large, and have a long switching fiber and large signal latency. LOTOS gates are quite stable under temperature fluctuations. But SOA gates and NOLM gates need temperature stabilization for normal operation. This is especially true for gates, which require severe temperature control for the switching fibers.

In summary, the advantages of LOTOS are nonlinearity in transmittance, a wide operating wavelength range, an ultra short gating window, low switching energy, compactness, and stability.

B. Repetition Limit of LOTOS

The maximum repetition frequency of LOTOS is limited by the degradation of the transmittance of the optical gate. The degradation can be attributed to the thermal red shift of the absorption edge of the MQW.

Since the optical gate absorbs pumping optical power, absorbed power increases the temperature of the MQW. This could cause severe problems, such as the red shift of the absorption edge. The red shift could bring about extra absorption, which would make the transmittance decrease considerably. Therefore, I have to suppress the temperature rise as much as possible.

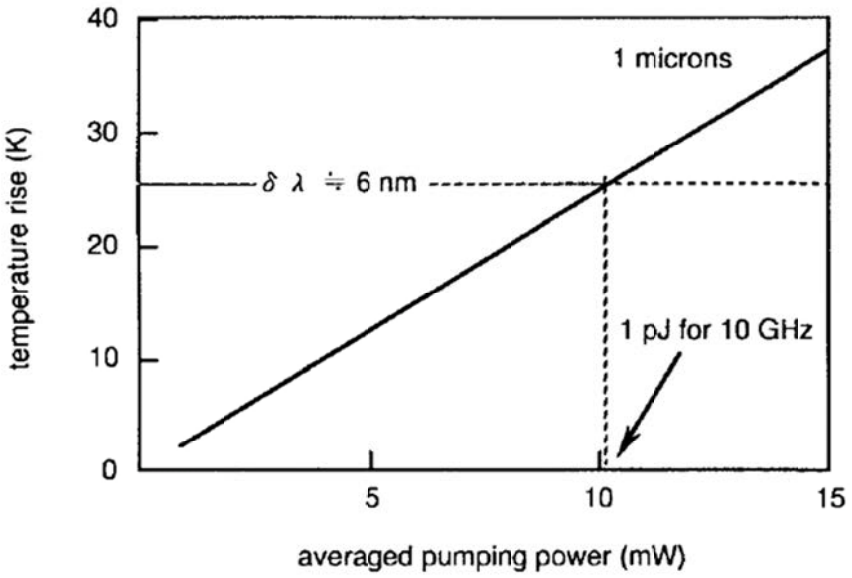

Fig. 5-2-17 Calculated temperature rise at pump-irradiated spot

The amount of absorbed optical power, and the heat resistance and heat capacity of the MQW are dominant factors affecting the temperature rise. Fig. 5-2-17 shows the calculated temperature rise at pump-irradiated spot as a function of averaged pumping power. The calculated temperature rise at the pumping power of 10 mW (1 pJ at 10-GHz repetition frequency) is 25 K for a 1-μm thick optical gate. Such a rise can cause a severe red shift of the absorption edge [70].

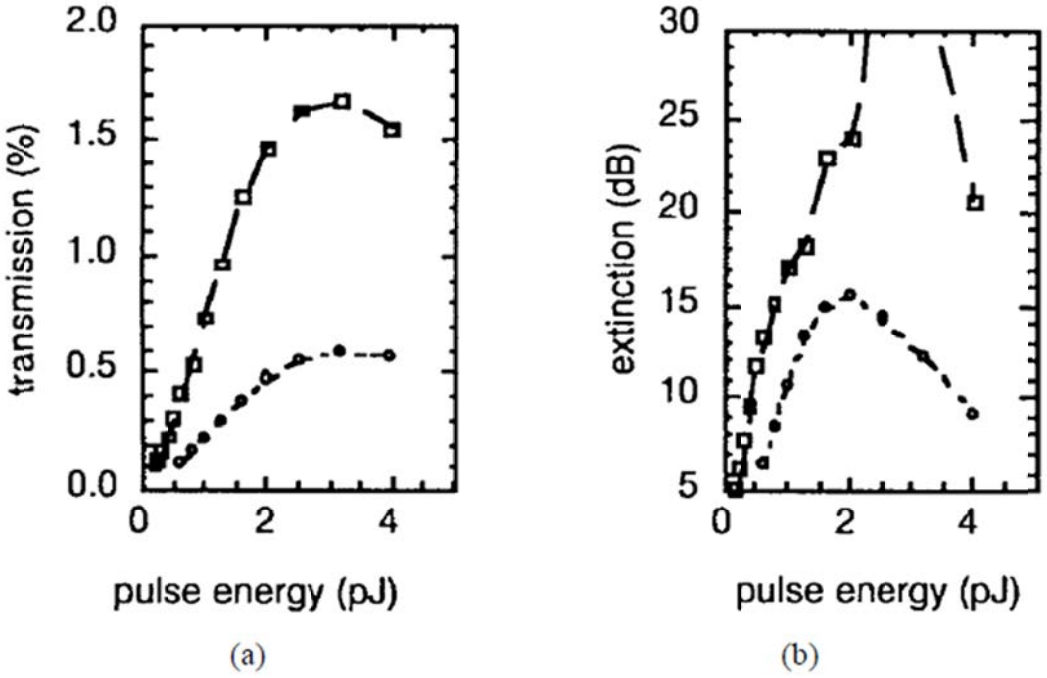

Fig. 5-2-18 Transmittance/extinction ratio of a 2-mm thick gate

This thermal effect was observed experimentally. Fig. 5-2-18 shows the transmittance of a 2-μm thick gate as a function of pump pulse energy for several repetition frequencies. Averaged pumping power is 1.2 mW at 2 pJ of pump pulse energy and 600-MHz repetition frequency. No degradation of transmittance was observed, but transmittance severely degraded at pumping powers above 10 mW at 5-GHz repetition frequency. This degradation could be attributed to the red shift at the absorption edge.

Reducing of switching energy is effective in suppressing the temperature rise that occurs when using thinner MQW layers. However a thinner MQW has a low extinction ratio in the OFF state. Therefore, I insert a DBR mirror layer between InP substrate and MQW layer to compensate for the degradation of the extinction ratio as discussed in sec. VI. C.

Switching energy is proportional to a volume concerning the saturation of absorption, and can be expressed as

$$E_{sw} = V N_c \frac{h c}{\lambda} \qquad \text{Eq. 5-2-22}$$

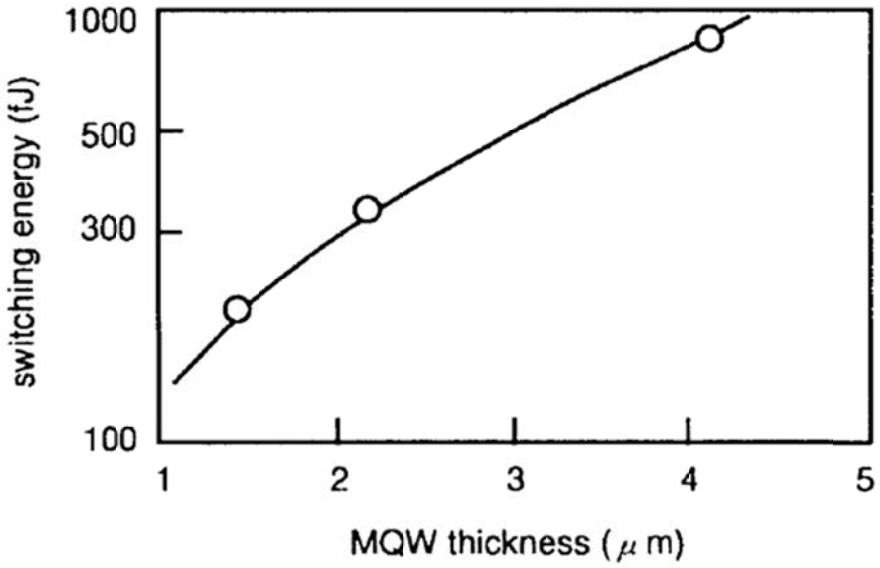

Fig. 5-2-19 Calculated switching energy

Tab. 5-2-5 Parameter descriptions for switching energy estimation

symbol	*meaning*
V	volume concerning a switching
N_c	carrier density needed for absorption
h	Plank constant
c	velocity of light
λ	wavelength of pumping light

Fig. 5-2-19 shows the calculated switching energy (E_{sw}). Table 5-2-5 summarizes the parameters used in this numerical estimation. Experimental values are plotted as a function of MQW thickness on the curve. The refractive index of the MQW layer is assumed to be 3.3. The volume (V) is a function of the irradiating spot radius and MQW layer thickness. The carrier density (N_c) required for a saturation of absorption is assumed to be 5×10^{17} cm^{-3}. Experimental E_{sw}'s are defined as the pump pulse energy required to achieve a 10-dB

extinction ratio, and they agree well with calculated values. This means, I have succeeded in the reduction of a switching energy. The reduction of E_{sw} relaxes the degradation of transmittance and enables 10 Gb/s operation. Further improvement of repetition frequency is expected by reducing E_{sw}, improving heat transfer, and cooling the MQW.

C. Optical bandwidth of LOTOS

I define the optical bandwidth of LOTOS as the wavelength range in which a high extinction ratio is maintained. The bandwidth is determined by MQW thickness and the absorption coefficient in the OFF state.

As I have pointed out in sec. IV. A. The DBR mirror layer is designed so that the intensity of reflected light from the DBR is equal to the intensity of light leaking from unsaturated MQW and so that the relative phase difference between the two light waves is $(2n - 1)\pi$ ($n = 1, 2, 3, \ldots$). Provided that the thickness of MQW and absorption coefficient in the OFF state is given, I can calculate the optimum reflectivity for the maximum extinction ratio.

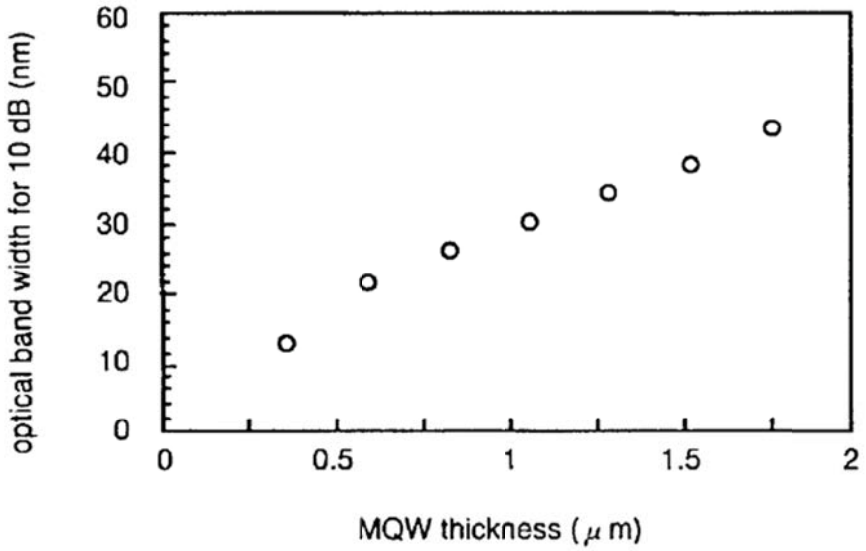

Fig. 5-2-20 Calculated bandwidth for more than a 10-dB extinction ratio

As I increase DBR reflectivity, multiple reflection of the light wave between the DBR and Au mirror will be effective in the ON state. Therefore, the optical bandwidth of high extinction ratio will decrease by this cavity effect. In other word, a Fabry-Perot cavity will be formed between the two layers. Fig. 5-2-20 shows the calculated bandwidth for more than a 10-dB extinction ratio. As I reduce MQW layer thickness, the bandwidth decreases. The bandwidth is 30 nm for a 1-μm thick MQW.

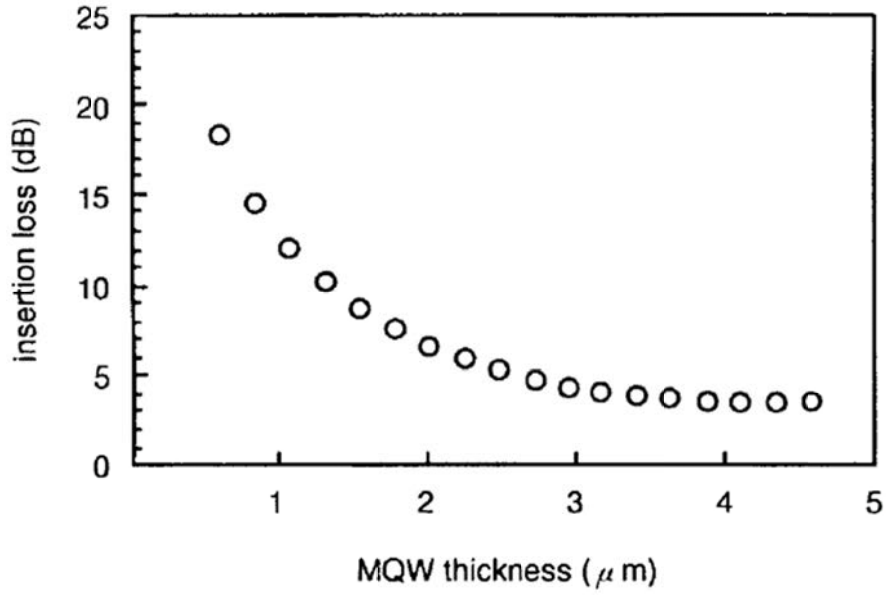

Fig. 5-2-21 Insertion loss as a function of MQW thickness

Even in the ON state, the gated light wave will be partially eliminated by destructive interference with the light wave reflected by the DBR mirror. The degradation of transmittance can be treated as an extra insertion loss. Fig. 5-2-21 shows the insertion loss as a function of MQW thickness. I optimized the reflectivity of the DBR mirror for each thickness in the calculation. The insertion loss increases with decreasing MQW thickness. In order to ensure the insertion loss is no more than 15 dB, the thickness of MQW layer should be no less than 1 μm. The optimized reflectivity is 13 % for 1 μm.

D. No wavelength change configuration

LOTOS is a surface-reflection-type optical gate. Therefore, I can separate the pump and probe pulses by their spatial trajectory using multiple input/output port lenses. Each isolated lens has the same focusing spots. Pump and probe lays have their own isolated trajectory but the same spot on the optical gate. Therefore, I can use the same wavelength for pump and probe pulses. There is no need for WDM couplers, optical band pass filters, or fiber Bragg gratings for channel separation. Because I have to share the N.A. for input/output ports, the maximum effective N.A. must be smaller than that for the single port WDM configuration. For optical regenerative repeaters, the wavelength of pump and probe pulses should be the same to achieve cascadability of regenerators. Therefore, it is important to realize the multi-port optics.

Section summary

In this section, I have proposed an all-optical discriminator having a nonlinear optical gate, and introduced performance parameters to quantify the discrimination performance of the gates. The clamping parameter η primally determine the discrimination performance. The η value for existing optical gates, such as NOLM and LOTOS, were estimated to be about 0.6. A simplified theoretical estimation using the parameters revealed that the discriminator can regenerate optical signal pulses and consequently suppress the ASE-noise-induced degradation of SNR sufficiently with the η values. In the estimation, the clamping at the "1" (mark) level of PDFs was more effective for recovery of SNR than at the "0" (space) level in the usual case where signal-ASE beat noise is a dominant noise source. I examined the discrimination performance experimentally utilizing the MQW optical gate, and confirmed the suppression by the reduction of the ASE-noise-induced power penalty at 0.6, 2.4, and 10 Gbit/s.

Summary of section 5

In sections 5.1 and 5.2, I proposed novel methods to mitigate OSNR impairment for upgrading transmission capacity.

One of the fundamental issues to improve OSNR in optical receiver with optical amplifiers is signal-ASE beat noise as I discussed in section 1.

In section 5.1, I proposed to utilize nonlinear phase matching in fiber four wave mixing process to suppress signal-ASE noise, since nonlinear phase matching induces nonlinear response in transmitting pumping wave. I used the nonlinear response to suppress the signal-ASE beat noise. I have designed the wavelength assignment for pumping wavelength and zero dispersion wavelength of optical fiber to maximize the nonlinear response. Then I evaluated the performance in experiment and confirmed the noise suppression performance by measuring eye diagram and bit error rates before and after the suppression.

In section 5.2, I have extended my approach to suppress not only signal-ASE noise but also timing jitter and waveform distortion in optical signal. I have proposed signal regenerator circuit with optical nonlinear gate. I have also modeled optical signal regenerator and calculated probability density function of photon number through the regenerator. I found non-Gaussian distribution after the nonlinear optical gate approaches Gaussian distribution by optical amplification and confirmed that we can apply Gaussian model when we use optical amplifier with sufficient gain after the nonlinear optical gate. In addition to that, I have evaluated SNR recovery performance both numerically and experimentally.

The contributions in sections 5.1 and 5.2 pioneered novel all-optical signal-ASE beat noise suppression. As of 2018, signal regeneration has been carried out by electrical digital circuit as usual. However, as transport capacity expands, power consumption of regenerator circuits will also inevitably increase. So to avoid energy catastrophe, some lower power dissipation approaches such as all-optical ones may have potential impact in the near future.

6. Approaches toward wider bandwidth WDM

6.1 Dispersion slope compensation

Background

40-Gbit/s/ch wavelength division multiplexing (WDM) is an attractive technique to increase overall transmission capacity toward future terabit/s networks [71-74]. However, in this case, a dispersion compensation and a guarantee of sufficient power margin for each 40-Gbit/s channel are essential to realize such high capacity WDM system.

Such large capacity WDM system required simultaneous broadband compensation of dispersion and dispersion slope. The complete broadband compensation of dispersion and dispersion slope of standard single-mode-fiber (SMF) was first tested in 40-Gbit/s/ch WDM transmission experiment [15] using reverse-dispersion-fiber (RDF). In case of DSF, however, it is difficult to realize such simultaneous compensation by using DCF because of its low dispersion per slope value.

In this section, I demonstrate 640-Gbit/s (16 ch x 42.7 Gbit/s) WDM transmission experiment over 100 km DSF using 25-nm bandwidth dispersion slope compensator that can exactly compensate the dispersion slope of DSF.

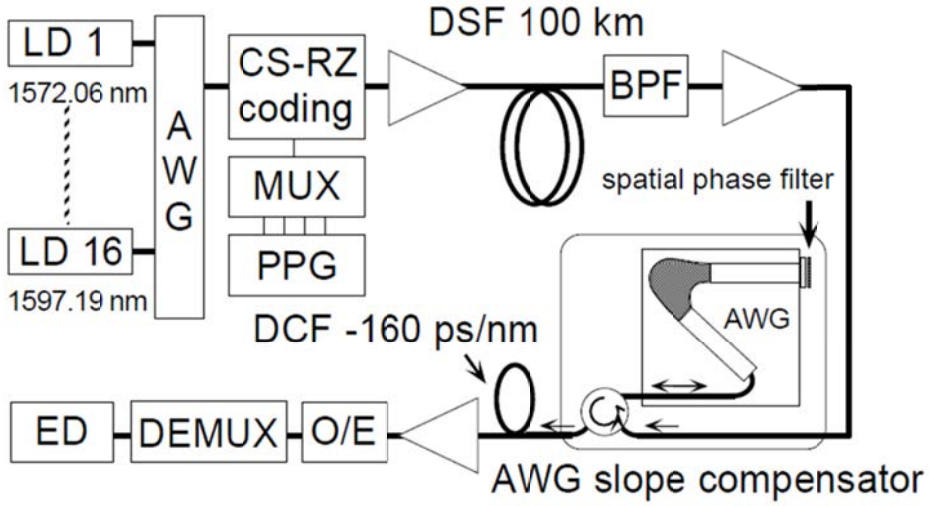

Fig. 6-1-1 Setup of the 16-ch WDM transmission experiment

3.2 THz bandwidth slope compensator

Dispersion slope compensator based on time-space conversion consists of arrayed-waveguide-grating (AWG), and a spatial filter [75] as shown in Fig. 6-1-1. Dispersion compensation is performed by decomposing the input waveform into its frequency components, modulating the phase of each component by a spatial phase filter, and reforming the waveform by combining the components. To compensate a dispersion slope of DSF, I designed and fabricated the spatial phase filter. Figure 6-1-2 shows the dispersion of the fabricated compensator. It has 0 ps/nm of dispersion at 1584.5 nm of wavelength that compensate only dispersion slope. The obtained slope was -7.1 ps/nm^2 that can compensate dispersion slope of 100 km of DSF.

16-ch x 42.7-Gbit/s WDM transmission experiment

Figure 6-1-1 shows the setup of the 16-ch WDM transmission experiment. 200-GHz-spaced 16 continuous wave (CW) light from laser diodes (LD) with wavelength ranging from 1572.06 nm (190.7 THz) to 1597.19 nm (187.7 THz) were simultaneously modulated and encoded into 42.7-Gbit/s carrier-suppressed return-to-zero (CS-RZ) format [31] having a word length of a 23rd-order pseudo random binary sequence (PRBS). For the CS-RZ encoding, two low-driving-voltage LiNbO3 (LN) Mach-Zehnder modulators [25] were used and driven by 42.7-Gbit/s electrically multiplexed signal generated by InP HEMT ICs [27] and a 21.4-GHz clock, respectively.

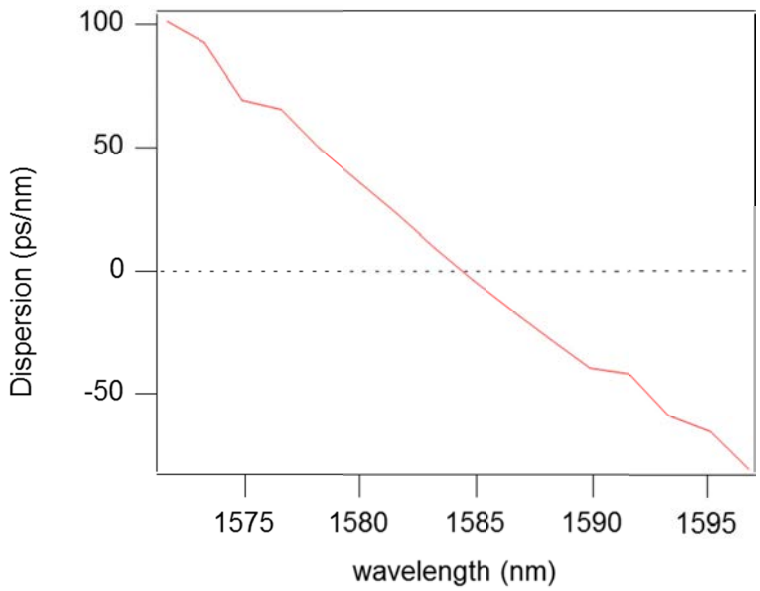

Fig. 6-1-2 Chromatic dispersion of the slope compensator

The encoded optical signal was amplified by a fluoride based erbium-doped fiber amplifier (EDFA) and was launched into 100 km of DSF. The fiber input power was set at +6.0 dBm/ch and +18.0 dBm in total. Since the CS-RZ code is tolerant with respect to the self phase modulation (SPM) of the transmission fiber, the optimum dispersion is kept around 0 ps/nm of dispersion at high fiber input power [76]. The transmitted signal was amplified, and one of the 16 channels was selected by the 1-nm bandwidth optical band-pass filter (OBPF). Then the dispersion slope and dispersion were individually compensated by the slope compensator which has the dispersion characteristics as shown in Fig. 6-1-2 and -160 ps/nm of DCF. The compensated signal was O/E converted and demultiplexed into 4x10-Gbit/s binary sequences for error detection after the final EDFA.

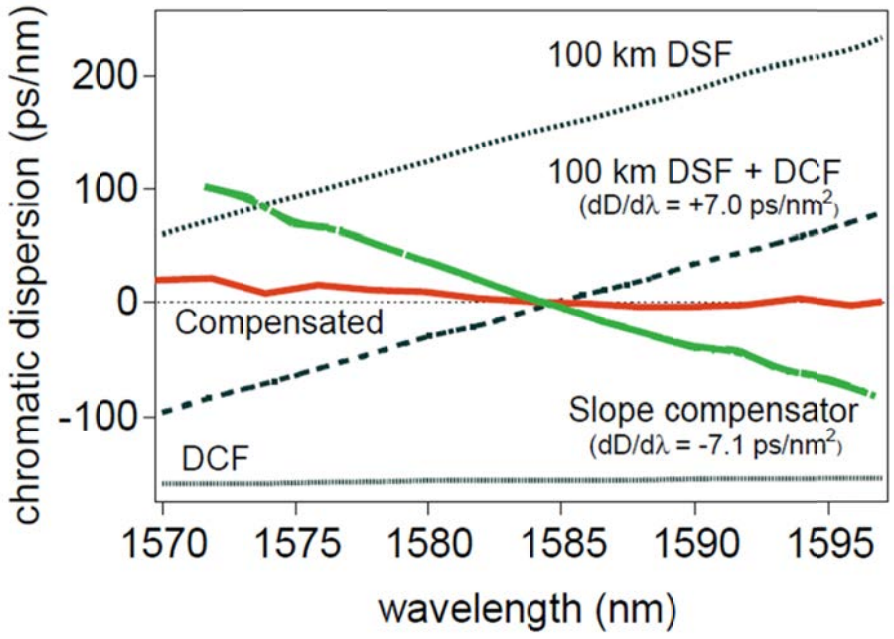

Fig. 6-1-3 Dispersion of 100 km DSF with both the dispersion slope compensator and DCF

Figure 6-1-3 shows the dispersion of 100-km DSF with both the dispersion slope compensator and DCF. Dispersion slope compensator based on time- space conversion consists of arrayed-waveguide-grating (AWG), and a spatial filter [75]. Dispersion slope compensation is performed by decomposing the input waveform into its frequency components, modulating the phase of each component by a spatial phase filter, and reforming the waveform by combining the components. To compensate a dispersion slope of DSF, I designed and fabricated the spatial phase filter. The measured dispersion slope of the compensator was -7.1 ps/nm^2 that can compensate the dispersion slope of 100 km of

DSF. The dispersion of only 100 km DSF, only DSF, only the slope compensator, and 100 km DSF with DCF are also shown in the figure for comparison. The residual dispersion was less than 10 ps/nm maximum in 25-nm bandwidth.

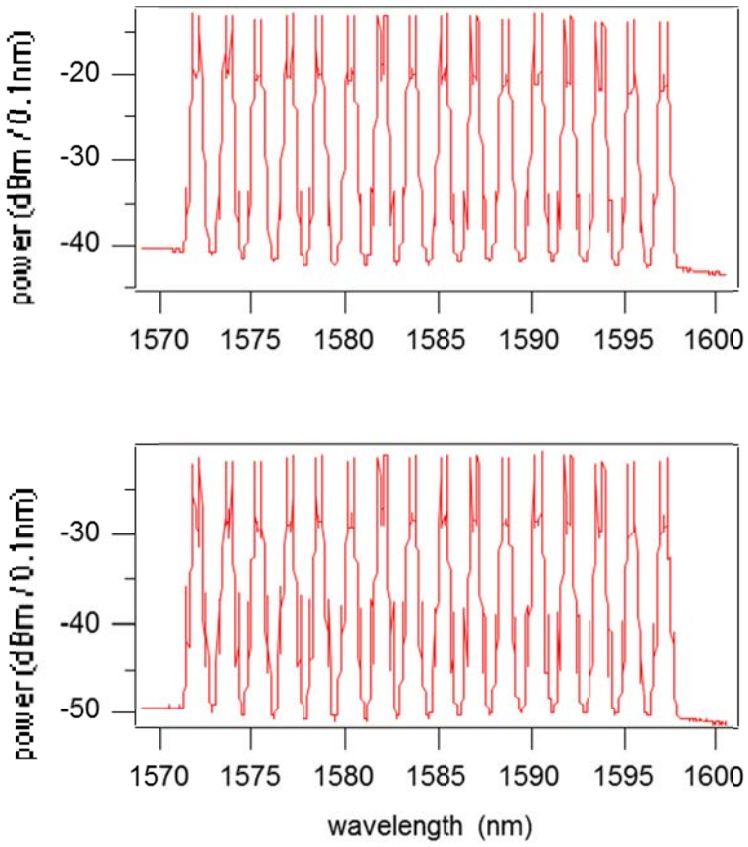

Fig. 6-1-4 Optical spectrum before and after transmission

The optical spectrum before and after transmission were shown in Fig. 6-1-4. I observed no four-wave-mixing (FWM) component, and signal-to-noise ratio (SNR) was sufficiently high after transmission.

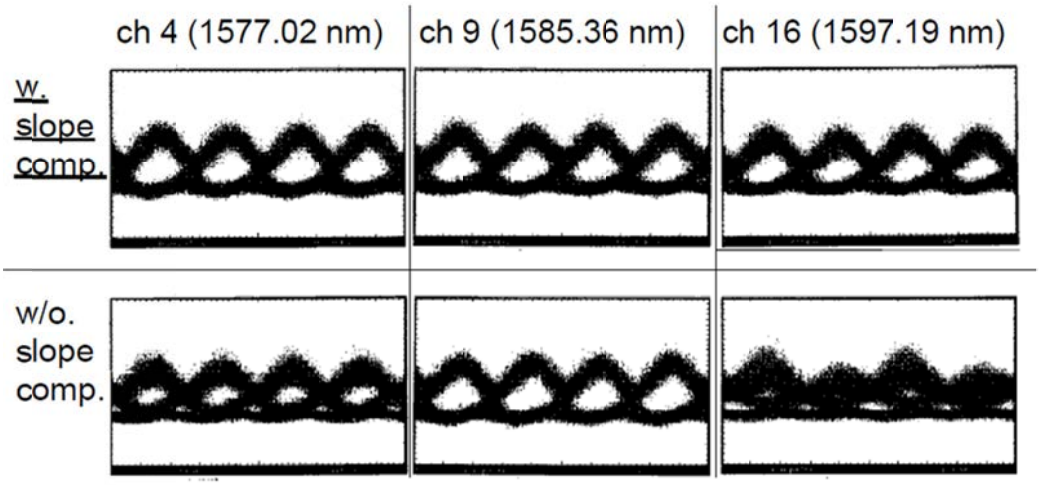

Fig. 6-1-5 Eye diagrams after transmission

Figure 6-1-5 shows the eye diagrams after transmission with and without the slope compensator. With slope compensation, a clear eye-opening was achieved as shown at left side. On the other hand, the eye-opening was severely degraded without slope compensation, except in the center wavelength region (ch 9). The measured receiver sensitivity is plotted in Fig. 6-1-6.

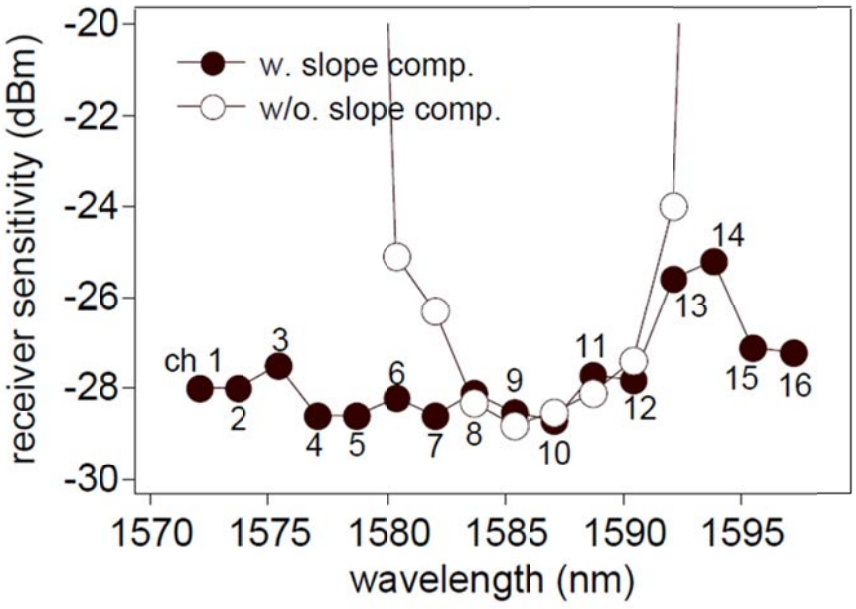

Fig. 6-1-6 Measured receiver sensitivity

All 16 channels could be transmitted when the slope compensator was included in the receiver. On the other hand, only the center wavelength region could be transmitted when there was no slope compensation. These results shows that 25-nm bandwidth dispersion and dispersion slope compensation in L-band DSF can be confirmed in 640 Gbit/s (16 ch x 42.7 Gbit/s) WDM configuration.

Section summary

A 25-nm bandwidth dispersion slope compensator based on time-space conversion using AWG was described. I investigated 640 Gbit/s (16 ch x 40 Gbit/s) DSF 100 km L-band transmission using the slope compensator in the receiver. All 16 channels were successfully transmitted with the compensator in place.

6.2 Optical virtual concatenation

Background

Parallelism is now penetrating into cutting edge applications, computers, and photonic networks to overcome the performance limitations resulting from using a single machine, single chip, or single lambda. The Scalable Adaptive Graphics Environment (SAGE) application developed at EVL accommodates 55 LCD displays driven by a 30 node cluster of PCs with the graphics rendering capacity approaching nearly a Tb/s. The high-end linux cluster BlueGene, installed at Lawrence Livermore National Laboratories (LLNL) and developed by IBM has 65536 PowerPC processors and 1152 GbE ports to communicate to other clusters. It is clear therefore that high-end applications and clusters need Tb/s capacity for their interconnections. I propose that an OXC-enabled photonic network will be the most promising way to realize TERAbit-LAN [77-79]. There is a large number of on-going activities [80-82] evaluating and promoting photonic networking. The OMNInet testbeds covers various kinds of applications including actual production services [81]. I can find a sophisticated classification of such photonic network solutions in [82]. Among various kinds of users, the TERAbit-LAN project aims to meet high-end interconnection requirements with high reliability and reasonable cost.

To meet high-end Tb/s class demand, parallelism as mentioned above will play an important role. Around the year 2006, the I/O capacity of a PC is limited to 10GbE. Thus multiple Network Interface Cards (NICs) will inevitably be required to support such demand. Even in a single PC, the PCI Express x32 interface which has 32 parallel lanes (each lane supports about 2 Gb/s) supports 64 Gb/s of capacity that exceeds the capacity of a conventional 10GbE NIC. On the other hand, the number of parallel wavelengths in a DWDM transport system is approaching and will exceed 100 channels. This suggests that new schemes or mechanisms to manage multiple parallel NICs and transport through photonic networks will be essential to ensuring high throughput over LAN or WAN.

The TERAbit-LAN project aims to develop such schemes or mechanisms to realize photonic networks that are tuned to accommodate terabit capacity communications which consist of a large number of parallel channels.

The TERAbit-LAN

Figure 6-2-1 shows a conceptual diagram of TERAbit-LAN. Three key components are needed: core optical cross connect switches (OXCs), transmission links, and end-interfaces. In this Figure, I have shown a star-topology as the simplest example, this is by no means a constraint of the overall framework. In this configuration, parallelism plays an important role in photonic switching and transport. The end-systems generate flows of traffic in parallel and request parallel connections to target remote interfaces. The TERAbit-LAN accepts parallel connection requests and allocates parallel lambdas or parallel L2 connections and configures the OXC to establish dedicated parallel connections between these two end-interfaces.

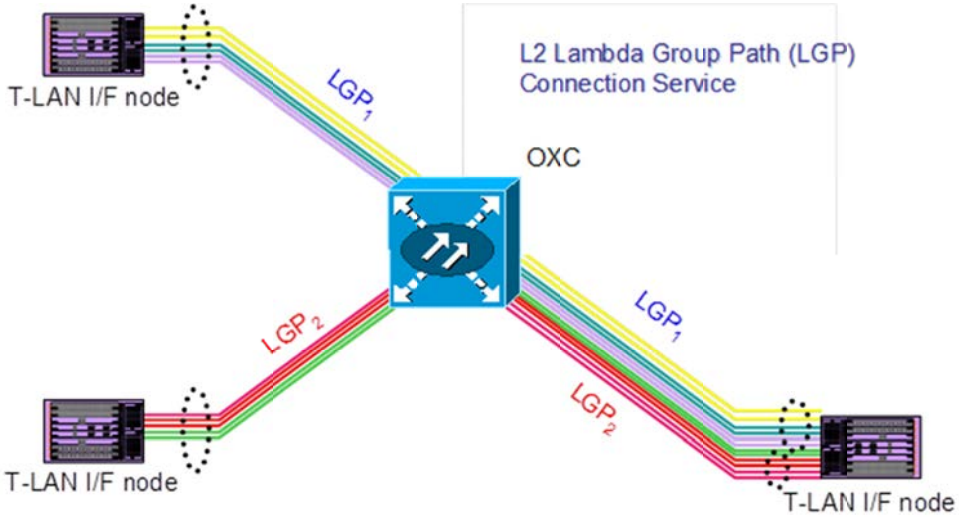

Fig. 6-2-1 Conceptual diagram of TERAbit-LAN

The First of the three key components is the OXC. I have developed an OXC prototype to serve as a core switch for TERAbit-LAN as shown in Figure 6-2-2 [83], in which an 8 x 8 Planar Lightwave Circuit (PLC) optical switch is equipped [83]. It supports various kinds of interface for both Network Node Interface (NNI) and User-Network Interface (UNI), and has a supervisory and control unit for management and signaling communication with Generalized Multi-Protocol Label Switching (GMPLS) capability within the Control-plane (C-plane). The interface cards can accommodate both 10GbE LAN-PHY, OC-192 (10GbE WAN-PHY). These incoming signals will be converted into 10G OTN signal (OTU2) format in the cards and launched into PLC optical switch. So all the optical switching will be done in OTN format.

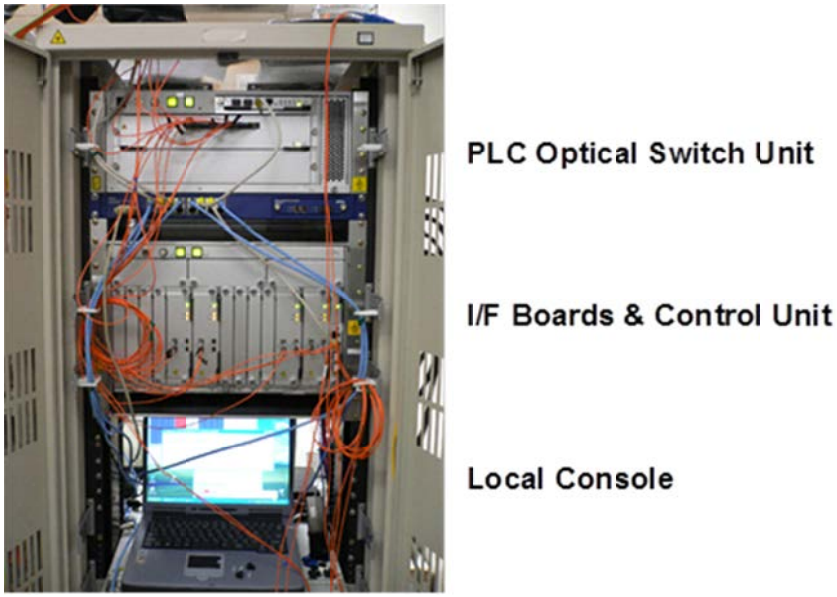

Fig. 6-2-2 OXC prototype

In order to realize 1Tbit/s capacity switching on an OXC based on 10GbE channels, I have to handle 100 channels or lambdas at the same time, and switch these lambdas individually. However, it appears impractical to extend the switching matrix to such high dimensions as it would be expensive, difficult to control, and unreliable.

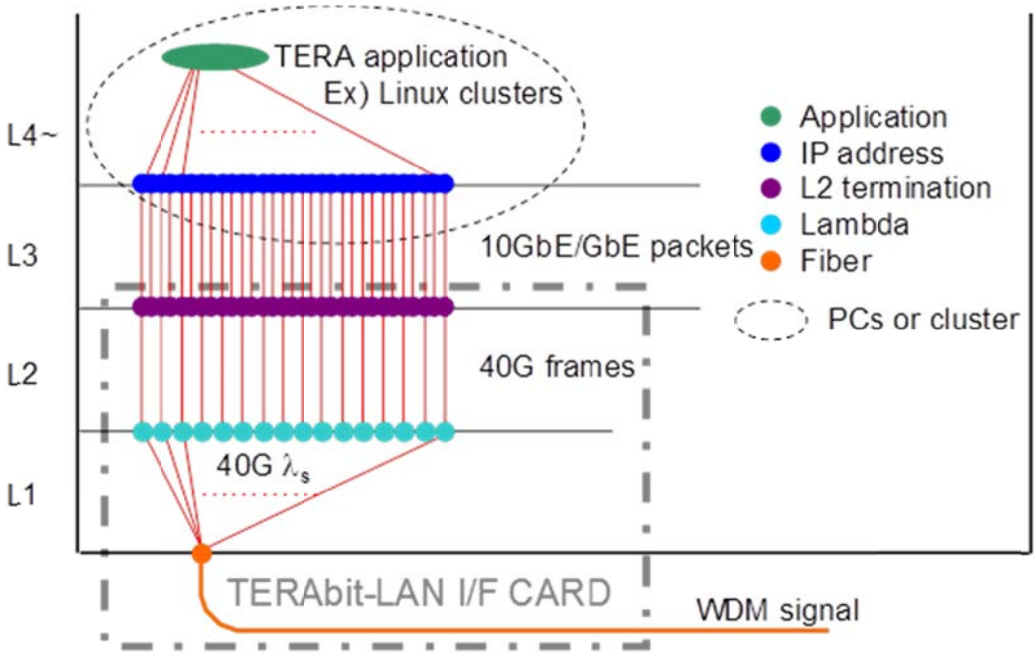

Fig. 6-2-3 Hypothetical TERAbit-LAN application

Figure 6-2-3 shows a hypothetical TERAbit-LAN application represented on a simplified OSI layer diagram from the viewpoint of future high-end applications. As I have described in the introduction, some high-end Grid applications (large-scale cluster computing, high-end visualization and, etc) require bandwidth which exceeds the maximum capacity of a single NIC. Inevitably, multiple NICs have to work together to meet such requirements. Since these NICs serve from a single application, I believe they should be concatenated to ensure the best performance for the application. These NICs will generate multiple lambdas for a single application. Therefore, these lambdas will be expected to be used as a group of lambda in a limited number of optical paths. These grouped lambdas should hence be switched and transported as a single path to simplify the switching complexity and to reduce cost.

The Terabit-LAN/WAN focuses on this parallelism in switching and transport of multiple lambdas. To realize parallel switching of these multiple lambda, Terabit-LAN/WAN adopts lambda group switching and establishes and the notion of a lambda group path (LGP). High-end application users would require multiple lambdas as a whole for their clusters, so a Terabit-LAN/WAN switch would provision and establish an LGP upon request of these applications. The number of lambdas in each LGP will be determined and provisioned by such applications. The Terabit-LAN/WAN switches these LGPs as a single end-to-end optical path. In comparison with the case where one would switch all the lambdas individually, LGP-based optical switching only requires a switching matrix dimension no larger than the number of LGPs. For example, when I switch 100 lambdas individually, I need roughly a 100 x 100-dimenstion optical switch. However, when I assume 10 lambdas can be grouped as an LGP, I need only a 10 x 10-dimenstion optical switch. LGP scheme could therefore reduce switching complexity, the load of the operating system, and consequently Capex/Opex of the photonic network system.

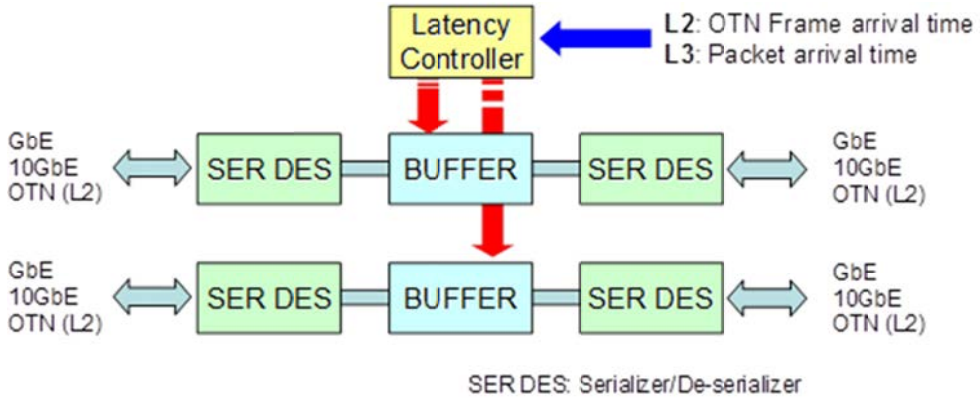

Fig. 6-2-4 Schematic configuration of an OVC circuit

The second key component is a transport or link system to support parallel lambdas. From the viewpoint of parallel transport of 10GbE/GbE lambdas over Terabit-LAN/WAN, relative latency deviations in each LGP could be a serious hindrance towards achieving high quality of service. This relative latency can arise for numerous reasons such as optical path diversity or group velocity dispersion in optical fibers. To overcome such issues, I have developed OVC (Optical Virtual Concatenation) [77]. The schematic configuration of an OVC circuit is shown in Figure. 6-2-4. It consists of serializer/de-serializer circuits, memory buffers, and a latency controller. The latency controller detects relative latency deviation among OTN frame arrival times for L2 implementation or Ethernet packet arrival times for L3 implementation. It is an analogous to virtual concatenation in SDH/Sonet. I have extended it to multiple lambdas with the aid of ITU-T G.709 OTN [29]. OVC can be realized in L2 by OTN (Optical Transport Network) function as defined in ITU-T Recommendation G.709. OVC can completely compensate for the aforementioned relative latency deviations to achieve virtual terabit bulk transport. I can achieve OVC accuracy of a single bit or timeslot (e.g. 0.1 ns for 10Gb/s). OVC functionality can be realized also in L3. For this implementation, relative deviation of packet arrival time could be used to de-skew each channel to provide virtual bulk transport. However, the accuracy of OVC in L3 will degrade to milliseconds. With the help of OVC, visualization applications, clusters, and high-end PCs will not suffer any impairment that could result from the relative latency deviation in a single LGP.

The third key component of TERAbit-LAN consists of the end-interfaces. Around the year 2006, GbE/10GbE interface cards are a popular interconnect for PCs or clusters, and of course these cards can be used to connect to TERAbit-LAN. OVC functionality can be achieved in L3 by monitoring the relative latency deviation of packet arrival or Round-Trip

Time. However I also hope to develop a TERAbit-LAN card solution (Figure 8-3). The solution accepts L2 connections or lambdas into one TERAbit-LAN card and can generate a WDM signal intended for an OXC node.

The capacity of a single channel is approaching 40Gb/s, and we have developed a 40Gb/s link system which is fully compliant with the ITU-T G.709 standard [45]. The system can accept both GbE and 10GbE clients and transport by using advanced modulation schemes [31] with automatic group velocity dispersion (GVD) compensation [84, 85] which ensures highly reliable operation of the system. In the near future, TERAbit-LAN will employ LGP-enabled OXC, 40 Gbit/s/ch links with OVC, and will accept multiple 10GbE channels as a single link.

The Scalable Adaptive Graphics Environment (SAGE)

The Scalable Adaptive Graphics Environment (SAGE) [86-88] is a middleware system for managing visualization and high-definition video streams for viewing on ultra-high-resolution displays such as EVL's 100 Megapixel LambdaVision tiled LCD display wall. SAGE consists of Free Space Manager, SAGE Application Interface Library (SAIL), SAGE Receiver, and User Interface (UI client) as shown in the figure 6-2-5. The Free Space Manager gets user commands from UI clients and controls pixel streams between SAIL and the SAGE Receivers. SAIL captures output pixels from applications, and streams them to appropriate SAGE Receivers. A SAGE Receiver can get multiple pixel streams from different applications, and displays streamed pixels on multiple tiles. Remote visualization applications (such as 3D rendering, remote desktop, video streams, and large 2D maps) stream their rendered pixels (or graphics primitives) to SAGE, allowing for any given layout onto the displays (e.g. the output of arbitrary M by N pixel rendering cluster nodes can be streamed to X by Y pixel display screens).

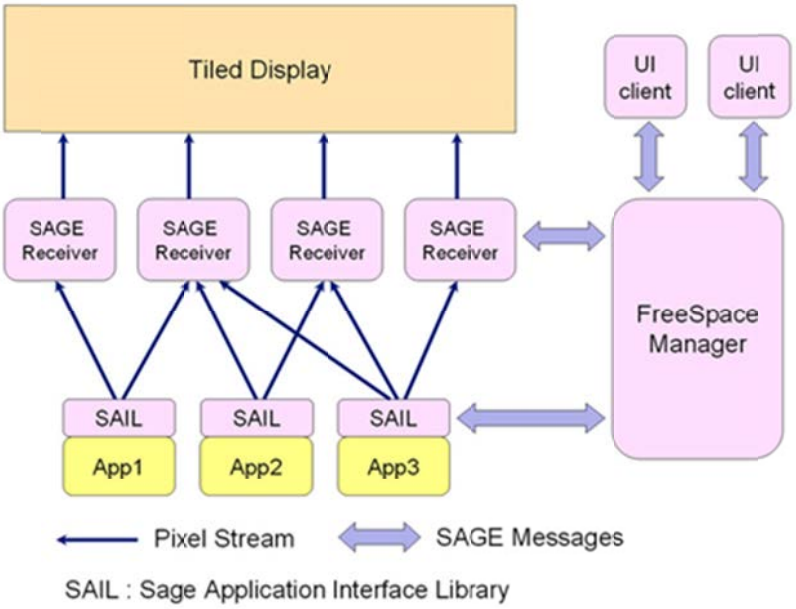

Fig. 6-2-5 The Scalable Adaptive Graphics Environment

The Technology and iGrid Real-time Demonstration

I. Network configuration

Figure 6-2-6 shows the network configuration for the demonstration. The SAGE sender PC is placed in EVL/Chicago and generates two parallel GbE video streams from its two GbE NICs. Each stream consists of half of a 3200x1200 graphics animation. GbE vlans were set up from EVL to iGrid so that each of the streams followed decidedly different network paths to reach their destination. To demonstrate OVC functionality in an LGP, and to demonstrate its path restoration capability, I installed our OXC system at EVL. The L2 switch accepts GbE channels and maps them into 10GbE LAN-PHY signals. Then the 10GbE signals were converted to G.709 OTU2. Optical switching is performed on the OTN signal. The switched OTN signal was converted back into 10GbE LAN-PHY and then into GbE signals.

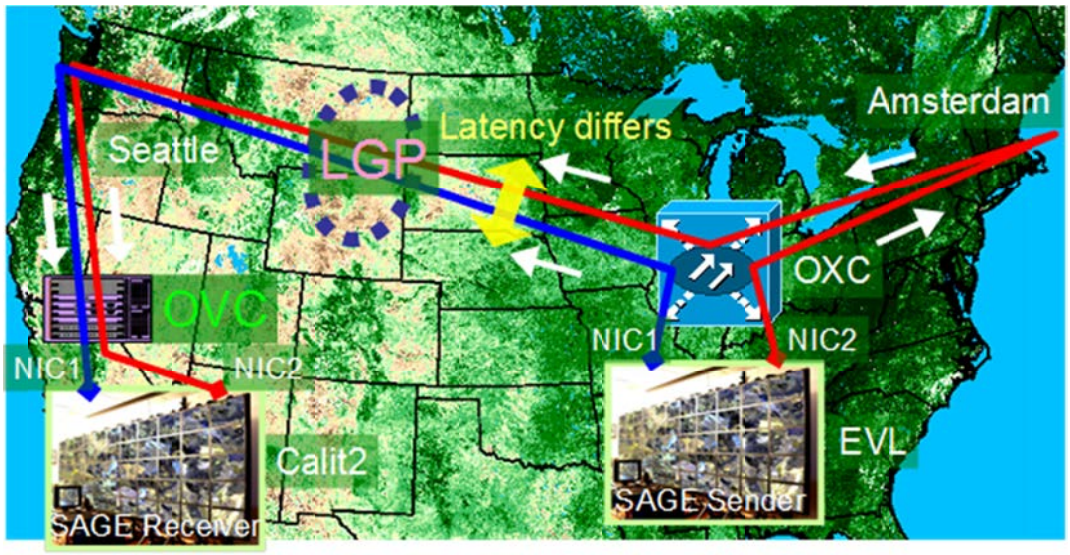

Fig. 6-2-6 Network configuration for the demonstration

Under normal conditions, these two GbEs would be transported to iGrid on two vlans (3707 and 3708) over CAVEwave. Thus there is no relative latency difference between the two links. The SAGE receiver PC would then stitch together the two halves of the image for display.

In the event of a fault in a GbE link, the OXC could switch to a restoration path to save the channel (the restoration path is provisioned in advance.) For this demonstration, I prepared entirely different paths (one through Amsterdam, but both originating from EVL) with significantly differing latency to show that OVC was able to transparently resynchronize the two flows. I also installed a network emulator which was kindly provided by Anue Systems Inc. for my demonstration to simulate expected latency from Amsterdam, should the real link fail during the workshop.

II. OXC system

The configuration of the OXC system used in the demonstration is shown in Figure 6-2-7. It consists of an 8 x 8 switching unit, 10GbE LAN-PHY interface cards, GMPLS-enabled control unit, and a L2 switching unit. The L2 switch accepted GbE client signals and mapped them into 10GbE LAN-PHY signals. Then the 10GbE signal was passed to the OXC I/F card which converted the incoming 10GbE LAN-PHY signal into 10G OTU2 signal which is

compliant with ITU-T G.709 standard. All the optical switching was carried out as an OTN standard signal.

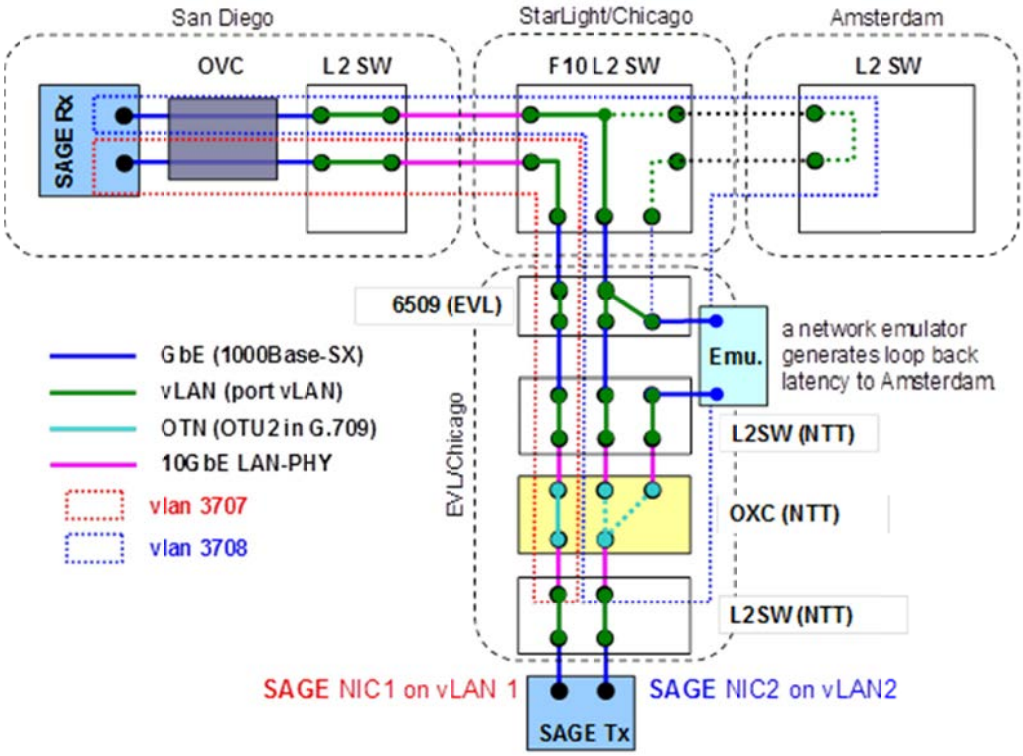

Fig. 6-2-7 Configuration of the OXC system

III. OVC implementation

There are two possible implementations for OVC function as discussed in The TERAbit-LAN section. These include L2 solution by OTN frame or L3 solution by Ethernet packet. As for the scale of latency deviations, I am supposing about 200 ms at maximum. It could be the case when a path restoration in global scale occurred. In my OVC hardware, I have implemented 1 GB of buffer that can sufficiently support around 500ms of latency which is enough to meet with global scale path diversity. In the demonstration, OVC functionality was realized in L3 by integrating a latency detection module and a latency controller as shown in Figure 6-2-4. Ideally OVC function should be implemented in L2 to realize highest accuracy. For such a purpose, all the networking equipment including L2 switches, routers, and repeaters must be compliant with the G.709 standard. But unfortunately, not all the equipments were ready to conform to standard. Thus I adopted L3 OVC configuration in the demonstration. The latency detection module detected RTT for

each channel in a LGP. Then the differences in relative latency that were calculated by the obtained RTT times was used to control the latency control unit. The restored path had excessive latency of about 175ms which has significantly impaired quality of streaming from EVL. To ensure to keep quality of streaming, I have to compensate the latency deviation less than about several tens of ms to avoid visible deterioration. The OVC circuit I have implemented has less than 1 ms of accuracy of compensation which is sufficient for this purpose. For L2 implementation, absolute latency determined by a change of geographical distance is a main component. In global scale systems, some small latency induced by electrical regeneration in link systems will also be needed to be considered. For L3 implementation, I need to consider store and forward latency to route packets. Usually, this latency component will be the secondarily large next to the absolute latency, and it will be statistically distributed. So I have averaged over 3 seconds to get a stable value for compensation. In other words, I have compensated at a fixed averaged value instead of packet by packet compensation. The averaging time could be optimized depending on network condition. I will be able to decrease it when I have no congestion, since I can expect stable, not scattered latency deviation. However, when I faced severe congestion and large number of packet loss, I can hardly get stable averaged latency to compensate. When the congestion had cleared, I can get a stable latency deviation and OVC will re-start within 3 seconds as I mentioned above. In my demo, I developed TCL scripts on Windows OS to measure RTT and average, and to control the latency controller. In the demonstration problems occurred in the loop-back connection through Amsterdam, so the equivalent relative latency of 180ms was provided by the network emulator placed between a port of the OXC and a port in Cisco 6509 which was connected to StarLight's E1200.

IV. SAGE with multi-network support

SAGE was improved to accommodate multiple network connections to demonstrate OVC functionality in the TERAbit-LAN project. Figure 6-2-8 shows a schematic of SAGE's new multi-network capability. A single SAGE application can use multiple IP addresses or multiple NICs and the bandwidth allocation or splitting on the SAGE window can be arbitrary configured. On the sender side, traffic of an application running on a SAGE window was split into two streams depending on the location of the application on the window. When the application ran on only left half of the SAGE window, the traffic was pushed out from only one NIC which corresponds to the window. In the actual demonstration, I placed a real-time streaming application at the center of a SAGE window.

Therefore, almost equal amounts of traffic were output from both NICs and received in the receiver side in Calit2.

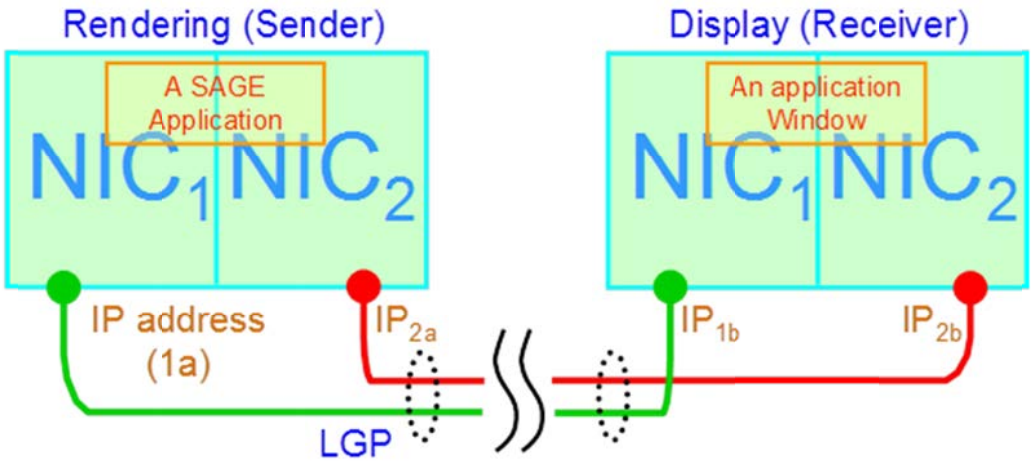

Fig. 6-2-8 Schematic of SAGE's new multi-network capability

V. LIVE streaming from EVL

Figure 6-2-9 shows a snapshot of the demonstration station. I had placed a moving toy in front of the HD camera which was located in EVL/Chicago so that the audience could easily see tearing between the two video streams in real-time. In the control condition where there is no relative latency deviation in two constituent channels in a LGP, there was no tearing noticed on the display screen. Then, when an intentional fault occurred in a channel, audiences could clearly notice tearing in the video feed. The tearing resulted from additional latency induced by a change in optical route restored by the OXC system. When I turned the OVC circuit ON, the tearing was suppressed immediately. The recovery time needed was on the order of a few seconds, due to some time needed to detect and determine relative latency differences between the two GbE channels. I have encountered severe bandwidth fluctuation and sometimes intermittent connection to EVL/Chicago in the former part of my demo timeslot. But in the last 30 minutes, the network performance recovered well and showed good throughput. I achieved 320-400Mbit/s of peak bandwidth used for each vlan in the demo.

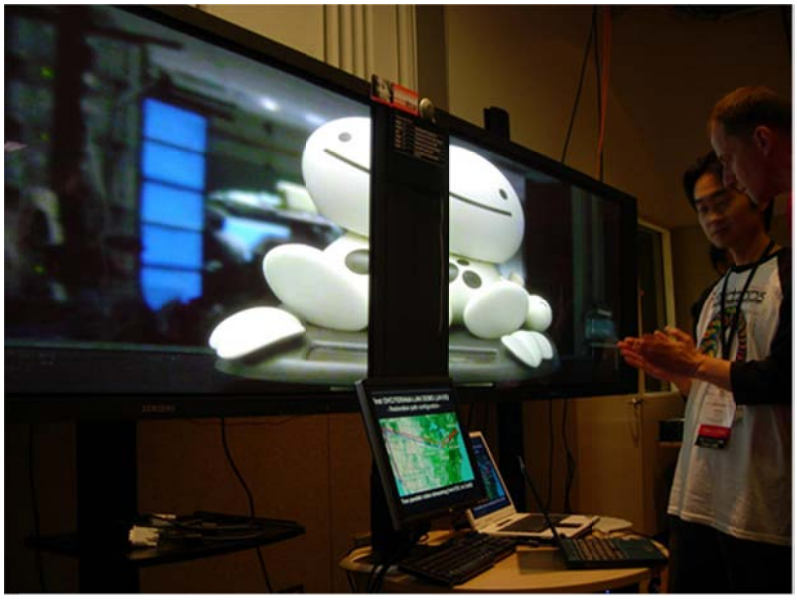

Fig. 6-2-9 Snapshot of the demonstration station

Section summary

In this section, I have successfully demonstrated OVC functionality in a TERAbit-LAN LGP with a high-performance graphics stream application. An OXC placed in EVL/Chicago established an LGP between EVL/Chicago and Calit2/San Diego. In the demonstration, OVC was realized in L3 by simple latency detection and control, since OTN-enabled transport layer was not available in end-to-end. But I am anticipating that the G.709 OTN standard will penetrate into the transport network and fully realize the TERAbit-LAN and OVC concept. In my demo, I have investigated in a live streaming application. To collect information concerning accuracy of latency compensation needed for applications, I will investigate similar kinds of tests to wider extent of applications such as tightly interactive ones. In addition, I have tested OVC in a LGP with two parallel vlans in the demo, and they were static, since I was focusing on OVC in this time. I plan to implement a novel c-plane network which can accepts required number of lambdas in a LGP from end-hosts and can configure end-hosts and optical switches to establish a LGP dynamically.

At the time I proposed OVC concept, there had been no means to implement OVC in OTN network and/or Ethernet network. Thus I implemented the idea in L3 by simple latency detection and control. After the proposal, client interface capacity such as Ethernet has been expanding continuously as I have predicted in this section and the direction toward OVC and LGP have been emerging for the time being. Looking at the standardization bodies,

Optical Internetworking Forum (OIF) is now discussing FlexE specifications which align to the LGP concept I have proposed and ITU-T is also considering FlexO specifications which has the similar direction.

6.3 Programmable resiliency

Background

For years, the main and dominant network service was a voice call and carrier network has been designed to support such services so far. However, emerging video-related services are about to explode, which are stimulated and supported by strong penetration of smart and mobile devices. Corresponding traffic volume and traffic pattern will differ significantly from the one of the legacy telephone service [89-90]. The traffic will be terminated more and more in metro area. Such traffic for dynamic caching will be no longer star-like pattern but multidirectional. In addition to that, traffic will be generated by machines or servers, in contrast to humans in phone calls. So the traffic prediction or estimation and adaptation to that will be a big issue [91-92]. For such purpose, dynamic and agile feature will be essential part for future metro area network. As for agility enhancement, mesh-like topology will have more potential than ring, and could be one of the candidates to serve those upcoming services. In addition to that, most carriers are forced to achieve further cost reduction including operational cost to support still increasing traffic with saturating revenue. From the technical point of view, parallelism in optical transport such as multi-carrier transmission will be expected in beyond 100G era [93].

In this section, I propose i-ANP^2 architecture which will fit in with the parallelism and enhances agility of photonic network. It also realizes highly cost-effective protection and drastic reduction of operational expenditure (OPEX).

i-ANP^2 architecture

Figure 6-3-1 shows the basic architecture of i-ANP^2 in comparison with conventional approach to achieve hit-less protection against a single failure in optical path in the transport network. In the conventional approach, we need a protection path for each working path as shown in Fig. 6-3-1a. As a result, we need doubled optical paths.

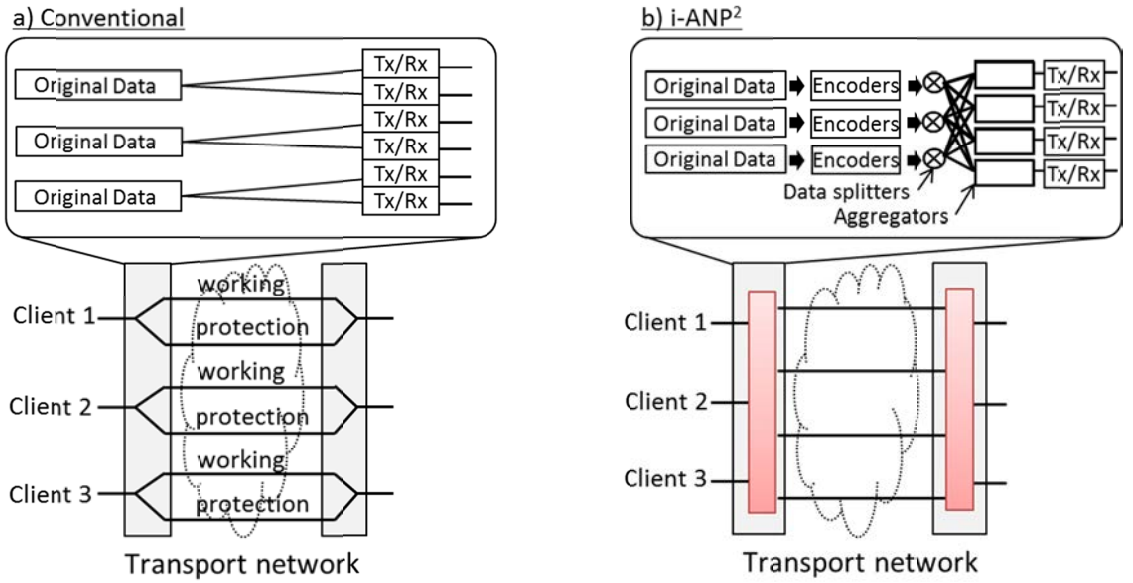

Fig. 6-3-1 Basic architecture of i-ANP²

In i-ANP², the original digital data are firstly erasure-encoded with designed redundancy for protection as shown in Fig. 6-3-1b. The encoder/decoder consists of (2N, N) block code which can correct N symbols and is belong to MDS (Maximum Distance Separable) code, such as Reed-Solomon code. The redundancy needed for a single failure is 1/(n-1), where n stands for the number of parallel optical paths to which encoded digital data is distributed over. Here, I need 33% of redundancy (n=4) to protect against a single failure in optical path. The encoded data are then split into multiple parts with a defined block size and launched into corresponding aggregators. Each aggregator collects the split data from those encoders and transfers them to the transmitter circuit. The data are then transmitted through parallel optical paths. At the destination site, the transmitted data are received and sent to the aggregators where the incoming data are de-aggregated. The data combiners collect the split data blocks and reconstruct the data. Then the data are erasure-decoded to regenerate the original digital data. This architecture will fit in with the parallelism in optical transport. I can programme the redundancy by changing the number of sub-carriers.

Main advantages

In contrast to the error correction codes used for transmission where frequency of error occurrence distributes statistically, a data loss by a component failure is deterministic. Therefore, I can recover the loss completely without a single bit loss. I can realize protection against a single failure with 33% of spare resource in contrast to 100% in a

conventional one. Therefore, I can expect reduction of CAPEX which correspond to the reduced resource. In the conventional approach, we need a dedicated protection path for each working path. On the other hand, the proposed approach can achieve efficient sharing of spare resource.

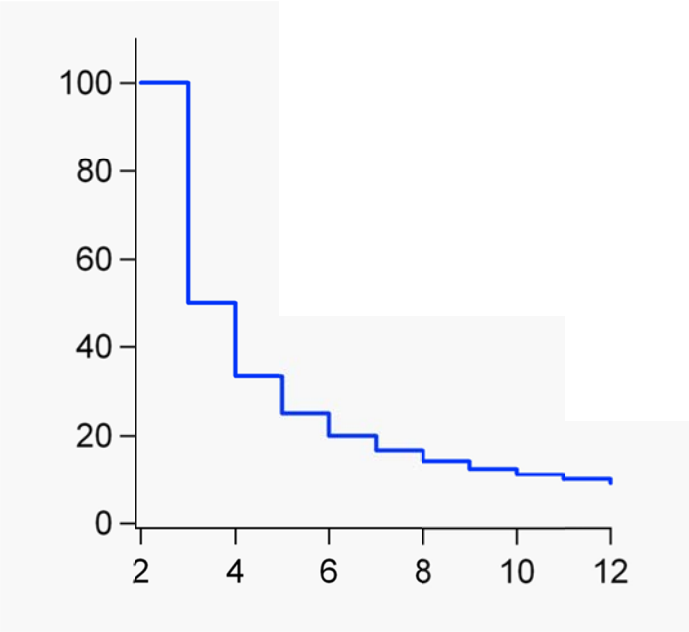

Fig. 6-3-2 Comparison of spare resource

The required spare resource needed is shown in Fig. 6-3-2. in comparison to a conventional 1+1 protection. As I increase the number of parallel connections, I can further improve the efficiency of network resource usage. These parallel channels can be wavelengths, optical carriers, and so on, depending on the entities which should be needed to have enhanced robustness.

Figure 6-3-3 summarizes the performance of i-ANP^2 as a function of the amount of spare resource and service interruption time in comparison to legacy technologies. 1+1 protection provide hitless protection but suffer maximum cost of 100% of spare resource. Automatic protection switching will also need 100% of spare resource and will suffer service interruption from switching time. Shared protection with centralized control approach requires less spare resource but cannot avoid long service interruption resulted from computation time of restoration path. The i-ANP^2 can provide hitless protection with reduced spare resource.

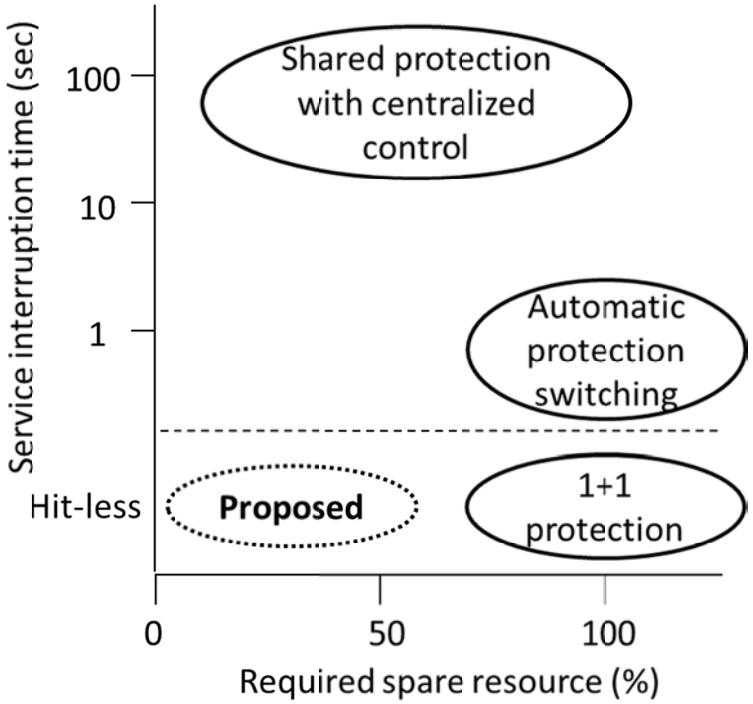

Fig. 6-3-3 Spare resource and service interruption.

Toward OPEX reduction

Not only the CAPEX, the i-ANP^2 can reduce OPEX. For simplicity, I will suppose that a truck-roll for a repair operation will be needed when a fault in transponders in the network occurred, which is one of the frequent cause. And I consider the operational cost from the truck-roll only and suppose that it is proportional to the number of truck-roll needed. Thus, I can estimate the OPEX by evaluating the probability of a fault that occurs in the network.

Only a single and more faults among these systems will cause system failure and service interruption. The failure probability of such a system can be estimated by the following equation; 1-(1-p)N, supposing all the components have the same outage probabilities and the total number of the components as p and N, respectively. With the help of i-ANP^2, a single fault of the component will be completely masked and no impact on transport services. I define a single failure protection by i-ANP^2 as "+1 protection." I can compute the probability of a system failure by the following equation; 1-((1-p)N + Np(1-p)N-1), since double and more failures will cause a system failure.

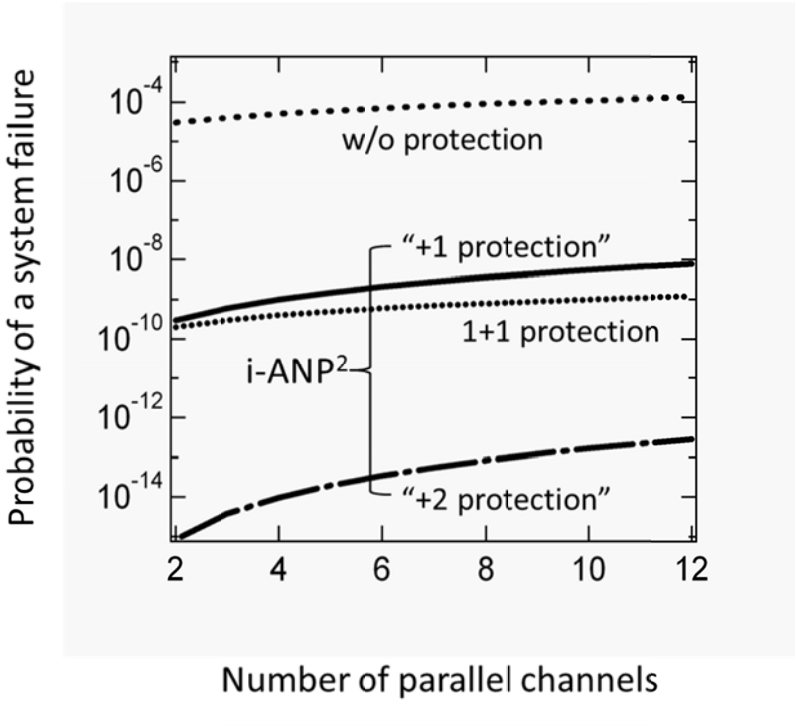

Fig. 6-3-4 Probability of a system failure.

Figure 6-3-4 shows the probabilities of a system failure as a function of the number of parallel channels that consists of a connection. Here, I have supposed averaged outage probability p of each component as 10^{-5} as an example. Thanks to the i-ANP^2 architecture, the probability of a system failure is drastically reduced. The failure probability is programmable by changing the redundancy in i-ANP^2. Thus, I can expect drastic reduction of OPEX of truck roll for repair operation with reduced CAPEX in comparison with 1+1 protection.

Change of maintenance operation

The amount of redundancy is programmable and I can change it intentionally to protect against double or triple faults with minimized cost. Therefore, I can leave single or double faults as it is, since they will not impact transport services. This will make a drastic change in workflow in maintenance operation from "truck roll" to "schedule maintenance". We will no longer need round-the-clock workers to support transport network and will further reduce corresponding OPEX of the network.

Enhanced agility with mesh-like topology

The i-ANP^2 can mask not only failures of optical paths but also reconfiguration or moves of optical network or optical paths, respectively. Therefore, I can optimize transport network without any impact on transport services. From the viewpoint of network topology, mesh-like topology has maximum agility in nature. So I can expect the combination of the i-ANP^2 and mesh-like topology can decouple transport infrastructure with maximum agility from transport service. This decoupling will make it possible to adapt unpredictable and volatile traffic from cloud-based services with minimum cost without having to worry about service interruption.

Section summary

In this section, I have proposed i-ANP^2 architecture which enabled cost-efficient protection over optical transport network. It can reduce spare resource needed for protection against failures of components that consists of optical paths with the help of effective spare resource sharing realized by i-ANP^2. The reduction ratio of spare resource was 66% (from 100% to 33%) for 4 parallel channels and can be enhanced as I increase the parallel number. The architecture also reduces operational cost resulted from truck-roll to repair transport equipment failures by suppressing outage probability in several order of magnitude with significantly reduced CAPEX. Moreover, the architecture decouples transport service from transport infrastructure. Thus, I can optimize transport infrastructure to meet volatile traffic from cloud-like services without any impact on transport services.

To evaluate advantage of the proposed architecture, I have conducted a government funded project to evaluate the proposed idea in 4 parallel channel configuration [94]. We have implemented data splitters, aggregators, and erasure encoding for OTN frames [45] to protect data transmission from channel failure. I have confirmed robustness against network failure which is equivalent to legacy 1+1 protection scheme with less than 50% of network resource, and achieved the highest score "S" (Excellent) for our project [95].

At the beginning of 21st century, we are facing rapid falling of working population because of aging society and falling birth rate. Operation and maintenance of network services have been relying on significant amount of labour work so far. Therefore, we need to change the way we operate and maintenance our network into the one where we need less or minimized labour work. One of the potential candidates to overcome these issues could be to enhance robustness of the network with minimum additional cost. The proposed method will serve to establish such maintenance-free network infrastructure in the near future. For such purpose, we also need to consider utilizing artificial intelligence

(AI) for network operation. So we have to proceed in both hardware and software aspect to realize such next generation maintenance-free network.

Summary of section 6

In sections 6.1 through 6.3, I proposed novel approaches to mitigate impairments resulted from WDM transmission.

One of the issues for WDM transmission is GVD deviation over wide wavelength range used for WDM transmission. In addition to that, in the era when client capacity exceeds transmission capacity of a single wavelength channel, we need novel mechanism that enables to use plural wavelength channels as a whole to carry the big client signal. As we increase the number of wavelength channels for a client, outage probability as a whole will increase, since total number of components in such a system will increase also. Thus, some mitigation technique against a single or a few failures of constituent wavelength channels will also be indispensable.

In section 6.1, I proposed novel compensation method for GVD deviation over L-band in dispersion shifted fiber. The method is based on space-time conversion circuit. I have designed phase filter to meet GVD deviation in L-band of G.653 optical fibers and confirmed successful transmission over 100-km G.653 fiber with the compensator.

In section 6.2, I proposed novel concept of optical virtual concatenation that accommodate large capacity client signal with plural physical connections such as wavelengths channels. To disseminate and promote such direction, I have conducted real-time demonstration and presented to academic and industrial community in global network by implementing the concept using L3 technologies.

In section 6.3, I proposed novel impairment mitigation technique which could be applicable to OVC circuits. The technique can achieve programmable resiliency with minimum network resource by using erasure coding over plural optical channels.

The contributions in sections 6.1 through 6.3 pioneered essential technologies, which will play important role in future large capacity optical transport network with multiple wavelengths channels. GVD slope compensation, OVC, and iANP2 will be expected to contribute for realizing large capacity and reliable future optical transport network.

7. Conclusion

The Thesis presents novel techniques for impairments mitigations resulted from transmission of digital optical signal through optical fibers.

Toward further enhancement of transmission speed (bitrate), group velocity dispersion and polarization mode dispersion in optical transmission fibers are the obstacles to challenge. I have proposed novel modulation formats through investigation of penalty resulted from group velocity dispersion implementing optical time-division multiplexing circuit with variable optical phase control capability. This work opened new horizon of phase-shift keying in optical communication systems to reduce symbol rate and overcome ISI from group velocity dispersion and polarization mode dispersion. The proposed signal format has three symbol points without degradation of inter symbol distance, so symbol rate was decreased by 2/3 and improved tolerance against above impairments. After this invention, one more symbol was added and implemented for 40 Gbit/s commercial systems.

In addition to that, I have proposed novel spectral mode splitting method for group velocity dispersion measurement by focusing spectral mode orthogonality. The basic understanding of spectral mode orthogonality has been used for further upgrade of wavelength multiplexing, such as optical orthogonal frequency division multiplexing (O-OFDM) toward realizing more capacity. Moreover, cutting edge digital coherent transmission systems implemented automatic dispersion detection mechanism, which is based on this work for automatic compensation by digital coherent signal processor.

For polarization mode dispersion, I have conducted field experiment in Germany to evaluate actual impairment and relation to modulation formats and forward error correction. This work provided basic understanding for system design considering PMD. Based on the tolerance measured in this field experiment, actual 40 Gbit/s systems had been designed to avoid system outage caused by temporal change of 1^{st} and 2^{nd} order PMD.

As a result, group velocity dispersion and polarization mode dispersion are accommodated via novel impairment-tolerant modulation techniques and compensation method. Precise manipulation of optical phase is a key technology for such applications and these techniques discussed in this Thesis have been the pioneering work toward such direction.

In addition to those, recovery of optical signal to noise ratio is one of the fundamental issue in optical communication systems. The Thesis discussed some challenging works of simple all-optical or electro-optical approaches to overcome these issues. To recover optical signal to noise ratio after optical transmission, suppression of signal-ASE beat noise suppression is essential. I have proposed fiber nonlinearity-based method to suppress the

noise and confirmed effective suppression by both experiment and numerical simulation. In addition to these, I have investigated nonlinear optical gate to realize 3R regeneration. Not only the signal-ASE beat noise, retiming function has been also implemented by this approach. During the discussion, I have presented probability density function output from all-optical nonlinear gate approaches the Gaussian distribution. Therefore, simple OSNR treatment can be applied to this application.

For further extend optical bandwidth toward more large capacity transmission, dispersion slope of group velocity dispersion, some concatenation method to aggregate to support large capacity client, and enhancement of reliability with less equipment cost will be mandatory. I have proposed wide band dispersion slope compensator based on space-time conversion technique and confirmed successful transmission of wide-band L-band transmission over dispersion-shifted optical fibers.

Also I have proposed optical virtual concatenation concept and demonstrated the concept by using multiple lambdas and high-end large capacity visualizing applications. After the proposal, client interface capacity such as Ethernet has been expanding continuously and the direction toward OVC and LGP have been emerging for the time being. Looking at the standardization bodies, Optical Internetworking Forum (OIF) is now discussing FlexE specifications which align to the LGP concept I have proposed and ITU-T is also considering FlexO specifications which has the similar direction.

As we increase the number of wavelength channels, the total number of components that consist of transport systems will also expand. Thus failure rate of total transmission systems will increase accordingly. To avoid this issue, I have proposed novel transmission architecture that supports programmable resiliency and achieves higher robustness (lower failure rate) with minimum resource. Moreover, we are confronting now is how we operate further complicating network with less labor work. Moreover, aging society and low birthrate have been becoming inevitable issue where we are gradually suffering lacking of labor power. So the next generation transport system should meet such issues. The proposed architecture can realize enhanced resiliency or robustness against failures with minimized additional expense. This will help to reduce track-roll for maintenance operation for network.

Formerly, network has been mainly owned and operated by telecom operators including AT&T, DT, BT, NTT and so on. When we look at the current circumstance in optical transport, as optical transport systems has matured, transport cost per bit decreased dramatically. By the help of the cost reduction, diversified global service providers emerged including over-the-top (OTT) service providers such as Google, Amazon, Facebook, etc. Network

architecture and traffic pattern in such providers also differs from legacy telecom-based one to data center-based one, since their network has been for mainly inter- and intra-data center connection. Reliability or availability requirements also differ. Telecom operators need high availability such as five 9s, since they provide network service itself. On the other hand, OTT operators provide virtualized services on top of their network. They secure high availability by virtualization of their services, so do not rely on high reliability of each network connection.

So the global market of network equipment now is being split into two segments. One is for traditional telecom operators and another is for OTT operators. Depending on their service characteristics, requirements for network equipment differs. Telecom operators need aggregation-based network to accommodate various clients and rich Operation, Administration, and Maintenance (OAM) mechanism to diagnose faults and recover network service promptly. OTT operators require large capacity and relatively short reach data center interconnections with reduced OAM mechanism.

The modulation formats, encoding algorithms, optical devices and so forth may differ depending on the use cases as discussed above, because the required optical reach and transmission capacity will differ for each use case. However, as for the impact of my Thesis, for both use cases, standard single mode optical fibers will be still deployed. Therefore, GVD and PMD should be accommodated in the upcoming data center era.

The original idea I have proposed for GVD measurement is based on optical implementation. After the proposal of the idea, digital signal processing technologies including high-speed Analog-to-Digital-Converters (ADC) and Digital-to-Analog-Converters (DAC) has progressed a lot, so almost all signal processing related to optical impairment mitigations has been carried out in digital regime. In the development of GVD measurement in 100G transport systems, the proposed idea has been implemented in digital signal processing circuit where spectral mode splitting has been realized for digital signal and corresponding filtering has been also realized in digital filters. As for the statistical design for PMD, based on the basic understanding pioneered by my work, additional long term field trials had carried out for candidate modulation formats and reached the final design.

Recently, to overcome the upper limit of standard single mode optical fibers, space division multiplexing technology is being developed for future transmission media. Even in such a case, GVD and PMD impairment should be accommodated. Accordingly, my contribution in this Thesis continues to serve highly accurate impairment mitigation against GVD and PMD for higher capacity transmission systems for both telecom and OTT services. Contributions such as OVC and iANP2 will provide possible options to serve ultra large capacity and resilient transport link in future network.

At the beginning of the year 2017, Ministry of Internal affairs and Communications (MIC) hosted a working group discussion toward future network. It says that with regard to decreasing working population in Japan, network should work by much less expert or labor power. Therefore, programmable resiliency realized by my proposal may contribute to future large capacity optical network which will be maintained by less operational work.

Acknowledgments

I am grateful to Prof. Iwao Sasase, Prof. Hiroyuki Tsuda, Prof. Naoaki Yamanaka, Prof. Tomoaki Otsuki and Prof. Satoru Okamoto of Keio University for their direction and support. I also thank Dr. Masahito Tomizawa, Dr. Yutaka Miyamoto, Dr. Ryutaro Kawamura, Mr. Shoichiro Kuwahara, Mr. Yoshiaki Kisaka, Dr. Naofumi Shimizu of NTT Laboratoris, Prof. Masaki Asobe of Tokai University, Prof. Ken-ichi Sato of Nagoya University, Dr. Mikio Yoneyama, Dr. Hiromu Toba, and Mr. Kazuo Hagimoto of NTT Electronics Corporation for their fruitful discussions and advices. The figures published in IET Electronics Letters are reproduced by permission of the Institution of Engineering & Technology in this Thesis. Information on the original papers is referred in each section.

Appendix

I define γ as

$$1 + \gamma \equiv \frac{\langle \sigma^2 \rangle_{II}}{\langle n \rangle_{II}} \tag{A-1}$$

where γ degradation coefficient of light input to amplifiers. γ equals to zero means a coherent state. Therefore, the excessive noise component can be expressed as,

$$G_\beta^2 \gamma \langle n \rangle_{II} = G_\beta^2 (\langle \sigma^2 \rangle_{II} - \langle n \rangle_{II}) \tag{A-2}$$

Here, the variance of the input of amplifier β can be expressed by discrimination parameter η, the output variance of amplifier α and optical loss of the attenuator β as

$$\langle \sigma \rangle_{II} = \eta \, L_\beta \langle \sigma \rangle_\alpha \tag{A-3}$$

Since amplifier β compensates for the loss of optical attenuator β, the value of the loss coincides with the optical gain of the amplifier. Therefore,

$$L_\beta = \frac{1}{G_\beta} \tag{A-4}$$

Combining equations (A-2), (A-3), and (A-4),

$$G_\beta^2 \gamma \langle n \rangle = G_\beta \left\{ \frac{\eta^2}{G_\beta} \langle \sigma^2 \rangle_\alpha - G_\beta \langle n \rangle_{II} \right\} \tag{A-5}$$

References

1.

[1] Govind P. Agrawal: 'Fiber-Optic Communication Systems,' 2002 John Wiley & Sons, Inc., pp. 64-65.

[2] A. Sano et al., "Automatic dispersion equalization by monitoring extracted-clock power level in a 40-Gbit/s, 200-km transmission line," in Dig. ECOC1996, TuD.3.5, (1996)

[3] H. Ooi et al., "40-Gbit/s x 32 ch automatic dispersion compensation with VIPA variable dispersion compensators," in Dig. OECC / IOOC2001, Post-Deadline Paper (2001)

[4] A. Sano et al., "Adaptive dispersion equalization by monitoring relative phase shift between spacing-fixed WDM signals," IEEE J. Lightwave Technol., Vol. 19, No. 3, pp. 336-344, (2001)

[5] Hirano, A. et al., "Dispersion Tolerant 80-Gbit/s Carrier-Suppressed Return-to-Zero (CS-RZ) Format Generated by Using Phase- and Duty-Controlled Optical Time Division Multiplexing (OTDM) Technique," IEICE TRANSACTIONS on Communications Vol.E85-B No.2 pp.431-43.

[6] Hirano, A. et al., "A Novel Mode-Splitting Detection Scheme in 43-Gb/s CS-and DCS-RZ Signal Transmission," IEEE J. Lightwave Technol., Vol. 20, No. 12, pp. 2029-2034, (2002)

[7] Hirano, A. et al., "Field trial of 43 Gbit/s CS-RZ OTN system in PMD-limited transmission links," Electron. Lett., 2004, Vol. 40, No. 15, pp. 957-958.

[8] K. Smith, and J. K. Lucek, "All-optical signal regenerator," CLEO'93, CPD23, pp. 1/46-2/47, 1993.

[9] M. Jinno, and M. Abe, "All-optical regenerator based on nonlinear fiber sagnac interferometer," Electron. lett., 28, pp. 1350-1352, 1992.

[10] A. Dupas, L. Billes, J. C. Simon, B. Landousies, M. Henry, F. Ratovelomanana, A. Enard, and N. Vodjdani,"Progress towards a pan-european WDM network: 3600 km, 2.5 Gbit/s cascade of all optical 2R regenerator/wavelength converters and 400 km uncompensated standard fibre sections," ECOC'97, 5, pp. 85-88, 1997.

[11] D. Chiaroni, B. Lavigne, A. Jourdan, L. Hamon, C. Janz, and M. Renaud,"New 10 Gbit/s 3R NRZ optical regenerative interface based on semiconductor optical amplifiers for all-optical networks," ECOC'97, 5, pp. 41-44, 1997.

[12] Hirano, A. et al., "All-optical limiter circuit based on four-wave mixing in optical fibres," Electron. Lett., 1998, Vol. 34, No. 14, pp. 1410-1411.

[13] Hirano, A. et al., ”Simple 2R repeater using direct coupling of UTC-PD and EA modulator,” Optical Amplifiers and Their Applications, ThC2, Nara Japan, June 9, 1999.

[14] Hirano, A. et al., ”All-optical discrimination based on nonlinear transmittance of MQW semiconductor optical gates,” Journal of Lightwave Technology, Vol. 17, Issue 5, pp. 873- (1999).

[15] Yonenaga K., Matsuura A., Kuwahara S., Yoneyama M., Miyamoto Y., Hagimoto K., and Noguchi K.: ‘Dispersion-compensation-free 40 Gbit/s x 4-channel WDM transmission experiment using zero-dispersion-flattened transmission line’ OFC’98 PD, 1998, pp. 20.

[16] Hirano, A. et al., “640 Gbit/s (16 channel/spl times/42.7 Gbit/s) WDM L-band DSF transmission experiment using 25 nm bandwidth AWG dispersion slope compensator,” Electron. Lett., 2000, Vol. 36, No. 19, pp. 1638-1639.

[17] René-Jean Essiambre, Gerard Foschini, Peter Winzer, and Gerhard Kramer, ” Capacity Limits of Fiber-Optic Communication Systems,” Journal of Lightwave Technology, OFC2009 paper OThL1, (2009).

[18] Hirano, A. et al.,”The first functional demonstration of optical virtual concatenation as a technique for achieving Terabit networking,” Future Generation Computer Systems, Volume 22, Issue 8, October 2006, Pages 876–883.

[19] Hirano, A. et al.,”Cost Effective and Robust Optical Network by Inversely Aggregated Networking with Programmable Protection Architecture,” Electronics Letters, vol. 50, no. 20, pp. 1459-1461, September 2014.

2.

[20] Kawanishi, S. et al., "3 Tbit/s OTDM/WDM transmission experiment," OFC99, PD1, 1999.

[21] Takara, H. et al., "Integrated optical time division multiplexer based on planar lightwave circuit," Electron. Lett., Vol. 35, No. 15, pp. 1263-1264, 1999.

[22] Yonenaga, K. et al.,"320-Gbit/s, 100-km WDM repeaterless transmission using fully encoded 40-Gbit/s optical duobinary channels with dispersion tolerance of 380 ps/nm," ECOC2000, pp. 75-76, 2000.

[23] Ishikawa, G. et al.,"80-Gbit/s (2 x 40-Gbit/s) transmission experiments over 667-km dispersion-shifted fiber using Ti:LiNbO3 OTDM modulator and demultiplexer ," ECOC96, Vol. 5, pp. 37-40, 1996.

[24] Shake, I. et al., "High-repetition-rate optical pulse generation by using chirped optical pulses," Electron Lett., Vol. 34, pp. 792-793, 1998.

[25] Noguchi K., Mitomi O., and Miyazawa H.: 'Push-pull type ridged Ti:LiNbO3 optical modulator' IEICE Trans. Electron., 1996, E79-C, (1), pp. 27-31.

[26] Sato, K. et al., "Chirp-compensated 40 GHz semiconductor modelocked lasers integrated with chirped gratings," Electron. Lett., Vol. 34, No. 20, pp. 1944-1946, 1998.

[27] Otsuji T., Yoneyama M., Imai Y., Enoki T., and Umeda Y.: '64 Gbit/s 2:1 multiplexer IC using InAlAs/InGaAs/InP HEMTs' Electron. Lett., 1997, Vol. 33, No. 17, pp. 1488-1489.

[28] Takara, H. et al., "100 Gbit/s optical signal eye-diagram measurement with optical sampling using organic nonlinear optical crystal," Electron Lett., Vol. 32, pp. 2256-2258, 1996.

[29] Yoneyama, M. et al., "Fully electrical 40-Gbit/s TDM system prototype and its application to 160-Gbit/s WDM transmission," OFC99, ThI6-1, pp. 128-130, 1999.

[30] Miyamoto, Y. et al., "Dispersion-tolerant RZ signal transmission using baseband differential code and carrier suppressed modulation," ECOC98, TuD12, pp. 351-352, 1998.

3.

[31] Miyamoto Y., Hirano A., Yonenaga K., Sano A., Toba H., Murata K., and Mitomi O.: '320 Gbit/s (8 x 40 Gbit/s) WDM transmission over 367 km with 120 km repeater spacing using carrier-suppressed return-to-zero format' Electron. Lett., 1999, Vol. 35, No. 23, pp. 2041-2042.

[32] Y. Miyamoto, K. Yonenaga, A. Hirano, A. Sano, S. Kuwahara, H. Kawakami, H. Toba, K. Murata, M. Fukutoku, Y. Yamane, H. Miyazawa, T. Ishibashi, and T. Sato, "320-Gbit/s (8 x 40 Gbit/s) WDM field experiment over 281-km installed dispersion-shifted fiber using carrier-suppressed return-to-zero pulse format," Technical Digest of OECC'99 post-deadline paper, vol. 2, pp. 5-8, 1999.

[33] K. Yonenaga, Y. Miyamoto, A. Hirano, A. Sano, S. Kuwahara, H. Kawakami, H. Toba, K. Murata, M. Fukutoku, Y. Yamane, K. Noguchi, T. Ishibashi, and K. Nakajima, "320 Gbit/s WDM filed experiment using 40 Gbit/s ETDM channels over 176 km dispersion-shifted fiber with nonlinearity-tolerant signal format," IEE Electron. Lett., vol. 36, pp.153-155, 2000.

[34] Breuer, D., Enner, K., and Petermann, K.: 'Comparison of NRZ- and RZ-modulation format for 40-Gbit/s TDM standard-fibre systems,' ECOC'96, Vol. 2, pp. 199-202, 1996.

[35] Y. Miyamoto, K. Yonenaga, A. Hirano and M. Tomizawa, "N x 40-Gbit/s DWDM transport system using novel return-to-zero formats with modulation bandwidth reduction," IEICE Trans. Commun., vol. E85-B, no. 2, pp. 374-385, 2002.

[36] A. Hirano et al., "Expanded dispersion tolerance by SSB direct detection in Duobinary Carrier-Suppressed RZ signal transmission," in Dig. OAA2001, OTuD2, (2001).

[37] A. Hirano, S. Kuwahara, Y. Miyamoto, and K. Murata, "A Novel dispersion compensation scheme based on phase comparison between two SSB signals generated from a spectrally filtered CS-RZ signal," Technical Digest of OFC'2002, WE2, 2002.

[38] K. Sato, A. Hirano, N. Shimizu, T. Ohno, and H. Ishii, "Dual mode operation of semi conductor mode-locked lasers for anti-phase pulse generation," Technical Digest of OFC'2000, ThW3, 2000.

[39] M. Tomizawa, Y. Kisaka, A. Hirano and Y. Miyamoto, "Error correction without additional redundancy by novel optical receiver with diverse detection," Technical Digest of OFC'2002, WX7, 2002.

[40] Yonenaga, K. Miyamoto, Y., Toba, H., Murata, K., Yoneyama, M., Yamane, Y., and Miyazawa H.: '320-Gbit/s, 100-km WDM repeaterless transmission using fully

encoded 40-Gbit/s optical duobinary channels with dispersion tolerance of 380 ps/nm' ECOC'2000, pp. 75-76.

[41] L. Boivin, and G. J. Pendock,: "Receiver sensitivity for optically amplified RZ signals with arbitrary duty cycle," in Dig. OAA'99, ThB4, 1999.

[42] K. Murata, T Otsuji, T. Enoki, and Y. Umeda, "Exclusive OR/NOR IC for > 40Gbit/s optical transmission systems," IEE Electron. Lett., Vol. 34, No. 8, pp. 764-765, 1998.

[43] S. Kuwahara, A. Hirano, Y. Miyamoto, and K. Murata, "Automatic dispersion compensation for WDM system by mode-splitting of tone-modulated CS-RZ signal," submitted to ECOC'2002.

[44] W. Idler, S. Bigo, Y. Frignac, B. Franz, and G. Veith, "Vestigial side band demultiplexing for ultra high capacity (0.64 bit/s/Hz) transmission of 128x40 Gb/s channels," submitted to ECOC'2002.

4.

[45] ITU-T Recommendation G.709, Interfaces for the Optical Transport Network (OTN), 2003..

[46] Weiershausen, W., Scholl, H., Kuppers, F., Leppla, R., Hein, B., Burkhard, H., Lach, E., and Veith, G.: '40 Gb/s field test on an installed fiber link with high PMD and investigation of differential group delay impact on the transmission performance', in Tech. Digest of OFC99, 3, pp. 125-127

[47] Tomizawa, M., Kisaka, Y., Ono, T., Miyamoto, Y., and Tada, Y.: 'FEC performance in PMD limited high-speed optical transmission systems', in Tech. Digest of ECOC2000, 2, pp. 97-99

[48] Kisaka, Y., Tomizawa, M., Kuwahara, S., and Miyamoto Y.: 'First- and higher-order PMD tolerance of carrier-suppressed return-to-zero format with forward error correction', in Tech. Digest of ECOC2001, pp. 438-439

[49] Xie, C., and Moller, L.: 'Polarization mode dispersion induced impairments in different modulation format systems', in Tech. Digest of OFC2003, TuO1

[50] Allen, C., Kondamuri, P.K., Richards, D.L., and Hague, D.C.: 'Measured temporal and spectral PMD characteristics and their implications for network-level mitigation approaches', IEEE J. of Lightwave Technol., 2003, 21, pp. 79-86

[51] Ciprut, P., Gisin, B., Gisin, N., Passy, R., Von Der Weld, P., Prieto, F., and Zimmer, C.W.:'Second-order polarization mode dispersion: impact on analog and digital transmissions', 1998, J. Lightwave Technol., 16, pp. 757-771

[52] Ono, T., Yano, Y., Garrett, J., A., Nagel, J., A., Dickerson, M., J., Cvijetic, M.: '10 Gb/s PMD compensation field experiment over 452 km using principal state transmission method', in Tech. Digest of OFC'2000, PD44

5.1

[53] K. Inoue, "A simple expression for optical FDM network scale considering fiber four-wave mixing and optical amplifier noise," J. Lightwave Technol., 13, pp. 856-861, 1995.

[54] K. Inoue, and H. Toba, "Wavelength conversion experiment using fiber four-wave mixing," IEEE Photon. Tech. Lett., 4, pp. 69-72, 1992.

[55] P. A. Andrekson, N. A. Olsson, J. R. Simpson, T. Tanbun-ek, R. A. Logan, and M. Haner,"16-Gbit/s all-optical demultiplexing using four-wave mixing," Electron. lett., 27, pp. 922-924, 1991.

[56] X. Zhang, and B. F. Jorgensen, "Analysis of optical phase conjugation using four-wave mixing in a dispersion-shifted fibre," IEEE Proc.-Optoelectron., 143, pp. 195-199, 1996.

[57] G. P. Agrawal, "Nonlinear fiber optics," Academic Press, Inc., 1989.

5.2

[58] H. Kurita, T. Shimizu, and H. Yokoyama,"All-optical clock extraction at bit rates up to 80 Gbit/s with monolithic mode-locked laser diodes," CLEO'97, CTuJ5, 1997.

[59] O. Kamatani, S. Kawanishi, and M. Saruwatari,"Prescaled 6.3 GHz clock recovery from 50 Gbit/s TDM optical signal with 50 GHz PLL using four-wave mixing in a traveling-wave laser diode optical amplifier," Electron. lett., 30, pp. 807-809, 1994.

[60] R. Takahashi, Y. Kawamura, T. Kagawa, and H. Iwamura,"Ultrafast 1.55-um photoresponses in low-temperature-grown InGaAs/InAlAs quantum wells," Appl. Phys. Lett., 65, pp. 1790-1792, 1994.

[61] R. Takahashi, Y. Kawamura, and H. Iwamura,"1.55 micro meter ultrafast surface-reflection all-optical switching using low-temperature-grown Be-doped strained MQWs," ECOC'94, PD113-116, 1994.

[62] H. Kobayashi, R. Takahashi, Y. Matsuoka, and H. Iwamura,"Ultrafast all-optical switch using low-temperature-grown InGaAs/InAlAs multiple quantum well," 4th International workshop on femtosecond technology, pp. 28-30, 1997.

[63] H. Tsuda, A. Hirano, R. Takahashi, K. Sato, and K. Hagimoto,"All-optical pulse discrimination experiment using a low-temperature-grown multiple quantum well optical switch," Electron. lett., 32, pp. 365-366, 1996.

[64] A. Hirano, H. Tsuda, K. Hagimoto, R. Takahashi, Y. Kawamura, and H. Iwamura,"10 ps pulse all-optical discrimination using a high-speed saturable absorber optical gate," Electron. lett., 31, pp. 736-737, 1995.

[65] A. Hirano, H. Kobayashi, H. Tsuda, R. Takahashi, M. Asobe, K. Sato, and K. Hagimoto,"10-Gbit/s RZ all-optical discrimination using a refined saturable absorber optical gate," Electron. lett., 34, pp. 198-199, 1998.

[66] K. Shimoda, H. Takahasi, and C. H. Towns,"Fluctuations in amplification of quanta with application to maser amplifiers," J. Phys. Soc. Japan, 12, pp. 686-700, 1957.

[67] S. Carusotto,"Quantum statistics of light after one-photon interaction with matter," Phys. Rev. A, 11, pp. 1629-1633, 1975.

[68] E. B. Rockower, N. B. Abraham, and S. R. Smith,"Evolution of the quantum statistics of light," Phys. Rev. A, 17, pp. 1100-1112, 1978.

[69] K. Sato, I. Kotaka, Y. Kondo, and M. Yamamoto,"Actively mode-locked strained-InGaAsP multiplequantum-well lasers integrated with electroabsorption modulators and distributed Bragg reflectors," OFC'95, TuI2, pp. 37-38, 1995.

[70] T. Ishibashi,"Gallium arsenide and related compounds," Oiso, p587, 1981.

6.1

[71] Veith, G.: 'European 40 Gbit/s field tests,' ECOC'99, 1999, Vol. 2, pp. 82-83.

[72] Nielsen N. T., Stentz J. A., Hansen B. P., Chen J. Z., Vengsarkar, S. D., Strasser A. T., Rottwitt K., Park H. J., Stulz S., Cabot S., Feder S. K., Westbrook S. P., and Kosinski G. S.: '1.6 Tb/s (40 x 40 Gbit/s) transmission over 4 x 100 km nonzero-dispersion fiber using hybrid Raman/Erbium-doped inline amplifiers' ECOC'99 PD, 1999, pp. 26-27.

[73] Elbers –P. J., Scheerer C., Farbert A., Glingener C., Schopflin A., Gottwald E., and Fischer G.: '3.2 Tbit/s (80 x 40 Gbit/s) bidirectional DWDM/ETDM transmission' ECOC'99 PD, 1999, pp. 32-33.

[74] Miyamoto Y., Yonenaga K., Kuwahara S., Tomizawa M., Hirano A., Toba H., Murata K., Tada Y., Umeda Y., and Miyazawa H.: '1.2-Tbit/s (30 x 42.7 Gbit/s ETDM optical channel) WDM transmission over 376 km with 125-km spacing using forward error correction and carrier-suppressed RZ format' OFC'2000 PD, 2000, pp. 26.

[75] Tsuda H., Kurokawa T., Okamoto K., Ishii T., Naganuma K., Inoue Y., and Takenouchi H.: 'Second- and third-order dispersion compensation using a high resolution arrayed-waveguide grating' ECOC'98, 1998, Vol. 1, pp. 533-534.

[76] Hirano A., Miyamoto Y., Yonenaga K., Sano A., and Toba H.: '40 Gbit/s L-band transmission experiment using SPM-tolerant carrier-suppressed RZ format 'Electron. Lett., 1999, Vol. 35, No. 25, pp. 2213-2215.

6.2

[77] Masahito Tomizawa, Jun Yamawaku, Yoshihiro Takigawa, Masafumi Koga, Yutaka Miyamoto, Toshio Morioka, Kazuo Hagimoto, Terabit-LAN with optical virtual concatenation for grid applications with super computers, Proceedings of OFC2005, paper OthG6, 2005.

[78] TERAbit-LAN. http://www.evl.uic.edu/cavern/terabitlan/.

[79] Symposium Panels in iGrid2005, Advances toward economic and efficient Terabit LANs and WANs http://www.igrid2005.org/program/symposium_panels.html.

[80] StarLight. http://www.startap.net/starlight/.

[81] Joe Mambretti, Recent Progress on TransLight, OptIPuter, OMNInet and Future Trends toward Lambda Grids, Proceedings, CPT2005 8th International Symposium on Contemporary Photonics Technology, January 12-14, 2005, Tokyo, Japan.

[82] Cees de Laat, Erik Radius, Steven Wallace, The Rationale of the current optical networking initiatives, Future Generation Computer Systems 19 (2003) 999-1008.

[83] Toshio Watanabe, Shunichi Sohma, Takashi Goh, Tomohiro Shibata, Hiroshi Takahashi, Compact 8 x 8 Silica-based PLC switch with compressed arrangement, in Tech. Digest of ECOC2004, Th3.6.3, 2005.

[84] Akira Hirano, Yutaka Miyamoto, Novel modulation formats in ultra-high-speed optical transmission systems, and their applications, in Tech. Digest of OFC2004, invited paper ThM1, 2004.

[85] Shoichiro. Kuwahara, Akira Hirano, Hiroji Masuda, Hiroto Kawakami, Yutaka Miyamoto, Mikio Yoneyama, Yoshiaki Kisaka, Kenji Sato, Masahito Tomizawa, Yasuhiko Tada, Tomoko Sawabe, Teturo Fujii and Kazushige Yonenaga, WDM field demonstration of 43 Gbit/s/channel path provisioning by automatic dispersion compensation using tone modulated CS-RZ signal, Tech. Digest of ECOC2003, paper Tu1.6.2, 2003.

[86] Byungil Jeong, Luc Renambot, Rajvikram Singh, Andrew Johnson, Jason Leigh, High-Performance Scalable Graphics Architecture for High-Resolution Displays, EVL Technical Document Technical publication 20050824_Jeong, 2005.

[87] Renambot, L., Rao, A., Singh, R., Jeong, B., Krishnaprasad, Naveen, Vishwanath, V., Chandrasekhar, V., Schwarz,N., Spale, A., Zhang, C., Goldman, G., Leigh, J., Johnson, A., SAGE: the Scalable Adaptive Graphics Environment, In Proceedings of WACE 2004, Nice, France, September 2004.

[88] SAGE. http://www.evl.uic.edu/cavern/sage/

6.3

[89] Bell laboratories/Alcatel-Lucent; ‘Metro network traffic growth and architecture impact study;’ http://resources.alcatel-lucent.com/asset/171568; December 2013.

[90] Yoo, J., Kim, J., Won, Y., Kim, H., Park, S., and Ha, T.: ‘Traffic characteristics of modern video streaming service,’ International Journal of Innovation, Management and Technology, Vol. 3, No. 3, pp. 236-240. 2012.

[91] Feurer, M., Woodward, S. L., Kim, I., Palacharla, P., Wang, X., Zhang, Q., and Bihon, D.: ‘Simulations of traffic growth in a ROADM network with a growing topology,’ Proc. OFC2014, M2B.3, 2014.

[92] Kadohata, A.: ‘Adaptive reconfiguration of sub-lambda and wavelength paths for unpredictable traffic demands,’ Proc. OFC2014, W4A.5, 2014.

[93] Mizuno, T., Kobayashi, T., Takara, H., Sano, A., Kawakami, H., Nakagawa, T., Miyamoto, Y., Abe, Y., Goh, T., Oguma, M., Sakamoto, T., Sasaki, Y., Ishida, I., Takenaga, K., Matsuo, S., Saitoh, K., and Morioka, T.: ’12-core x 3-mode dense space division multiplexed transmission over 40 km employing multi-carrier signals with parallel MIMO equalization,’ Proc. OFC2014, Th5B.2, 2014.

[94] NICT sponsored research project #171B01:”Research on elastic optical network” https://www.nict.go.jp/collabo/commission/k_171b.html#block_top2, 2016.

[95] NICT sponsored research project #171B01:”Research on elastic optical network” https://www.nict.go.jp/collabo/commission/itaku_hyoka_h28last.html#171b01, 2017.

【Journal Papers used in the Thesis】

(1) A. Hirano, Y. Yamada, T. Tanaka, T. Oda, K. Shintaku and T. Inui,“Cost Effective & Robust Optical Network by Inversely Aggregated Networking with Programmable Protection Architecture,” Electronics Letters, Volume 50, Issue 20, pp. 1459 – 1461 (2014).

(2) A. Hirano, L. Renambot, B. Jeong, J. Leigh, A. Verlo, V. Vishwanath, R. Singh, J. Aguilera, A. Johnson, T. A. DeFanti, L. Long, N. Schwarz, M. Brown, N. Nagatsu, Y. Tsukishima, M. Tomizawa, Y. Miyamoto, M. Jinno, Y. Takigawa, O. Ishida, “The first functional demonstration of optical virtual concatenation as a technique for achieving Terabit networking,” Future Generation Computer Systems, Volume 22, Issue 8, pp. 876–883 (2006).

(3) A. Hirano, S. Kuwahara, M. Yoneyama, Y. Kisaka, M. Tomizawa, Y. Miyamoto, W. Weiershausen, R. Leppla, O. Leminger, F. Rumpf, R. Herber, A. Mattheus, A. Gladisch, “Field trial of 43 Gbit/s CS-RZ OTN system in PMD-limited transmission links,” Electronics Letters, Volume 40, Issue 15, pp. 957 – 958 (2004).

(4) A. Hirano, Y. Miyamoto, S. Kuwahara, M. Tomizawa, K. Murata, “A Novel Mode-Splitting Detection Scheme in 43-Gb/s CS-and DCS-RZ Signal Transmission,” Journal of Lightwave Technology, Volume 20, Issue 12, pp. 2029-2034 (2002).

(5) A. Hirano, M. Asobe, K. Sato, Y. Miyamoto, K. Yonenaga, H. Miyazawa, M. Abe, H. Takara, I. Shake, “Dispersion Tolerant 80-Gbit/s Carrier-Suppressed Return-to-Zero (CS-RZ) Format Generated by Using Phase- and Duty-Controlled Optical Time Division Multiplexing (OTDM) Technique,” IEICE TRANSACTIONS on Communications Volume E85-B No.2 pp.431-437 (2002).

(6) A. Hirano, K. Yonenaga, Y. Miyamoto, H. Toba, H. Takenouchi, H. Tsuda, “640 Gbit/s (16 channel×42.7 Gbit/s) WDM L-band DSF transmission experiment using 25 nm bandwidth AWG dispersion slope compensator,” Electronics Letters, Volume 36, Issue 19, pp. 1638 – 1639 (2000).

(7) A. Hirano, H. Tsuda, H. Kobayashi, R. Takahashi, M. Asobe, K. Sato, K. Hagimoto,“All-optical discrimination based on nonlinear transmittance of MQW semiconductor optical gates,” Journal of Lightwave Technology, Volume 17, Issue 5, pp. 873-884 (1999).

(8) A. Hirano, T. Kataoka, S. Kuwahara, M. Asobe, Y. Yamabayashi, “All-optical limiter circuit based on four-wave mixing in optical fibres,” Electronics Letters, Volume 34, Issue 14, pp. 1410‐1411 (1998).

【Other Journal Papers】

(1) Masanori Nakamura, Fukutaro Hamaoka, Asuka Matsushita, Kengo Horikoshi, Hiroshi Yamazaki, Munehiko Nagatani, Akihide Sano, Akira Hirano, Yutaka Miyamoto, "*Coded 8-Dimensional QAM Technique Using Iterative Soft-Output Decoding and Its Demonstration in High Baud-Rate Transmission*," Journal of Lightwave Technology, Volume 35, Issue 8 pp. 1369-1375 (2017).

(2) Takafumi Tanaka, Tetsuro Inui, Akihiro Kadohata, Wataru Imajuku, Akira Hirano, "*Mult-iperiod IP-Over-Elastic Network Reconfiguration With Adaptive Bandwidth Resizing and Modulation*. Journal of Optical Communications and Networking, " Vol. 8, Issue 7, pp. A180-A190 (2016)

(3) Akihiro KADOHATA, Takafumi TANAKA, Atsushi WATANABE, Akira HIRANO, Hiroshi HASEGAWA, Ken-ichi SATO, "*Differential Reliability Path Accommodation Design and Reconfiguration in Virtualized Multi-Layer Transport Network*, "IEICE Transactions on Communications, Vol.E98-B No.11 pp.2151-2159 (2015)

(4) M. Yoshida, K. Yonenaga, and A. Hirano, "*Dispersion insensitive demodulation using spectral symmetry of real-valued signals,*" . Electronics Letters, Volume 51, Issue 24, pp.2024-2026 (2015)

(5) F. Hamaoka, S. Okamoto, K. Horikoshi, K. Yonenaga, A. Hirano, and Y. Miyamoto, "*Mode-selective coherent detection technique for low-complexity mode division multiplexing systems*," Electronics Letters, Volume 51, Issue 23, pp. 1899 – 1900 (2015).

(6) Akihiro KADOHATA, Atsushi WATANABE, Akira HIRANO, Hiroshi HASEGAWA, Ken-ichi SATO, "*Pre-Adjustment Rerouting for Wavelength Defragmentation in Optical Transparent WDM Networks*," IEICE Transactions on Communications, Vol.E98-B No.10, pp.2014-2021 (2015).

(7) Akihiro Kadohata, Atsushi Watanabe, Akira Hirano, "*Sub-lambda and Wavelength Path Reconfiguration in Multi-layer Transport Networks [Invited]*," Journal of Optical Communications and Networking, Vol. 7, Issue 3, pp. A432-A439 (2015).

(8) Akira Hirano, Yoshiaki Yamada, Takafumi Tanaka, Tetsuya Oda, Kengo Shintaku, Tomoki Inui, "*Cost effective and robust optical network by inversely aggregated networking with programmable protection architecture*," Electronics Letters, Volume 50, Issue 20, pp. 1459 – 1461 (2014).

(9) Zhi-Shu Shen, Hiroshi Hasegawa, Ken-Ichi Sato, Takafumi Tanaka, Akira Hirano, "*A novel elastic optical path network that utilizes bitrate-specific anchored frequency slot arrangement*," Optics Express, vol. 22(3), pp. 3169-79, (2014).

(10) Takafumi Tanaka, Akira Hirano, Masahiko Jinno, "*Advantages of IP over elastic optical networks using multi-flow transponders from cost and equipment count aspects*," Optics Express, vol., 22(1), pp. 62-70, (2014).

(11) Masahiko Jinno, Hidehiko Takara, Kazushige Yonenaga, Akira Hirano, "*Virtualization in Optical Networks from Network Level to Hardware Level [Invited]*. Journal of Optical Communications and Networking," vol. 5(10), pp. A46-A56, (2013).

(12) Takafumi Tanaka, Akira Hirano, Masahiko Jinno, "*Impact of Transponder Architecture on the Scalability of Optical Nodes in Elastic Optical Networks*," IEEE Communications Letters, vol. 17(9), pp. 1846-1848, (2013).

(13) Akihiro Kadohata, Akira Hirano, Fumikazu Inuzuka, Atsushi Watanabe, Osamu Ishida, "*Wavelength Path Reconfiguration Design in Transparent Optical WDM Networks*. Journal of Optical Communications and Networking," vol. 5(7), pp. 751-761, (2013).

(14) Tatsumi Takagi, Hiroshi Hasegawa, Ken-Ichi Sato, Yoshiaki Sone, Akira Hirano, Masahiko Jinno, "*Impact of Elastic Optical Paths That Adopt Distance Adaptive Modulation to Create Efficient Networks*," IEICE Transactions on Communications, vol. E95.B(12), pp. 3793-3801, (2012).

(15) Masahiko Jinno, Hidehiko Takara, Yoshiaki Sone, Kazushige Yonenaga, Akira Hirano, "*Multi-flow Optical Transponder for Efficient Multilayer Optical Networking*," IEEE Communications Magazine, vol. 50(5), pp. 56-65, (2012).

(16) Akihiro Kadohata, Akira Hirano, Mitsunori Fukutoku, Takuya Ohara, Yoshiaki Sone, Osamu Ishida, "*Multi-Layer Greenfield Re-Grooming with Wavelength Defragmentation*," IEEE Communications Letters, vol. 16(4), pp. 530-532, (2012).

(17) Masahiko Jinno, Hidehiko Takara, Yoshiaki Sone, Kazushige Yonenaga, Akira Hirano, "*Elastic Optical Path Network Architecture: Framework for Spectrally-Efficient and Scalable Future Optical Networks*," IEICE Transactions on Communications, vol. E95.B(3), pp. 706-713, (2012).

(18) Masahiko Jinno, Takuya Ohara, Yoshiaki Sone, Akira Hirano, Osamu Ishida, Masahito Tomizawa, "*Elastic and adaptive optical networks: Possible adoption scenarios and future standardization aspects*," IEEE Communications Magazine, vol. 49(10), pp. 164-172, (2011).

(19) Bartlomiej Kozicki, Hidehiko Takara, Takafumi Tanaka, Yoshiaki Sone, Akira Hirano, Kazushige Yonenaga, Masahiko Jinno, "*Distance-Adaptive Path Allocation in Elastic Optical Path Networks*," IEICE Transactions on Communications, vol. 94-B(7), pp. 1823-1830, (2011).

(20) Yukio Tsukishima, Michiaki Hayashi, Tomohiro Kudoh, Akira Hirano, Takahiro Miyamoto, Atsuko Takefusa, Atsushi Taniguchi, Shuichi Okamoto, Hidemoto Nakada, Yasunori Sameshima, Hideaki Tanaka, Fumihiro Okazaki, Masahiko Jinno, "*Grid Network Service-Web Services Interface Version 2 Achieving Scalable Reservation of Network Resources Across Multiple Network Domains via Management Plane*," IEICE Transactions on Communications, vol. 93-B(10), pp. 2696-2705, (2010).

(21) Masahiko Jinno, Bartlomiej Kozicki, Hidehiko Takara, Atsushi Watanabe, Yoshiaki Sone, Takafumi Tanaka, Akira Hirano, "*Distance-Adaptive Spectrum Resource Allocation in Spectrum-Sliced Elastic Optical Path Network*," IEEE Communications Magazine, vol. 48(8-48), pp. 138 - 145, (2010).

(22) Yukio Tsukishima, Yasunori Sameshima, Akira Hirano, Masahiko Jinno, Tomohiro Kudoh, Fumihiro Okazaki, "*Multi-Layer Lambda Grid With Exact Bandwidth Provisioning*

Over Converged IP and Optical Networks," Journal of Lightwave Technology, vol. 27(12), pp. 1776-1784, (2009).

(23) Akira Hirano, Luc Renambot, Byungil Jeong, Jason Leigh, Alan Verlo, Venkatram Vishwanath, Rajvikram Singh, Julieta Aguilera, Andrew Johnson, Thomas A. DeFanti, Lance Long, Nicholas Schwarz, Maxine Brown, Naohide Nagatsu, Yukio Tsukishima, Masahito Tomizawa, Yutaka Miyamoto, Masahiko Jinno, Yoshihiro Takigawa, Osamu Ishida, "*The first functional demonstration of optical virtual concatenation as a technique for achieving Terabit networking*," Future Generation Computer Systems, vol. 22(8-22), pp. 876-883, (2006).

(24) Y. Tsukishima, A. Hirano, M. Jinno, "*Application-aware synergetic network control technology demonstrated in a field trial in US nationwide photonic network*," NTT Technical Review, vol. 4, No. 9, pp. 53-60, (2006).

(25) H. Masuda, K. Sato, A. Hirano, Y. Miyamoto, "*Pump-wavelength detuning method for forward pumped distributed Raman amplification systems*," Electronics Letters, vol. 2005(10-41), pp. 608-610, (2005).

(26) A. Hirano, S. Kuwahara, M. Yoneyama, Y. Kisaka, M. Tomizawa, Y. Miyamoto, W. Weiershausen, R. Leppla, O. Leminger, F. Rumpf, R. Herber, A. Mattheus, A. Gladisch, "*Field trial of 43 Gbit/s CS-RZ OTN system in PMD-limited transmission links*," Electronics Letters, vol. 40(15-40), pp. 957-958, (2004).

(27) Werner Weiershausen, Ralph Leppla, Ottokar Leminger, Frank Rumpf, Ralf Herber, Arnold Mattheus, Andreas Gladisch, Akira Hirano, Yoshiaki Kisaka, Yutaka Miyamoto, Shoichiro Kuwahara, Mikio Yoneyama, Masahito Tomizawa, "*PMD outage measurements in a joint field trial of a 43-Gbit/s NTT WDM transmission system within DT's installed fiber environment*," Procedia - Social and Behavioral Sciences, (2004).

(28) Akira Hirano, Shoichiro Kuwahara, Mikio Yoneyama, Yoshiaki Kisaka, Masahito Tomizawa, Yutaka Miyamoto, Werner Weiershausen, Ralph Leppla, Ottokar Leminger, Frank Rumpf, Ralf Herber, Arnold Mattheus, Andreas Gladisch, "*PMD-limited*

transmission with CS-RZ and NRZ in joint field trial: 43-Gbit/s NTT's transport system in DT's installed fiber environment," Procedia - Social and Behavioral Sciences, (2004).

(29) H. Masuda, H. Kawakami, S. Kuwahara, A. Hirano, K. Sato, Y. Miyamoto, "*1.28 Tbit/s (32 × 43 Gbit/s) field trial over 528 km (6 × 88 km) DSF using L-band remotely-pumped EDF/distributed Raman hybrid inline amplifiers*,"Electronics Letters, vol. 39(23-39), pp. 1668-70, (2003).

(30) S. Kuwahara, A. Hirano, H. Masuda, H. Kawakami, Y. Miyamoto, M. Yoneyama, Y. Kisaka, K. Sato, M. Tomizawa, Y. Tada, T. Sawabe, T. Fujii, K. Yonenaga, "*WDM field demonstration of path provision by automatic dispersion compensation using tone modulated CS-RZ signal*," Electronics Letters, vol. 39(22-39), pp. 1601 – 1603, (2003).

(31) M. Tomizawa, Y. Kisaka, A. Hirano, M. Yoneyama, Y. Miyamoto, "*Error controlling optical receiver with diverse detection*," Electronics Letters, vol. 39(13-39), pp. 1002 – 1004, (2003).

(32) R. Kasahara, Y. Inoue, M. Ishii, A. Hirano, Y. Miyamoto, H. Takahashi, Y. Hibino, "*Cyclic and rectangular passband optical bandpass filter using AWG pair*,"Electronics Letters, vol. 39(12-39), pp. 910 - 911, (2003).

(33) M. Tomizawa, A. Hirano, S. Ishibashi, T. Sakamoto, "*International Standardization Activities on Optical Interfaces*," NTT Technical Review, vol. 1, No. 3, pp. 85-89, (2003).

(34) T. Ohara, H. Takara, A. Hirano, K. Mori, S. Kawanishi, "*40-Gb/s × 4-channel all-optical multichannel limiter utilizing spectrally filtered optical solitons*," IEEE Photonics Technology Letters, vol. 15(5-15), pp. 763 - 765, (2003).

(35) Y. Kisaka, A. Tomizawa, A. Hirano, S. Kuwahara, Y. Miyamoto, "*Compact-spectrum RZ signal generated by single-stage push-pull type Mach-Zehnder modulator for DWDM transmission*," Electronics Letters, vol. 39(3-39), pp. 304 - 306, (2003).

(36) S. Kuwahara, Y Miyamoto, A Hirano, "*Automatic chromatic dispersion compensation using alternating chirp signal for installation of high-speed transmission systems*," Journal of Lightwave Technology, vol. 20(12), pp. 2044-2051, (2003).

(37) Yutaka Miyamoto, Akira Hirano, Shoichiro Kuwahara, Masahito Tomizawa, Yasuhiko Tada, *"Novel modulation and detection for bandwidth-reduced RZ formats using duobinary-mode splitting in wideband PSK/ASK conversion*. Journal of Lightwave Technology, vol. 20(12), pp. 2067-2078, (2003).

(38) Y. Miyamoto, H. Masuda, A. Hirano, S. Kuwahara, Y. Kisaka, H. Kawakami, M. Tomizawa, Y. Tada, S. Aozasa, *"S-band WDM coherent transmission of 40 x 43-Gbit/s CS-RZ DPSK signals over 400 km DSF using hybrid GS-TDFAs/Raman amplifiers*," Electronics Letters, vol. 38(24-38), pp. 1569-1570, (2002).

(39) Akira Hirano, Yutaka Miyamoto, Shoichiro Kuwahara, Masahito Tomizawa, Koichi Murata, *"A novel mode-splitting detection scheme in 43-Gb/s CS- and DCS-RZ signal transmission*," Journal of Lightwave Technology, vol. 20(12), pp. 2029, (2002).

(40) Yutaka Miyamoto, Tomoyoshi Kataoka, Kazushige Yonenaga, Masahito Tomizawa, Akira Hirano, Shoichiro Kuwahara, Yasuhiko Tada, *"WDM field trials of 43Gb/s/channel transport system for optical transport network*," Journal of Lightwave Technology, vol. 20(12), pp. 2115-2128, (2002).

(41) A. Hirano, Y. Miyamoto, K. Yonenaga, S. Kuwahara, H. Miyazawa, K. Murata, K. Sato, Y. Tada, *"SSB direct detection scheme in duobinary-carrier-suppressed RZ transmission*," Electronics Letters, vol. 38(12-38), pp. 585 - 587, (2002).

(42) A. Hirano, S. Kuwahara, Y. Miyamoto, K. Murata, *"Dispersion accommodation scheme comparing relative bit-phase of two SSB signals generated from spectrally filtered CS-RZ signal*. Electronics Letters, vol. 38(12-38), pp. 580 - 582, (2002).

(43) S. Kuwahara, K. Yonenaga, Y. Miyamoto, Y. Kisaka, K. Sato, A. Hirano, T. Ono, A. Matsuura, M. Tomizawa, T. Kataoka, Y. Tada, H. Toba, K. Hagimoto, N. Hirayama, H. Asai, *"1 Tbit/s (25 × 43 Gbit/s) field trial using 43-Gbit/s/ch OTN interface prototype*," IEICE Transactions on Communications, vol. E85B(2), pp. 470-477, (2002).

(44) A. Hirano, M. Asobe, K. Sato, Y. Miyamoto, K. Yonenaga, H. Miyazawa, M. Abe, H. Takara, I. Shake, *"Dispersion tolerant 80-Gbit/s carrier-suppressed return-to-zero (CS-RZ) format generated by using phase- and duty-controlled optical time division multiplexing*

(OTDM) technique," IEICE Transactions on Communications, vol. E85B(2), pp. 431-437, (2002).

(45) Y. Miyamoto, K. Yonenaga, A. Hirano, M. Tomizawa, "*N x 40-Gbit/s DWDM transport system using novel Return-to-Zero formats with modulation bandwidth reduction*," IEICE Transactions on Communications, vol. E85B(2), pp. 374-385, (2002).

(46) Y. Miyamoto, K. Yonenaga, A. Hirano, H. Toba, K. Murata, H. Miyazawa, "*100 GHz-spaced 8×43 Gbit/s DWDM unrepeatered transmission over 163 km using duobinary-carrier-suppressed return-to-zero format*," Electronics Letters, vol. 37(23-37), pp. 1395 – 1396, (2001).

(47) S. Kuwahara, K. Yonenaga, Y. Miyamoto, Y. Kisaka, K. Sato, A. Hirano, T. Ono, A. Matsuura, M. Tomizawa, T. Kataoka, Y. Tada, H. Toba, N. Hirayama, H. Asai, "*1 Tbit/s field trial with 100 GHz spacing over 91 km SMF using 43 Gbit/s/channel OTN interface prototype*," Electronics Letters, vol. 37(14-37), pp. 904 - 906, (2001).

(48) H. Takenouchi, T. Goh, T. Ishii, A. Hirano, "*8 THz bandwidth dispersion-slope compensator module for multiband 40 Gbit/s WDM transmission systems using an AWG and spatial phase filter*," Electronics Letters, vol. 37, pp. 777 - 778, (2001).

(49) A. Hirano, K. Yonenaga, Y. Miyamoto, H. Toba, H. Takenouchi, H. Tsuda, "*640 Gbit/s (16 channel×42.7 Gbit/s) WDM L-band DSF transmission experiment using 25 nm bandwidth AWG dispersion slope compensator*," Electronics Letters, vol. 36, pp. 1638-1639, (2000).

(50) Hiroyuki Tsuda, Hirokazu Takenouchi, Akira Hirano, Takashi Kurokawa, Katsunari Okamoto, "*Performance analysis of a dispersion compensator using arrayed-waveguide gratings*," Journal of Lightwave Technology, vol. 18(8-18), pp. 1139-1147, (2000).

(51) N. Shimizu, K. Murata, A. Hirano, Y. Miyamoto, H. Kitabayashi, Y. Umeda, T. Akeyoshi, T. Furuta, N. Watanabe, "*40 Gbit/s monolithic digital OEIC composed of unitravelling-carrier photodiode and InP HEMTs*," Electronics Letters, vol. 36(14-36), pp. 1220 - 1221, (2000).

(52) Y. Miyamoto, K. Yonenaga, S. Kuwahara, M. Tomizawa, A. Hirano, H. Toba, K. Murata, Y. Tada, Y. Umeda, H. Miyazawa, "*1.2 Tbit/s (30×42.7 Gbit/s ETDM channel) WDM*

transmission over 3×125 km with forward error correction," Electronics Letters, vol. 36(9-36), pp. 812 - 813, (2000).

(53) K. Sato, A. Hirano, N. Shimizu, T. Ohno, H. Ishii, "*Optical millimetre-wave generation by dual-mode operation of semiconductor modelocked lasers*," Electronics Letters, vol. 36(4-36), pp. 340 - 342, (2000).

(54) K. Yonenaga, A. Hirano, S. Kuwahara, Y. Miyamoto, H. Toba, K. Sato, H. Miyazawa, "*Temperature-independent 80 Gbit/s OTDM transmission experiment using zero-dispersion-flattened transmission line*," Electronics Letters, vol. 36(4-36), pp. 343 - 345, (2000).

(55) K. Yonenaga, Y. Miyamoto, A. Hirano, A. Sano, S. Kuwahara, H. Kawakami, H. Toba, K. Murata, M. Fukutoku, Y. Yamane, K. Noguchi, T. Ishibashi, K. Nakajima, "*320 Gbit/s WDM field experiment using 40 Gbit/s ETDM channels over 176 km dispersion-shifted fibre with nonlinearity-tolerant signal format*," Electronics Letters, vol. 36(2-36), pp. 153 - 155, (2000).

(56) A. Hirano, Y. Miyamoto, K. Yonenaga, A. Sano, H. Toba, "*40 Gbit/s L-Band Transmission Experiment Using SPM-Tolerant Carrier-Suppressed RZ Format*," Electronics Letters, vol. 35(25-35), pp. 2213 - 2215, (2000).

(57) Y. Miyamoto, A. Hirano, K. Yonenaga, A. Sano, H. Toba, K. Murata, O. Mitomi, "*320 Gb/s (8 × 40 Gb/s) WDM transmission over 367 km with 120 km repeater spacing using carrier-suppressed return-to-zero format*," Electronics Letters, vol. 35(23-35), pp. 2041 - 2042, (1999).

(58) H. Tsuda, H. Takenouchi, T. Ishii, K. Okamoto, T. Goh, K. Sato, A. Hirano, T. Kurokawa, C. Amano, "*Spectral encoding and decoding of 10Gbit/s femtosecond pulses using high resolution arrayed-waveguide grating*," Electronics Letters, vol. 35(14-35), pp. 1186 - 1188, (1999).

(59) K. Sato, A. Hirano, N. Shimizu, I. Kotaka, "*High-frequency and low-jitter optical pulse generation using semiconductor mode-locked lasers*," IEEE Transactions on Microwave Theory and Techniques, vol. 47(7-47), pp. 1251 - 1256, (1999).

(60) Y. Kisaka, A. Hirano, M. Yoneyama, N. Shimizu, "*Simple 2R repeater based on EA modulator directly driven by uni-travelling-carrier photodiode*," Electronics Letters, vol. 35(12-35), pp. 1016 - 1017, (1999).

(61) K. Sato, A. Hirano, H. Ishii, "*Chirp-Compensated 40-GHz Mode-Locked Lasers Integrated With Electroabsorption Modulators and Chirped Gratings*," IEEE Journal of Selected Topics in Quantum Electronics, vol. 5(3-5), pp. 590 - 595, (1999).

(62) Akira Hirano, Hiroyuki Tsuda, Hideki Kobayashi, Ryo Takahashi, Masaki Asobe, Kenji Sato, Kazuo Hagimoto, "*All-optical discrimination based on nonlinear transmittance of MQW semiconductor optical gates*," Journal of Lightwave Technology, vol. 17(5-17), pp. 873 - 884, (1999).

(63) K. Sato, A. Hirano, M. Asobe, H. Ishii, "*Chirp-compensated 40 GHz semiconductor modelocked lasers integrated with chirped gratings*," Electronics Letters, vol. 34(20-34), pp. 1944 - 1945, (1998).

(64) A. Hirano, T. Kataoka, S. Kuwahara, M. Asobe, Y. Yamabayashi, "*All-optical limiter circuit based on four-wave mixing in optical fibres*," Electronics Letters, vol. 34(14-34), pp. 1410 - 1411, (1998).

(65) M. Asobe, A. Hirano, Y. Miyamoto, K. Sato, K. Hagimoto, Y. Yamabayashi, "*Noise reduction of 20 Gbit/s pulse train using spectrally filtered optical solitons*," Electronics Letters, vol. 34(11-34), pp. 1135 - 1136, (1998).

(66) K. Sato, I. Kotaka, A. Hirano, M. Asobe, Y. Miyamoto, N. Shimizu, K. Hagimoto, "*High-repetition frequency pulse generation at 102 GHz using modelocked lasers integrated with electroabsorption modulators*," Electronics Letters, vol. 34(8-34), pp. 790 - 792, (1998).

(67) M. Asobe, Y. Miyamoto, A. Hirano, M. Yoneyama, H. Okamura, K. Hagimoto, H. Masuda, K. Aida, "*Simultaneous transmission of bandwidth-weighted TDM and WDM signals within a wideband optical amplifier gain-band*," Electronics Letters, vol. 34(5-34), pp. 487 - 488, (1998).

(68) K. Yonenaga, A. Hirano, M. Yoneyama, Y. Miyamoto, K. Hagimoto, K. Noguchi, "*Expansion of tolerable dispersion range in a 40 Gbit/s optical transmission system using an optical duobinary signal*," Electronics Letters, vol. 34(4-34), pp. 385 - 386, (1998).

(69) A. Hirano, H. Kobayashi, H. Tsuda, R. Takahashi, M. Asobe, K. Sato, K. Hagimoto, "*10 Gbit/s RZ all-optical discrimination using refined saturable absorber optical gate*," Electronics Letters, vol. 34(2-34), pp. 198 - 199, (1998).

(70) K. Wakita, K. Yoshino, A. Hirano, S. Kondo, Y. Noguchi, "*Very-high-speed and low driving-voltage modulator modules for a short optical pulse generation*," IEICE Transactions on Electronics, vol. E81C(2), pp. 175-179, (1998).

(71) M. Yoneyama, A. Sano, T. Kataoka, A. Hirano, T. Otsuji, K. Sato, H. Miyazawa, K. Hagimoto, "*40 Gbit/s optical repeater circuit using InAlAs/InGaAs HEMT digital IC modules*," Electronics Letters, vol. 33(23), pp. 1977-1978, (1997).

(72) M. Asobe, A. Hirano, K. Hagimoto, K. Sato, K. Naganuma, "*Noise and chirping characteristics of mode-locked laser diodes integrated with electroabsorption modulator*," Electronics Letters, vol. 33(10-33), pp. 883 - 885, (1997).

(73) A. Sano, T. Kataoka, H. Tsuda, A. Hirano, K. Murata, H. Kawakami, Y. Tada, K. Hagimoto, K. Sato, K. Wakita, K. Kato, Y. Miyamoto, "*Field experiments on 40 Gbit/s repeaterless transmission over 198 km dispersion-managed submarine cable using a monolithic mode-locked laser diode*," Electronics Letters, vol. 32(13-32), pp. 1218 - 1220, (1996).

(74) H Tsuda, A Hirano, R Takahashi, K Sato, K. Hagimoto, "*2.4Gbit/s all-optical pulse discrimination experiment using a high-speed saturable absorber optical*," Electronics Letters, vol. 32(4), pp. 365, (1996).

(75) Akira Hirano, Shunji Kitamoto, Tatsuya.Yamada, Shin Mineshige, Jun Fukue, "*Accretion Disk Structure and Branch Behavior of Cygnus X-2*," The Astrophysical Journal, vol. 446(1), pp. 350, (1995).

(76) A. Hirano, H. Tsuda, K. Hagimoto, R. Takahashi, Y. Kawamura, H. Iwamura, "*10ps pulse all-optical discrimination using a high-speed saturable absorber optical gate*," Electronics Letters, vol. 31(9), pp. 736-737, (1995).

(77) Shunji Kitamoto, Akira Hirano, Kenji Kawashima, Sigenori Miyamoto, Fumiaki Nagase, Nicholas E. White, Alan P. Smale, Yang Soong, Masaru Matsuoka, Nobuyuki Kawai, Atsumasa Yoshida, "*Orbital Period Changes of Cygnus X-3*," Publications- Astronomical Society of Japan, vol. 47, pp. 233-238, (1995).

(78) Shin Mineshige, Akira Hirano, Shunji Kitamoto, Tatsuya Yamada, Jun Fukue, "*Time-dependent disk accretion in X-ray Nova MUSCAE 1991*," The Astrophysical Journal, vol. 426(1), pp. 308-312, (1994).

(79) S. Mineshige, F. Honma, A. Hirano, S. Kitamoto, T. Yamada, J. Fukue, "*Temperature Profiles of Accretion Disks in X-Ray Binaries*," NATO ASI Series book series, vol. 417 Theory of Accretion Disks – 2, pp. 187-193, (1994).

(80) H. Tsunemi, K. Hayashida, K. Tamura, S. Nomoto, M. Wada, A. Hirano, E. Miyata, "*Detection of X-ray polarization with a charge coupled device*," Nuclear Instruments and Methods in Physics Research Section A Accelerators Spectrometers Detectors and Associated Equipment, vol. 321(3), pp. 629-631, (1992).

【Full-length Papers in International Conferences】

(1) M. Jinno, T. Ohara, Y. Sone, A. Hirano, O. Ishida, M. Tomizawa, "*Introducing elasticity and adaptation into the optical domain toward more efficient and scalable optical transport networks*," Kaleidoscope: Beyond the Internet? - Innovations for Future Networks and Services, ITU-T, pp. 1-7, (2010).

(2) Werner Weiershausen, Ralph Leppla, Ottokar Leminger, Frank Rumpf, Ralf Herber, Arnold Mattheus, Andreas Gladisch, Akira Hirano, Yoshiaki Kisaka, Yutaka Miyamoto, Shoichiro Kuwahara, Mikio Yoneyama, "*OTU3 transmission with 43-Gbit/s-CS-RZ signals over installed G.652 fiber infrastructure and accelerated PMD outage evaluation*," Proceedings of SPIE - The International Society for Optical Engineering, vol. 5596, pp. 1117-1129, (2004).

(3) Masahito Tomizawa, Yoshiaki Kisaka, Akira Hirano, Yutaka Miyamoto, "*Error control and modulation/detection techniques in WDM transmission systems*," Proceedings of SPIE - The International Society for Optical Engineering, vol. 5247, p. 266-275, (2003).

(4) Akira Hirano, Yutaka Miyamoto, Shoichiro Kuwahara, "*Spectral mode splitting scheme: Application to 40-Gbit/s RZ-ASK and RZ-PSK transmission*," Proceedings of SPIE - The International Society for Optical Engineering, vol. 5247, pp. 307-320, (2003).

(5) Akira Hirano, Yutaka Miyamoto, Masahito Tomizawa, "*Impact of modulation formats on 40-Gbit/s/ch WDM networks*," Proceedings of SPIE - The International Society for Optical Engineering, vol. 4872, pp. 11-23, (2002).

【International Conference Papers】

(1) Masanori Nakamura, Fukutaro Hamaoka, Asuka Matsushita, Hiroshi Yamazaki, munehiko nagatani, akihide sano, Akira Hirano, Yutaka Miyamoto, "*120-GBaud Coded 8 Dimensional 16QAM WDM Transmission Using Low-Complexity Iterative Decoding Based on Bit-Wise Log Likelihood Ratio*," Optical Fiber Communication Conference, W4A.3, (2017).

(2) Fukutaro Hamaoka, Seiji Okamoto, Kengo Horikoshi, Kazushige Yonenaga, Akira Hirano, Yutaka Miyamoto, "*Mode and Polarization Division Multiplexed Signal Detection with Single Coherent Receiver Using Mode-Selective Coherent Detection Technique*," Optical Fiber Communication Conference, Th3A.6, (2016).

(3) Kengo Shintaku, Yoshiaki Yamada, Shoukei Kobayashi, Akira Hirano, Yusuke Koizumi, "*High-availability optical multi-carrier interface for operational expenditure reduction*," 21st Asia-Pacific Conference on Communications (APCC), (2015).

(4) Takafumi Tanaka, Tetsuro Inui, Wataru Imajuku, Akira Hirano, "*Subcarrier restoration for survivable multi-flow transponders in elastic optical networks*," 21st Asia-Pacific Conference on Communications (APCC), (2015).

(5) Akihiro Kadohata, Takafumi Tanaka, Atsushi Watanabe, Akira Hirano, Hiroshi Hasegawa, Ken-ichi Sato, "*Path accommodation design and reconfiguration for different reliability classes in virtualized multi-layer transport network*," Opto-Electronics and Communications Conference (OECC), (2015).

(6) Takafumi Tanaka, Akira Hirano, "*An in-operation IP-over-optical network planning method that supports unpredictable IP traffic transitions*," European Conference on Optical Communication, 21-25 Sept. (2014).

(7) Takuya Oda, Akihiro Kadohata, Atsushi Watanabe, Akira Hirano, "*Optical network optimization considering maintenance-related operational expenditure*," European Conference on Optical Communication, 21-25 Sept. (2014).

(8) T. Tanaka, A. Hirano, M. Jinno, "*Impact of Multi-flow Transponder on Equipment Requirements in IP over Elastic Optical Networks*," Optical Communication (ECOC 2013), 39th European Conference and Exhibition, (2013).

(9) Akihiro Kadohata, Takafumi Tanaka, Fumikazu Inuzuka, Atsushi Watanabe, Akira Hirano, "*Wavelength Defragmentation Algorithm for Transparent Multi-ring Networks with Multiple Fibers per Link*," Optical Fiber Communication Conference and Exposition and the National Fiber Optic Engineers Conference (OFC/NFOEC), OW3A.7, (2013).

(10) Masahiko Jinno, Akira Hirano, "*Toward Deeply Virtualized Elastic Optical Networks*," Optical Fiber Communication Conference and Exposition and the National Fiber Optic Engineers Conference (OFC/NFOEC), NM2E.2, (2013).

(11) Zhi-shu Shen, H. Hasegawa, K.-I. Sato, T. Tanaka, A. Hirano, "*A Novel Semi-flexible Grid Optical Path Network That Utilizes Aligned Frequency Slot Arrangement*," Optical Communication (ECOC 2013), 39th European Conference and Exhibition, (2013).

(12) Akira Hirano, "*Design Plasticity in Elastic Optical Network for Unpredictable Traffic*," European Conference and Exhibition on Optical Communication, Mo.1.D.5, (2012).

(13) Akira Hirano, "*Highly efficient and reconfigurable networking technologies*," Opto-Electronics and Communications Conference (OECC), (2012).

(14) Shun Kosaka, Hiroshi Hasegawa, Ken-ichi Sato, Takafumi Tanaka, Akira Hirano, Masahiko Jinno, "*Shared Protected Elastic Optical Path Network Design that Applies Iterative Re-optimization based on Resource Utilization Efficiency Measures*," European Conference and Exhibition on Optical Communication, (2012).

(15) Fumikazu Inuzuka, Akihiro Kadohata, Takafumi Tanaka, Yoshiaki Sone, Akira Hirano, Atsushi Watanabe, Osamu Ishida, "*Optical path accommodation efficiency with provisioning order in Least Fragmentation algorithm*," Opto-Electronics and Communications Conference (OECC), (2012).

(16) Takafumi Tanaka, Akira Hirano, Masahiko Jinno, "*Performance Evaluation of Elastic Optical Networks with Multi-Flow Optical Transponders*," European Conference and Exhibition on Optical Communication (ECOC), (2012).

(17) T. Tanaka, A. Hirano, M. Jinno, "*Comparative study of optical networks with grid flexibility and traffic grooming*," 10th International Conference on Optical Internet (COIN), (2012).

(18) A. Kadohata, A. Hirano, F. Inuzuka, A. Watanabe, O. Ishida, "*Wavelength defragmentation design for multi-fiber WDM networks*," 10th International Conference on Optical Internet (COIN), (2012).

(19) Tatsumi Takagi, Hiroshi Hasegawa, Ken-ichi Sato, Yoshiaki Sone, Akira Hirano, Masahiko Jinno, "*Disruption Minimized Spectrum Defragmentation in Elastic Optical Path Networks that Adopt Distance Adaptive Modulation*," European Conference and Exhibition on Optical Communication (ECOC), Mo.2.K.3, (2011).

(20) Masahiko Jinno, Yoshiaki Sone, Hidehiko Takara, Akira Hirano, Kazushige Yonenaga, Shingo Kawai, "*IP Traffic Offloading to Elastic Optical Layer Using Multi-flow Optical Transponder*," European Conference and Exhibition on Optical Communication (ECOC), Mo.2.K.2, (2011).

(21) Yoshiaki Sone, Akira Hirano, Akihiro Kadohata, Masahiko Jinno, Osamu Ishida, "*Routing and Spectrum Assignment Algorithm Maximizes Spectrum Utilization in Optical Networks*," European Conference and Exhibition on Optical Communication (ECOC), Mo.1.K.3, (2011).

(22) Akihiro Kadohata, Akira Hirano, Yoshiaki Sone, Osamu Ishida, "*Wavelength Path Reconfiguration to Reduce Fragmentation and Number of Operations in WDM Mesh Networks*," European Conference and Exhibition on Optical Communication (ECOC), Mo.2.K.5, (2011).

(23) Takafumi Tanaka, Yoshiaki Sone, Akira Hirano, Osamu Ishida, "*Efficient resource sharing scheme based on path duration in transport network*," Opto-Electronics and Communications Conference (OECC), Kaohsiung, Taiwan (2011).

(24) Yoshiaki Sone, Akira Hirano, Akihiro Kadohata, Osamu Ishida, "*Efficient routing and wavelength assignment algorithm minimizes wavelength fragmentations in WDM mesh networks*," Opto-Electronics and Communications Conference (OECC), Kaohsiung, Taiwan (2011).

(25) Takuya Ohara, Mitsunori Fukutoku, Akihiro Kadohata, Akira Hirano, Takeshi Kawai, Tetsuro Komukai, Masahiro Suzuki, Shigeki Aisawa, Tetsuo Takahashi, Masahito

Tomizawa, Osamu Ishida, Shinji Matsuoka, "*Optimized Multi-Layer Optical Network using In-service ODU / Wavelength Path Re-grooming*," NFOEC, NMC5, (2011).

(26) Tatsumi Takagi, Hiroshi Hasegawa, Ken-ichi Sato, Yoshiaki Sone, Bartlomiej Kozicki, Akira Hirano, Masahiko Jinno, "*Dynamic Routing and Frequency Slot Assignment for Elastic Optical Path Networks that Adopt Distance Adaptive Modulation*," OFC, OTuI7, (2011).

(27) H. Takara, B. Kozicki, Y. Sone, T. Tanaka, A. Watanabe, A. Hirano, K. Yonenaga, M. Jinno, "*Distance-Adaptive Super-Wavelength Routing in Elastic Optical Path Network (SLICE) with Optical OFDM*," 36th European Conference and Exhibition on Optical Communication (ECOC), (2010).

(28) B. Kozicki, H. Takara, A. Watanabe, Y. Sone, T. Tanaka, A. Hirano, K. Yonenaga, M. Jinno, "*Distance-adaptive spectrum allocation in SLICE considering optical filtering effects*," Opto-Electronics and Communications Conference (OECC), 2010.

(29) Akira Hirano, "*Recent Progress on Optical Transmission Systems*. The Review of Laser Engineering (APLS), pp. 1314-1315, (2008).

(30) Yukio Tsukishima, Yasunori Sameshima, Akira Hirano, Masahiko Jinno, Tomohiro Kudoh, Fumihiro Okazaki, "*Multi-layer lambda Grid properly using lambdas and sub-lambdas*," ECOC, (2008).

(31) Atsushi Taniguchi, Akira Hirano, Hidehiko Takara, Takashi Goh, Takayuki Mizuno, Akimasa Kaneko, Yoshinori Hibino, "*Wavelength Cross-Connect Switching System with Dynamic Capacity Control that uses PLC-based WSS*," 33rd European Conference and Ehxibition of Optical Communication (ECOC), (2007).

(32) Yukio Tsukishima, Akira Hirano, Naohide Nagatsu, Wataru Imajuku, Masahiko Jinno, Yoshinori Hibino, Yoshihiro Takigawa, Kazuo Hagimoto, Xi Wang, Luc Renambot, Byungil Jeong, Jason Leigh, Tom DeFanti, Alan Verlo, "*Lambda Sharing Demonstration via Traffic-Driven Lambda-on-Demand*," 33rd European Conference and Ehxibition of Optical Communication (ECOC), (2007).

(33) Tomohiro Kudoh, Shuichi Okamoto, Yukio Tsukishima, Hideaki Tanaka, Masahiko Jinno, Michiaki Hayashi, Atsuko Takefusa, Tomohiro Otani, Atsushi Taniguchi, Akira Hirano, Takahiro Miyamoto, Hidemoto Nakada, *"Network as a resource, G-lambda project and its architecture,"* gridnets, (2007).

(34) Steven R. Thorpe, Lina Battestilli, Gigi Karmous-Edwards, Andrei Hutanu, Jon Maclaren, Joe Mambretti, John H. Moore, Kamaraju Syam Sundar, Yufeng Xin, Atsuko Takefusa, Michiaki Hayashi, Akira Hirano, Shuichi Okamoto, Tomohiro Kudoh, Takahiro Miyamoto, Yukio Tsukishima, Tomohiro Otani, Hidemoto Nakada, Hideaki Tanaka, Atsushi Taniguchi, Yasunori Sameshima, Masahiko Jinno, *"G-lambda and EnLIGHTened: Wrapped In Middleware Co-allocating Compute and Network Resources Across Japan and the US,"* gridnets, (2007).

(35) Yukio Tsukishima, Akira Hirano, Naohide Nagatsu, Takuya Ohara, Wataru Imajuku, Masahiko Jinno, Yoshihiro Takigawa, Kazuo Hagimoto, Luc Renambot, Byungil Jeong, Jason Leigh, Tom Defanti, Alan Verlo, Linda Winkler, *"The First Application-driven Lambda-on-Demand Field Trial over a US Nationwide Network,"* OFC, (2006).

(36) Yukio Tsukishima, Akira Hirano, Naohide Nagatsu, Takuya Ohara, Wataru Imajuku, Masahiko Jinno, Yoshihiro Takigawa, Kazuo Hagimoto, Luc Renambot, Byungil Jeong, Jason Leigh, Tom DeFanti, Alan Verlo, Linda Winkler, *"Stable IP-Routing Link Restoration: GUNI Restoration for Data Link Failure Between Routers in a Nationwide Photonic Network,"* European Conference on Optical Communications, (2006).

(37) Akira Hirano, *"Handling Parallel Lambdas toward Terabit Networking,"* European Conference on Optical Communications, (2006).

(38) A. Hirano, *"Spectral mode splitting - Concepts and applications,"* 2004 IEEE/LEOS Workshop on Advanced Modulation Formats, (2004).

(39) Hiroji Masuda, Shoichiro Kuwahara, Hiroto Kawakami, Akira Hirano, Yutaka Miyamoto, Atsushi Mori, Tadashi Sakamoto, *"Ultra-wideband remotely-pumped EDF/DRA hybrid inline-repeater system using tellurite-based EDFs and 1500-nm pumping method,"* Optical Amplifiers and Their Applications OAA, OWB2, (2004).

(40) A Hirano, Y Miyamoto, "*Novel modulation formats in ultra-high-speed transmission systems, and their applications*," Optical Fiber Communication Conference, (2004).

(41) Hiroji Masuda, Hiroto Kawakami, Shoichiro Kuwahara, Akira Hirano, Kenji Sato, Yutaka Miyamoto, "*First field trial using novel two-stage remotely-pumped EDF/distributed Raman hybrid inline amplifiers with 1.28-Tbit/s (32 x 43 Gbit/s) capacity over 528-km (6 x 88 km) DSF in the L-band*," OAA, PD2, (2003).

(42) Yutaka Miyamoto, Akira Hirano, Shoichiro Kuwahara, "*Bandwidth-efficient RZ format for DWDM transmission using orthogonal duobinary mode splitting*,"OAA, MA1, (2003).

(43) A. Hirano, Y. Miyamoto, S. Kuwahara, "*Performances of CSRZ-DPSK and RZ-DPSK in 43-Gbit/s/ch DWDM G.652 single-mode-fiber transmission*," Optical Fiber Communications Conference, (2003).

(44) M. Tomizawa, Y. Kisaka, A. Hirano, Y. Miyamoto, "*PMD mitigation by frequency diverse detection receiver employing error-correction function*," 28th European Conference on Optical Communication, (2002).

(45) T Ohara, H. Takara, A Hirano, K Mori, S Kawanishi, "*40 Gbit/s × 4 channel, all-optical multi-channel limiter based on spectrally filtered optical solitons*," 28th European Conference on Optical Communication, (2002).

(46) S. Kuwahara, A. Hirano, Y. Miyamoto, K. Murata, "*Automatic dispersion compensation for WDM system by mode-splitting of tone-modulated CS-RZ signal*," 28th European Conference on Optical Communication, (2002).

(47) M. Tomizawa, Y. Kisaka, A. Hirano, Y. Miyamoto, "*Error correction without additional redundancy by novel optical receiver with diverse detection*," Optical Fiber Communication Conference and Exhibit, (2002).

(48) A. Hirano, S. Kuwahara, Y. Miyamoto, K. Murata, "*A novel dispersion compensation scheme based on phase comparison between two SSB signals generated from a spectrally filtered CS-RZ signal*," Optical Fiber Communication Conference and Exhibit, (2002).

(49) Yutaka Miyamoto, Akira Hirano, Shoichiro Kuwahara, Yasuhiko Tada, Koichi Murata, Hiroshi Miyazawa, "*Carrier-suppressed differential phase shift keying format for ultra-high-speed channel transmission*," OTuB2, OAA, (2002).

(50) Y. Kisaka, M Tomizawa, A Hirano, S. Kuwahara, Y Miyamoto, "*Novel compact-spectrum RZ signal generated by a single-stage push-pull type Mach-Zehnder modulator for DWDM transmission*," 28th European Conference on Optical Communication, (2002).

(51) Y. Miyamoto, S. Kuwahara, A. Hirano, Y. Tada, Y. Yamane, H. Miyazawa, "*Reduction of nonlinear crosstalk by carrier-suppressed RZ format for 100 GHz-spaced Nx43-Gbit/s WDM in non-zero dispersion shifted band*," 27th European Conference on Optical Communication, (2001).

(52) Akira Hirano, Yutaka Miyamoto, Kazushige Yonenaga, Shoichiro Kuwahara, Horoshi Miyazawa, Koichi Murata, Kenji Sato, Yasuhiko Tada, "*Expanded dispersion tolerance by SSB direct detection in duobinary-carrier-suppressed RZ signal transmission*," OTuD2, OAA, (2001).

(53) Y Miyamoto, K. Yonenaga, A Hirano, H. Toba, K Murata, H Miyazawa, "*Duobinary carrier-suppressed return-to-zero format and its application to 100 GHz-spaced 8×43-Gbit/s DWDM unrepeatered transmission over 163 km*," Optical Fiber Communication Conference and Exhibit, (2001).

(54) Yutaka Miyamoto, Kazushige Yonenaga, Shoichiro Kuwahara, Masahito Tomizawa, Akira Hirano, Hiromu Toba, Koichi Murata, Yasuhiko Tada, Yohtaro Umeda, Hiroshi Miyazawa, "*1-2-Tbit/s (30 x 42.7-Gbit/s ETDM optical channel) WDM transmission over 376 km with 125-km spacing using forward error correction and carrier-suppressed RZ format*," Optical Fiber Communication Conference, (2000).

(55) N. Shimizu, K. Murata, A. Hirano, Y. Miyamoto, H. Kitabayashi, Y. Umeda, T. Akeyoshi, T. Furata, N. Watanabe, "*40-Gbit/s monolithic digital OEIC composed of a uni-traveling-carrier photodiode and InP HEMTs*," Proceedings of Conference on Lasers and Electro-Optics, paper CWU5, San Francisco, California United States (2000).

(56) Y Miyamoto, K. Yonenaga, S. Kuwahara, M Tomizawa, A Hirano, H. Toba, K Murata, Y Tada, Y Umeda, H Miyazawa, *"1.2 Tbit/s (30×42.7 Gbit/s ETDM optical channel) WDMtransmission over 376 km with 125 km spacing using forward errorcorrection and carrier-suppressed RZ format*," Optical Fiber Communication Conference, (2000).

(57) K. Sato, A. Hirano, N. Shimizu, T. Ohno, H. Ishii, *"Dual mode operation of semiconductor mode-locked lasers for anti-phase pulse generation*," Optical Fiber Communication Conference, (2000).

(58) Hiroyuki Tsuda, Hirokazu Takenouchi, Tetsuyoshi Ishii, Katsunari Okamoto, Takashi Goh, Kenji Sato, Akira Hirano, Takashi Kurokawa, Chikara Amano, *"Photonic Spectral Encoder/Decoder Using an Arrayed-Waveguide Grating for Coherent Optical Code Division Multiplexing*," OFC, (1999).

(59) Akira Hirano, Yoshiakai Kisaka, Mikio Yoneyama, Naofumi Shimizu, *"Simple 2R repeater using direct coupling of UTC-PD and EA modulator*," ThC2, OAA, (1999).

(60) Yutaka Miyamoto, Akira Hirano, Kazushige Yonenaga, Akihide Sano, Hiromu Toba, Koichi Murata, Osamu Mitomi, *"320 Gbits/s (8x40)Gbits/s WDM transmission over 367-km zero-dispersion-flattened line with 120-km repeater spacing using carrier-suppressed return-to zeron pulse format*,"SN1, OAA, (1999).

(61) M. Yoneyama, Y. Miyamoto, T. Otsuji, A. Hirano, H. Kikuchi, T. Ishibashi, H. Miyazawa, *"Fully electrical 40-Gbit/s TDM system prototype and its application to 160-Gbit/s WDM transmission*," Optical Fiber Communication Conference and the International Conference on Integrated Optics and Optical Fiber Communication (OFC/IOOC), (1999).

(62) K Sato, A Hirano, M. Asobe, H Ishii, *"Chirp-compensated 40-GHz mode-locked lasers integrated withelectroabsorption modulators and chirped gratings*," IEEE 16th International Semiconductor Laser Conference, NARA, (1998).

(63) Y. Miyamoto, K. Yonenaga, A. Hirano, N. Shimizu, M. Yoneyama, H. Takara, K. Noguchi, K. Tsuzuki, *"1.04-Tbit/s DWDM transmission experiment based on alternate-polarization 80-Gbit/s OTDM signals*," 24th European Conference on Optical Communication, (1998).

(64) K. Wakita, K. Yoshino, A. Hirano, S. Kondo, Y. Noguchi, "*4-5 ps optical pulse generation with 40 GHz train from low driving-voltage modulator modules*," International Conference on Indium Phosphide and Related Materials, (1998).

(65) A. Hirano, H. Kobayashi, H. Tsuda, R. Takahashi, K. Sato, K. Hagimoto, "*10 Gbit/s all-optical pulse discriminator using a high-speed saturable absorber optical gate*," 11th International Conference on Integrated Optics and Optical Fibre Communications and 23rd European Conference on Optical Communications, (1997).

(66) K. Hagimoto, M. Yoneyama, A. Sano, A. Hirano, T. Kataoka, T. Otsuji, K. Sato, K. Noguchi, "*Limitations and challenges of single-carrier full 40-Gbit/s repeater system based on optical equalization and new circuit design*," Conference on Optical Fiber Communication, (1997).

(67) T. Kataoka, A. Sano, H. Tsuda, A. Hirano, K. Hagimoto, K. Sato, "*Equalization of 4.4 ps 100 mW pulse generated by monolithic mode-locked laser diode through 20 Gbit/s 1000-km transmission line*," Conference on Optical Fiber Communication, (1996).

(68) A. Hirano, H. Tsuda, R. Takahashi, Y. Kawamura, H. Iwamura, K. Hagimoto, "*An all-optical signal discrimination experiment using a high-speed saturable absorber optical gate*," CLEO-PR, (1995).

【Domestic Conference Papers】(In Japanese)

(1) Akira Hirano, "*Prospects of Optical Network for 2030*," Technical Committee Conference on Optical Network Industry and Technology, Nov. 14, No. 7, (1996).

(2) Akira Hirano, "*Prospects of Optical Network in the Post-Olympic Era*," Proceedings of the Society Conference of the Institute of Electronics, Information and Communication Engineers, BI-5-2, (2016).

(3) Fukutaro Hamaoka, Masanori Nakamura, Asuka Matsushita, Kengo Horikoshi, Hiroshi Yamazaki, Nobuhiko Hase, Akihide Sano, Akira Hirano, Yutaka Miyamoto, "*WDM long distance transmission experiment of 96 Gbaud optical modulation signal using DP-AM-DAC*," Proceedings of the Society Conference of the Institute of Electronics, Information and Communication Engineers 2016, B-10-64, (2016).

(4) Fukutaro Hamaoka, Seiji Okamoto, Kengo Horikoshi, Akira Hirano, Yutaka Miyamoto, "*Batch reception technology of mode multiplexed signals by mode selection coherent detection*," Technical research report of the Institute of Electronics, Information and Communication, Vol.116 No.164, OCS2016-20, (2016)..

(5) Seiji Okamoto, Mitsuteru Yoshida, Fukutaro Hamaoka, Akira Hirano, "*Adaptive pre-compensation of band narrowing and chromatic dispersion using pilot sequence*," Technical research report of the Institute of Electronics, Information and Communication, Vol.116 No.112, OCS2016-18, (2016).

(6) Fukutaro Hamaoka, Seiji Okamoto, Kengo Horikoshi, Kazushige Yonenaga, Akira Hirano, Yutaka Miyamoto, "*Batch reception technology of mode multiplexed signals by mode selection coherent detection*," Proceedings of the IEICE General Conference Proceedings, B-10-29, (2016).

(7) Asuka Matsushita, Kengo Horikoshi, Kazushige Yonenaga, Akira Hirano, "*Investigation of Forward Pumped Secondary Raman Amplification for Improvement of Transmission Line OSNR*," Proceedings of the IEICE General Conference Proceedings, B-10-36, (2016).

(8) Akira Hirano, "*Ultra high speed large capacity optical transmission technology*," Applied Physics Society Lightwave Sensing Study Group, Dec. 8, No. 8, (2015).

(9) Masanori Nakamura, Mitsuteru Yoshida, Kazushige Yonenaga, Akira Hirano, "*Construction method and basic characteristics evaluation of 8-dimensional light modulation using square QAM*," Technical research report of the Institute of Electronics, Information and Communication, Vol.115 No.276, OCS2015-53, (2015).

(10) Mitsuteru Yoshida, Kazushige Yonenaga, Akira Hirano, "*Blind wavelength dispersion estimation method using spectral symmetry*," Proceedings of the Society Conference of the Institute of Electronics, Information and Communication Engineers, B-10-23, (2015).

(11) Takafumi Tanaka, Akira Hirano, "*Application of multi-layer path design method considering traffic fluctuation to elastic optical network*," Technical research report of the Institute of Electronics, Information and Communication, Vol.115 No.93, OCS2015-13, (2015).

(12) Kengo Shintaku, Yoshiaki Yamada, Takuya Ohara, Takafumi Tanaka, Tetsuro Inui, Akira Hirano, "*Proposal of optical link reliability method for multicarrier transmission*," Proceedings of the IEICE General Conference Proceedings, B-10-75, (2015).

(13) Takafumi Tanaka, Akira Hirano, "*Multilayer path design method to efficiently accommodate geographically and temporally changing IP traffic*," Proceedings of the IEICE General Conference Proceedings, B-10-73, (2015).

(14) Yoshiaki Yamada, Takafumi Tanaka, Akihiro Kadohata, Akira Hirano, "*Implementation of variable redundancy code (MLRC) suitable for multi-lane transmission*," Proceedings of the Society Conference of the Institute of Electronics, Information and Communication Engineers, B-10-45, (2014).

(15) Takuya Oda, Akihiro Kadohata, Tetsuro Inui, Atsushi Watanabe, Akira Hirano, "*Study on optical network optimization method including maintenance cost for maintenance free optical network*," Technical research report of the Institute of Electronics, Information and Communication, Vol.114 No.195, OCS2014-38, (2014).

(16) Tetsuro Inui, Yoshiaki Yamada, Takafumi Tanaka, Takuya Oda, Kengo Shintaku, Akira Hirano, "*Proposal of Maintenance Free Oriented Optical Network and Demonstration of*

Basic Functions of Elementary Technologies," Technical research report of the Institute of Electronics, Information and Communication, Vol.114 No.108, OCS2014-18, (2014).

(17) Kei Kitamura, Yoshiaki Yamada, Mitsuhiro Teshima, Akira Hirano, "*A Study on Beyond 100 Gb / s Path Capacity Adjustment Method in Elastic Transport Network*," Proceedings of the IEICE General Conference Proceedings, B-10-31, (2014).

(18) Takuya Oda, Akihiro Kadohata, Atsushi Watanabe, Akira Hirano, "*Proposal of highly reliable optical link configuration technology considering maintenance operation*," Proceedings of the IEICE General Conference Proceedings, B-10-30, (2014).

(19) Takafumi Tanaka, Akira Hirano, Masahiko Jinno, "*Efficiency evaluation of IP over Elastic optical network using multi-flow transponder*," Technical research report of the Institute of Electronics, Information and Communication, Vol.113 No.391, OCS2013-97, (2014).

(20) Kei Kitamura, Yoshiaki Yamada, Mitsuhiro Teshima, Akira Hirano, "*Capacity variable accommodation technology for reconfigurable transponder for Beyond 100G*," Technical research report of the Institute of Electronics, Information and Communication, Vol.113 No.182, OCS2013-45, (2013).

(21) Akihiro Kadohata, Takafumi Tanaka, Fumikazu Inuzuka, Atsushi Watanabe, Akira Hirano, "*Wavelength defragmentation method based on wavelength path resource management*," Technical research report of the Institute of Electronics, Information and Communication, Vol.113 No.175, PN2013-17, (2013).

(22) Yoshiaki Yamada, Takafumi Tanaka, Kei Kitamura, Kenji Hisadome, Mitsuhiro Teshima, Akira Hirano, "*Proposal of Variable Redundancy FEC for Elastic Optical Network and Implementation and Evaluation by GPU*," Technical research report of the Institute of Electronics, Information and Communication, Vol.112 No.484, CAS2012-129, (2013).

(23) Takafumi Tanaka, Akira Hirano, Masahiko Jinno, "*Quantitative Evaluation of Optical Node Scale in Elastic Optical Network*," Proceedings of the IEICE General Conference Proceedings, B-10-79, (2013).

(24) Yohei Okubo, Akihiro Kadohata, Akira Hirano, "*Cost Comparative Evaluation of Traffic Grooming Method in Optical Multi-ring Network*," Proceedings of the IEICE General Conference Proceedings, B-12-18, (2013).

(25) Akihiro Kadohata, Akira Hirano, Fumikazu Inuzuka, Atsushi Watanabe, Osamu Ishida, "*Wavelength path reallocation design in multi-fiber environment*," Proceedings of the IEICE General Conference Proceedings, B-10-70, (2012).

(26) Fumikazu Inuzuka, Yoshiaki Sone, Akihiro Kadohata, Takafumi Tanaka, Atsushi Watanabe, Akira Hirano, Osamu Ishida, "*Evaluation of Least Fragmentation Method in Optical Path Wavelength Allocation Problem*," Proceedings of the IEICE General Conference Proceedings, B-10-122, (2012).

(27) Takafumi Tanaka, Yoshiaki Sone, Akira Hirano, Osamu Ishida, "*A Study on Efficient Accommodation Method of Multi Lane Optical Path in Optical Transparent Network*," Technical research report of the Institute of Electronics, Information and Communication, Vol.111 No.411, OCS2011-109, (2011).

(28) Akihiro Kadohata, Akira Hirano, Yoshiaki Sone, Osamu Ishida, "*Study on wavelength path reallocation method*," Technical research report of the Institute of Electronics, Information and Communication, Vol.111 No.297, OCS2011-96, (2011).

(29) Akihiro Kadohata, Akira Hirano, Yoshiaki Sone, Osamu Ishida, "*Optical path reallocation method considering reallocation procedure number count*," Proceedings of the Society Conference of the Institute of Electronics, Information and Communication Engineers, B-10-69, (2011).

(30) Takafumi Tanaka, Yoshiaki Sone, Akira Hirano, Osamu Ishida, "*A Study on Variable Lane Number Accommodation in Optical Path Network with Multi Lane Transport*," Proceedings of the Society Conference of the Institute of Electronics, Information and Communication Engineers, B-10-68, (2011).

(31) Takuya Ohara, Akihiro Kadohata, Takeshi Kawai, Takashi Ono, Masahiro Suzuki, Tetsuro Komukai, Akira Hirano, Mitsunori Fukutoku, "*Study on optoelectronic hybrid*

node," Technical research report of the Institute of Electronics, Information and Communication, Vol.111 No.92, OCS2011-25, (2011).

(32) Masahiko Jinno, Hidehiko Takara, Yoshiaki Sone, Kazushige Yonenaga, Akira Hirano, Shingo Kawai, "*Multi-flow optical transponder*," Technical research report of the Institute of Electronics, Information and Communication, Vol.111 No.92, OCS2011-21, (2011).

(33) Takuya Ohara, Mitsunori Fukutoku, Akihiro Kadohata, Akira Hirano, Takeshi Kawai, Tetsuro Komoni, Masahiro Suzuki, Shigeki Aizawa, Tetsuo Takahashi, Masahito Tomizawa, Osamu Ishida, Shinji Matsuoka, "*Optoelectronic hybrid node (1) - Optimization by re-grooming Multi-layer optical network -*," Proceedings of the IEICE General Conference Proceedings, B-10-112, (2011).

(34) Yoshiaki Sone, Akira Hirano, Masahiko Jinno, "*A Study on Optical Path Setting Control Method for Distance Adaptive Elastic Optical Path Network*," Proceedings of the Society Conference of the Institute of Electronics, Information and Communication Engineers, B-12-2, (2010).

(35) Takafumi Tanaka, Yoshiaki Sone, Koshituki Bartromel, Hidehiko Takara, Atsushi Watanabe, Akira Hirano, Masahiko Jinno, "*Distance Adaptive Spectrum Allocation Scheme for Elastic Optical Path Network*," Proceedings of the Society Conference of the Institute of Electronics, Information and Communication Engineers, B-12-1, (2010).

(36) Akihiro Kadohata, Atsushi Watanabe, Akira Hirano, Osamu Ishida, "*Transparent Optical Network Capable of Quick and Flexible Optical Path Accommodation Design*," Proceedings of the IEICE General Conference Proceedings, B-12-32, (2010).

(37) Yukio Tsukishima, Akira Hirano, Atsushi Taniguchi, Wataru Imajuku, Masahiko Jinno, "*Demonstration of multi-domain compatible wavelength path virtual concatenation technology*," Proceedings of the Society Conference of the Institute of Electronics, Information and Communication Engineers, B-12-14, (2007).

(38) Akira Hirano, "*The latest trend of photonic network related technology - III -*," Technical research report of the Institute of Electronics, Information and Communication, Vol.106 No.281, PN2006-33, (2006).

(39) Akira Hirano, Yutaka Miyamoto, Shoichiro Kuwahara, "*Comparison of transmission characteristics of CSRZ-DPSK and RZ-DPSK in G.652 single mode fiber*," Proceedings of the Society Conference of the Institute of Electronics, Information and Communication Engineers, B-10-94, (2003).

【Holding Japanese patents】(In Japanese)

(1) Patent 6154788, transmission apparatus and transmission method, June 28, 2017
(2) Patent 6114464, transmission apparatus and transmission method, April 12, 2017
(3) Patent 6097158, failure recovery method and network management device, March 15, 2017
(4) Patent 6082357, communication system and redundant configuration setting method, February 15, 2017
(5) Patent 6077696, optical transmission system, February 8, 2017
(6) Patent 6077381, Communication system management apparatus, and communication system management method, February 8, 2017
(7) Patent 6057432, Multiplexer, optical path network and multiplexing method, January 11, 2017
(8) Patent 6046598, communication system, frame rate conversion apparatus, and frame rate conversion method, December 21, 2016
(9) Patent 5965352, communication system management apparatus, and communication system management method, August 3, 2016
(10) Patent 5937978, Network management system and network management method, June 22, 2016
(11) Patent 5898284, Communication network design apparatus and communication network design method, April 6, 2016
(12) Patent 5873576, High reliable path accommodation designing apparatus and method, March 1, 2016
(13) Patent 5835737, method of determining route and frequency band, 24th December 2015
(14) Patent 5814420, Matrix operation circuit and matrix operation method, November 17, 2015
(15) Patent 5778089, transmission / reception control device, transmission / reception control method and transmission / reception control program, September 16, 2015
(16) Patent 5748363, communication path designing apparatus, communication path designing method and communication path designing program, July 15, 2015
(17) Patent 5740020, Multi-lane transmission system, multi-lane transmission apparatus, and multi-lane transmission method, June 24, 2015
(18) Patent 5713446, path accommodation control method, May 7, 2015
(19) Patent 5700877, optical communication device and optical path switching device and network, April 15, 2015
(20) Patent 5687557, wavelength path reallocation method and upper layer path reallocation method, March 18, 2015

(21) Patent 5639550, Path reallocation method and apparatus, December 10, 2014
(22) Patent 5613633, Node device, communication system, fault switching method, October 29, 2014
(23) Patent 5613631, communication node apparatus and path allocation method, October 29, 2014
(24) Patent 5583851, transmission system and transmission method, September 3, 2014
(25) Patent 5574491, Multilayer integrated transmission apparatus and optimization method, August 20, 2014
(26) Patent 5565577, traffic accommodation designing method in bandwidth variable communication system, August 6, 2014
(27) Patent 5523578, frequency allocation method and apparatus, June 18, 2014
(28) Patent 5492684, Network maintenance / management method and system, May 14, 2014
(29) Patent 5455783, Optical communication network and communication path setting method and optical communication network management system and operation system, March 26, 2014
(30) Patent 5419740, path accommodation design method, February 19, 2014
(31) Patent 5398839, Band variable communication method, bandwidth variable communication apparatus, transmission band determination apparatus, transmission band determination method, node apparatus, communication path setting system, communication path setting method, January 29, 2014
(32) Patent 5262474, Signal control method and resource management network system, August 14, 2013
(33) Patent 5051593, communication device and quality / route control method and quality / route control program, October 17, 2012
(34) Patent 5038001, optical cross-connect device and wavelength group accommodation method, October 3, 2012
(35) Patent 4852491, optical cross-connect switch functional unit and optical cross-connect device, January 11, 2012
(36) Patent 4809820, distribution reservation method and reservation management device and distribution reservation program, November 9, 2011
(37) Patent 4809803, Signal control method in optical cross-connect device and optical cross-connect device, November 9, 2011
(38) Patent 4809802, Optical cross-connect device, signal control method in optical cross-connect system and optical cross-connect device, November 9, 2011

(39) Patent 4809801, Signal control method in optical cross-connect system and optical cross-connect system, November 9, 2011

(40) Patent 4768661, wavelength selection method and apparatus and program in wavelength group network, September 7, 2011

(41) Patent 4758388, Resource reservation control method and apparatus and program, August 24, 2011

(42) Patent 4758387, data packet transfer control method and system and program, August 24, 2011

(43) Patent 4717788, Cluster node and cluster node configuration method, July 6, 2011

(44) Patent 4717785, Network management apparatus and method, July 6, 2011

(45) Patent 4688911, reservation redesign method and resource management device and reservation redesign program, May 25, 2011

(46) Patent 4675796, Automatic dispersion compensation type optical transmission system, April 27, 2011

(47) Patent 4635026, Resource reservation control method and apparatus and system and program, February 16, 2011

(48) Patent No. 4621228, route searching method and apparatus and program in multi-layer network, January 26, 2011

(49) Patent 4612633, Processing method and device for determination of PMD-induced failure probability of optical transmission system, January 12, 2011

(50) Patent 4589939, connection information management method and apparatus and program, December 1, 2010

(51) Patent 4541367, Failure recovery method and packet communication device, September 8, 2010

(52) Patent 4509035, Optical fiber communication system using optical amplification, July 21, 2010

(53) Patent 4494401, optical transmission system, optical transmission device and optical reception device of optical transmission system, June 30, 2010

(54) Patent 4493439, optical communication method, 30th June 2010

(55) Patent 4361032, optical fiber communication system, 11th November 2009

(56) Patent 4282559, optical transmission method and optical transmission system, Jun. 24, 2009

(57) Patent 4278332, Optical transmitter and optical transmission system, Jun. 10, 2009

(58) Patent 4104999, optical transmitter, optical receiver, optical transmission system and optical transmission method, Jun. 18, 2008

(59) Patent 4087290, Reception circuit and digital transmission system, May 21, 2008

(60)Patent 4053473, Optical transmitter, February 27, 2008

(61) Patent 3987009, polarization mode dispersion compensation method and polarization mode dispersion compensation apparatus, October 3, 2007

(62) Patent 3953934, code conversion circuit, and optical transmission circuit, August 8, 2007

(63) Patent 3819332, Optical network and node device, September 6, 2006

(64) Patent 3811022, optical waveform shaping circuit, Aug. 16, 2006

(65) Patent 3790190, Digital transmission system, June 28, 2006

(66) Patent No. 3786901, Optical transmitter and optical transmission system, Jun. 21, 2006

(67) Patent No. 3776357, optical transmission system and optical transmission method, May 17, 2006

(68) Patent 3764686, optical transmission circuit, 12th April 2006

(69) Patent 3727520, Wavelength multiplex transmission system, December 14, 2005

(70) Patent 3727498, optical transmission system, December 14, 2005

(71) Patent 3708503, High Accuracy Wavelength Dispersion Measurement Method and Automatic Dispersion Compensation Type Optical Link System Using the Method, October 19, 2005

(72) Patent 3609008, optical transmission line, January 12, 2005

(73) Patent 3545673, optical communication device, optical transmitter and optical receiver, July 21, 2004

(74) Patent 3539716, semiconductor light source, July 7, 2004

(75) Patent 3524005, optical pulse generator, April 26, 2004

(76) Patent 3510995, optical transmission method and optical transmission device, March 29, 2004

(77) Patent 3472151, Optical 2R circuit, December 2, 2003

(78) Patent 3461121, Optical limiter circuit, October 27, 2003

(79) Patent 3447664, Optical transmitter and optical transmitter control method, September 16, 2003

(80) Patent 3444464, short pulse light source, September 8, 2003

(81) Patent 3428925, Optical transmission line, July 22, 2003

(82) Patent 3330875, Optical repeater, September 30, 2002

(83) Patent 3276097, optical limiter circuit, April 22, 2002